

Wroclaw University of Science and Technology
Faculty of Geoengineering, Mining and Geology
Machinery Systems Division

**Metody stochastycznego modelowania
drugiarniowych szeregów czasowych w zastosowaniu
do detekcji uszkodzeń lokalnych górniczych
maszyn wirnikowych**

**Vibration time series stochastic modeling
methods with application to local damage
detection in mining rotating machinery**

Jakub Obuchowski

Submitted in part fulfillment of the requirements for the degree of
Doctor of Philosophy in Mining and Engineering Geology of the Wroclaw University of
Science and Technology and
the Diploma of Faculty of Geoengineering, Mining and Geology, June 2016

Abstract

Text of the Abstract.

Acknowledgements

I would like to express (whatever feelings I have) to:

- My supervisor
- My second supervisor
- Other researchers
- My family and friends

Dedication

Dedication here.

‘Quote text here.’

Guy Quoted

Contents

List of Tables

List of Figures

Chapter 1

Introduction

Szkic troche na podstawie <http://kipworldblog.blogspot.com/2014/05/a-brief-outline-for-organisingwriting.html>

1.1 Motivation and Objectives

Motywacja do detekcji uszkodzen (elementow) maszyn gorniczych w ogole: Awarie, przestoje, podwyzszone narazenie na zbyt wysokie natezenie dzwieku na stanowisku pracy, niebezpieczne zdarzenia (dymy, pozary). Cele: wykrywanie uszkodzen (elementow) maszyn gorniczych we wczesnym stadium rozwoju uszkodzenia, aby zapobiec awariom i niebezpiecznym zdarzeniom, ograniczyc przestoje, dac mozliwosc na zaplanowanie remontow w odpowiednim czasie.

Alternatywnie: Motywacja do wykorzystania metod stochastycznych w analizie sygnalow drganiowych: Drgania maszyn maja charakter losowy ze wzgledu na...(nierownosci powierzchni elementow maszyn, tj. biezni i el. tocznych lozysk, kol zebatych). Ponadto, wpływ na postac sygnalu maja zrodla zewnetrzne (czujniki nie zbieraja jedynie drgan zwiazanych ze wzajemnym kotakiem kol zebatych czy biezni i elementow tocznych - kazdy kontakt z obudowa maszyny jest potencjalnym zrodlem dodatkowych składowych sygnalu drganiowego - zaklocen). Rowniez inne maszyny pracujace w poblizu sa potencjalnym zrodlem drgan zmierzonych na maszynie, ktorej elementy sa diagnozowane. W przypadku lozysk - losowosc spowodowana przez jitter (lozysko_b - stad local maxima a nie cyclostationarity) W niektórych maszynach mamy

do czynienia takze z losowo zmiennym obciążeniem (koparka kolowa). W przypadku wielu uszkodzeń występujących w jednej maszynie można oczekiwac roznego charakteru sygnałów związanych z tymi uszkodzeniami (deterministyczny, losowy). Cele: wykorzystać narzędzia oparte na metodach stochastycznych w celu uzyskania informacji o uszkodzeniu lokalnym, na podstawie sygnałów zmierzonych na maszynach górniczych w warunkach pracy kopalni.

1.2 Research Problem and Hypotheses

Tu po kolei wypunktuje problemy, które napotkalem w realizacji pracy (zaklocenia od maszyn pracujących w pobliżu - local maxima + selektory + filtrowanie z selektorów, przypadkowe impulsy - selektory + filtrowanie, jitter - local maxima + selektory (impulsowość zamiast cykliczności), zmiana obciążenia w koparce - PAR, dwa uszkodzenia - AR do usunięcia z sygnału jednego uszkodzenia + selektory z filtrowaniem do drugiego uszkodzenia) Hipoteza - zaproponowane narzędzia pozwalają na detekcję uszkodzeń lokalnych w maszynach górniczych w przypadku występowania wyżej wymienionych problemów, w czym przewyższają dotychczas stosowane metody.

1.3 Outline of the Thesis

Odpowiednik "The paper is structured as follows..."

1.4 Delimitations

Inne problemy występujące w detekcji uszkodzeń maszyn górniczych, które jednakże nie będą poruszane w pracy. Inne uszkodzenia, nie-lokalne. Uszkodzenia dwóch lożysk o identycznej budowie (częstotliwościach charakterystycznych). Analizy wielokanalowe (i wielowymiarowe).

Chapter 2

Background Theory

2.1 Introduction

Background: założenia dotyczące ujawniania się uszkodzeń lokalnych w sygnalach drganiowych (chwilowa zmiana sił, potem modulacja transmission path), wpływu zmiennego obciążenia, maszyn pracujących w pobliżu i środowiska pracy (przypadkowy kontakt z obudową) na postać sygnału drganiowego

teoria jitter

rodzaje uszkodzeń lokalnych, mechanizmy powstawania

Chapter 3

Literature review

3.1 Literature related to the topic/to the problems posed in the thesis

Przeglad literatury

Podsekcje dla kazdego z 5 problemow

1. Metody dekompozycji sygnału na składowe o prostszej strukturze
 - Krótkookresowa transformacja Fouriera (STFT)
 - Inne transformacje (t. falkowa, dekompozycja empiryczna)
2. Metody poszukiwania optymalnego pasma częstotliwościowego (składowe deterministyczne + sygnał impulsowy)
 - Selektory bazujące na momentach, kwantylach lub innych właściwościach sygnału
3. Filtracja sygnału na podstawie selektorów -Ustalenie granicznych poziomów selektorów
4. Modelowanie i filtracja sygnału na podstawie modelu autoregresyjnego (AR)
 - Metody estymacji parametrów modeli wysokiego rzędu z szumem gaussowskim i niegaussowskim
 - Stabilność dopasowanego modelu
5. Modelowanie sygnału drganiowego w zmiennych warunkach eksploatacyjnych

-Model AR o okresowo zmiennych współczynnikach (PAR z długim okresem zmienności)

3.2 Discussion

Dyskusja nad roznymi podejsciami, wady i zalety metod z literatury. Cos jak dyskusja nad roznymi metodami ustalenia poziomow granicznych selektorow.

3.3 Conclusions

Jak mozna poprawic (jak to poprawilem w pracy) metody z literatury.

Chapter 4

Methodology

Trzeba ustalic czy nazywac sekcje metodami (local maxima, odporne selektory, two-stage method, PAR) czy problemami (t-f map enhancement, selection of IFB, significance levels of selectors for filtering purposes, more than 1 damage, frequency modulation due to time-varying load) - raczej problemami

W kazdej sekcji metodologia, algorytm ze schematem, wyjasnienie poszczegolnych krokow (umotywowanie)

4.1 Time-frequency map enhancement - skompilowac z Fer-rara

In this section we present in details the local maxima method which was previously based on non-overlapping windows in short time Fourier transform [?]. Here we describe how to adapt it to highly-overlapping windows.

The local maxima method starts with a transformation which converts a signal in time domain into a two-dimensional map (time-frequency), where spikes in time domain become wide-band excitations. In this paper we use the short-time Fourier transform that is denoted by $\{STFT(t, f)\}_{t \in T, f \in F}$, where T is the set of time points and F stands for the set of frequencies

for which the transform is calculated. In the further analysis we assume $T = \{t_1, \dots, t_{\#T}\}$, where $\#T$ denotes number of elements of the set T . The STFT for random sample X_1, \dots, X_n , time point t_i and frequency f is defined as follows:

$$STFT(t_i, f) = \sum_{k=1}^n X_k \tilde{W}_{k-t_i} e^{jfk}, \quad (4.1)$$

where $\{\tilde{W}_k\}$ is the window sequence.

Once the map is obtained, time series related to each $f \in F$ are analyzed. For a given $f \in F$ and t_i we put $M(t_i, f) = 1$ if $|STFT(t_i, f)| = \max\{|STFT(t_k, f)| : i-r \leq k \leq i+r\}$ and $M(t_i, f) = 0$ elsewhere. The binary spectrogram obtained by applying this rule for every time series should have clearly visible wide-band excitations with small amount of local maxima between them if r is properly chosen. We suggest that r (called the minimal neighborhood length) should be as high as it is possible to theoretically preserve all the cyclic wide-band excitations related to damage in a rotating machine. In the non-overlapping windows case r is calculated as the highest integer value not greater than ratio of the expected time between the following disturbances to the STFT window length, both expressed in the same units, i.e. in samples or in a unit of time. The formula for r is:

$$r = \lfloor (fs/f\bar{f})/Nw - 1 \rfloor \quad (4.2)$$

where fs is the sampling frequency, $f\bar{f}$ is the fault frequency, Nw stands for the STFT window length and $\lfloor x \rfloor$ is the largest integer not greater than x . In the overlapping windows case we propose to modify equation (4.2) as follows:

$$r = \lfloor ((fs/f\bar{f})/Nw - 1)/(1 - Ov) \rfloor, \quad (4.3)$$

where Ov denotes overlap ratio, i.e. the ratio of the number of samples that each window overlaps to the window length. In the further analysis we use $Ov = 0.95$ and compare it to $Ov = 0$. In practice, there might be some deviations from the theoretical distance between local maxima. To illustrate this point, consider series of impulses of different height. It can be

caused both by random character of shocks and random background noise. Relaxation of the impulses, even in local damage case, takes a little of time so the real distance between local maxima in a particular time series might be a little smaller than theoretical. Moreover, some of rotating machines exhibit jitter (e.g. bearings) during operation under constant rotational speed, so the real distance might be a little higher or lower than the distance obtained by using equation (4.3).

The next step in our procedure is to calculate the vector of weights and combine it with the binary spectrogram obtaining the enhanced spectrogram. The latter one is formulated as follows:

$$ENH(t_i, f) = W(t_i)M(t_i, f), \quad (4.4)$$

where $W(t_i) = \frac{1}{\#F} \sum_{f \in F} M(t_i, f)$ is the vector of weights and $M(t_i, f)$ represents binary valued time series of the local maxima occurrence for a time point t_i and frequency f . Conversion of the time-frequency map $\{|STFT(t, f)|\}_{t \in T, f \in F}$ into the binary matrix $\{M(t, f)\}_{t \in T, f \in F}$ preserves energy-invariance, i.e. local maxima in a low-energy frequency bin are as significant as local maxima in other frequency bin. An impulse in the vector of weights calculated as average value of $\{M(t_i, f)\}_{f \in F}$, for a particular time t_i is present only if there is a significant number of local maxima at t_i , i.e. larger than in the case where local maxima at t_i are the result of random character of the signal. If there are no wideband excitations in the time-frequency map or frequency bands of the excitations are not significantly wide then the vector of weights has no pulses. Thus, in locally damaged machine case the enhanced time frequency map increases visibility of wideband excitations and decreases influence of high-energy components. In healthy machine case it presents time-frequency map without any pattern. Moreover, arithmetic mean in the formula for $W(t_i)$ makes the result invariant to number of points at which FFT is calculated.

In the next step of our procedure we propose to analyze the enhanced version of vector of

weights, i.e. vector calculated as follows:

$$V(t_i) = \frac{1}{\#F} \sum_{f \in F} ENH(t_i, f). \quad (4.5)$$

Formula 4.5 reduces noise present in $\{W(t)\}_{t \in T}$ putting highest values to time points at which the enhanced spectrogram $\{ENH(t, f)\}_{t \in T, f \in F}$ has wideband excitations instead of taking into account only binary matrix $\{M(t, f)\}_{t \in T, f \in F}$ (as in $\{W(t)\}_{t \in T}$).

One of the tools useful to estimate the fault frequency is the sample autocorrelation function (ACF). For a random sample Y_1, Y_2, \dots, Y_n the ACF is defined as follows:

$$R(k) = \frac{\sum_{i=1}^{n-|k|} (Y_i - \bar{Y})(Y_{i+k} - \bar{Y})}{\sqrt{\sum_{i=1}^n (Y_i - \bar{Y})^2}}, \quad (4.6)$$

where \bar{Y} is a sample mean of the random sample Y_1, Y_2, \dots, Y_n . The vector of weights (and its enhanced version) is a set of non-negative real numbers including a set of significantly higher values in the case of local damage. If time intervals between these values are equal, then the sample ACF should be higher at lags related to them. It was shown that even in the case of poor resolution on time scale the sample ACF is sufficient to estimate the fault frequency.

The main purpose to use overlapping windows is better resolution on time scale. In this paper it will be examined whether the sample ACF will still be useful in the case of better time resolution. What is more, this examination will be preceded by analysis of envelope spectra in both overlapping and non-overlapping cases.

The whole procedure is presented in Fig. 4.1

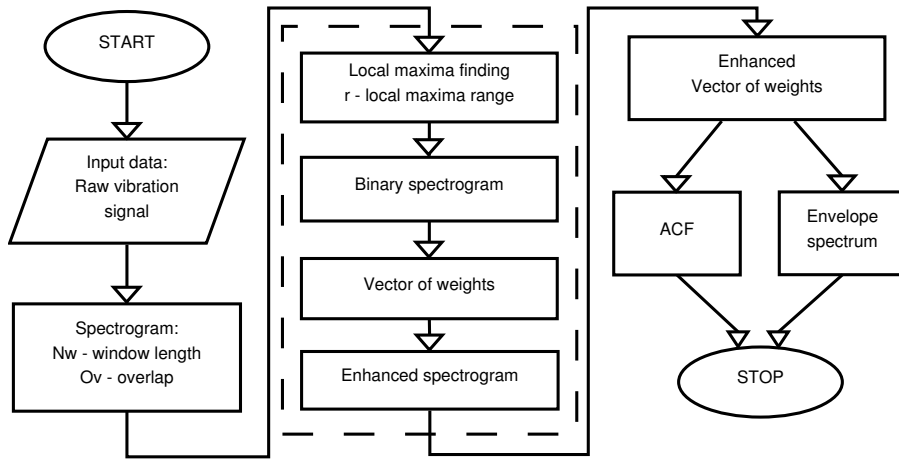


Figure 4.1: Diagram of time-frequency map enhancement procedure.

4.2 Selection of informative frequency band

In this section we introduce the novel procedure that leads to the local damage detection in rotating machinery. This procedure is based on the time-frequency representation of examined signal. More precisely, in the first step of our analysis we decompose the signal into set of narrowband sub-signals using a time-frequency representation. Here we propose to use the short-time Fourier transform (STFT) that is defined as follows [?]:

$$STFT(f, t) = \int_{-\infty}^{\infty} w(t - \tau) X(\tau) e^{2j\pi f \tau} d\tau, \quad (4.7)$$

where $w(t - \tau)$ is the shifted window and $X(\tau)$ is the input signal. Discrete version of equation (4.7) for observations X_1, X_2, \dots, X_N , time point $t \in T$ and frequency $f \in F$ is defined as follows:

$$STFT(t, f) = \sum_{k=0}^{N-1} X_k w(t - k) e^{2j\pi f k / N}. \quad (4.8)$$

In the second step of our analysis we use several statistics, called selectors, that can be useful as tools for assessment of the sub-signals. Each sub-signal is slice for a given narrow frequency range that arises after mentioned time-frequency decomposition. In this paper we extend the classical approach, where the kurtosis of sub-signals is calculated and propose new selectors based on statistical properties of examined sub-signals. The primary analysis of rotating ma-

achinery indicates that sub-signals related to machine in healthy condition are closer to Gaussian than sub-signals related to a damaged one, so some of the proposed statistics are based on the distance between empirical distribution of examined sub-signal and the base distribution, namely the Gaussian one. The selectors mentioned in this paper might be grouped with respect to their statistical properties. In the following subsections we describe the selectors grouped with respect to their statistical properties.

4.2.1 Moment-based selectors

One of the most popular selectors that might be applied to local damage detection of underlying signal is the spectral kurtosis (SK), [?]. The spectral kurtosis was first introduced as a statistical tool which can indicate not only non-Gaussian components in a signal, but also their locations in the frequency domain. The spectral kurtosis at the frequency band f is defined as follows [?]:

$$SK(f) = \#T \frac{\sum_{t \in T} |STFT(t, f)|^4}{(\sum_{t \in T} |STFT(t, f)|^2)^2} - 2, \quad (4.9)$$

where $\#T$ denotes the number of elements of the set T , i.e. number of time points at which STFT is calculated.

Since the spectral kurtosis is based on the fourth-order moment, this group of selectors will be complemented with a statistic which is based on both fourth and third moment, namely the Jarque-Bera statistic. It is strictly related to the Jarque-Bera test, which is a goodness-of-fit test of whether sample data has the skewness and kurtosis matching a normal distribution. This methodology is an extension of the widely used scheme where only the empirical kurtosis is being investigated. The JB statistic calculated for sub-signal corresponding to frequency band f is defined as:

$$JB(f) = \frac{\#T}{6} \left(S_f^2 + \frac{(K_f - 1)^2}{4} \right), \quad (4.10)$$

where S_f and K_f are the empirical skewness and kurtosis, respectively, calculated for given sub-signal corresponding to frequency band f .

The value of the JB statistic forms a random variable which converges to zero if the underlying distribution has skewness zero and kurtosis 3 (e.g. Gaussian). Any deviation from zero skewness and kurtosis equal to 3 increases the JB statistic. In this paper the JB statistic is one of the proposed selectors used for local damage detection. If the data come from a normal distribution, the JB statistic asymptotically has a chi-squared distribution with two degrees of freedom, so the statistic can be used to test the hypothesis that the data are derived from a Gaussian distribution. The null hypothesis is a joint hypothesis of the skewness being zero and the excess kurtosis being zero. As the definition of JB shows, any deviation from these values increases the JB statistic.

4.2.2 ECDF-based selectors

In this section we describe selectors based on the empirical cumulative distribution function (ECDF). The fundamental statistical property of them is that, for specific distributions, moments of a random variable might be infinite, while cumulative distribution function is always well-defined. Moreover, these two groups are different from the computational point of view - calculating ECDF requires sorting of the sample.

The first proposed selector in this group is a Kolmogorov-Smirnov statistic (KSS) that for sub-signal corresponding to the frequency band f is defined as follows [?, ?]:

$$KSS(f) = \sup_x |ECDF_f(x) - \Phi_f(x)|, \quad (4.11)$$

where Φ_f is the cumulative distribution function of the Gaussian distribution with parameters estimated from the sub-signal corresponding to the frequency band f . Therefore this function is given by:

$$\Phi_f(x) = \int_{-\infty}^x \frac{1}{\sqrt{2\pi\widehat{\sigma}_f^2}} \exp\left(-\frac{(x - \widehat{\mu}_f)^2}{2\widehat{\sigma}_f^2}\right) dx, \quad (4.12)$$

where $\widehat{\mu}_f$ is the empirical mean of the sub-signal $\{|STFT(t, f)|\}_{t \in T}$, and $\widehat{\sigma}_f$ is the empirical standard deviation of $\{|STFT(t, f)|\}_{t \in T}$. Moreover $ECDF_f(x)$ is the empirical cumulative distribution function calculated for the sub-signal corresponding to the frequency band f :

$$ECDF_f(x) = \frac{1}{\#T} \sum_{t \in T} \mathbf{1}\{|STFT(t_k, f)| \leq x\} \quad (4.13)$$

In the above definition $\mathbf{1}\{A\}$ denotes the indicator of the set A.

The idea of using the Kolmogorov-Smirnov statistic for spikiness detection is illustrated in

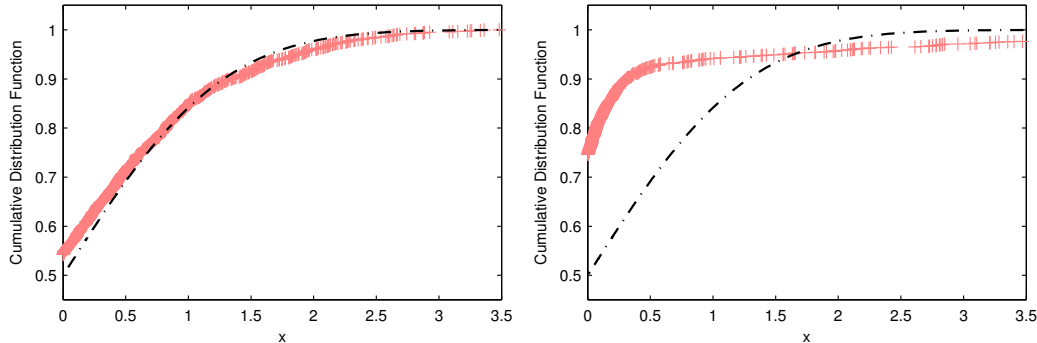


Figure 4.2: The empirical and theoretical (Gaussian) cumulative distribution functions for exemplary sub-signals from machine in good condition (left panel) and damaged one (right panel). The black dashed line represents the reference cumulative distribution function of Gaussian distribution.

Fig. 4.2, where we present the empirical and theoretical cumulative distribution functions for real data set analyzed in Sec. ???. In the left panel of Fig. 4.2 we show the cumulative distribution functions (empirical and theoretical - Gaussian) for sub-signal corresponding to the frequency $f = 2325$ Hz for machine in good condition while in the right panel for the damaged one. One can observe in the left panel the analyzed functions are closer than in the right panel, therefore the KSS for this frequency band has lower value for the sub-signal from machine in good condition.

In [?, ?] one can find more properties of the KSS statistic and statistical test based on it. We only mention here the KSS statistic tends to zero (almost surely) when number of elements in set T tends to infinity. Moreover the distribution of KSS statistic defined in (4.11) is normal. The first fact is a result of Glivenko-Cantelli theorem [?] while the second it is so called the distribution-free property.

The next statistic that might be a useful tool for informative band selection is an extension of the mentioned Kolmogorov-Smirnov. Similar to KSS , it is based on the distance between theoretical and empirical cumulative distribution functions for underlying sub-signal. The selector, called Anderson-Darling statistic, belongs to the Cramer-von Mises family of statistics which incorporate the idea of quadratic norm. The Cramer-von Mises statistic for frequency band f is defined by [?]

$$Q(f) = \#T \int_{-\infty}^{\infty} (ECDF_f(x) - \Phi_f(x))^2 \phi(x) dx \quad (4.14)$$

where $\phi(x)$ is a suitable function which puts weights to the squared difference $(ECDF_f(x) - \Phi_f(x))^2$. Moreover functions $ECDF_f(x)$ and $\Phi_f(x)$ are defined in (4.12) and (4.13), respectively. When $\phi(x) = 1$, $Q(f)$ is called the Cramer-von Mises statistic. In this case we denote it as CVM . If $\phi(x) = [\Phi_f(x)(1 - \Phi_f(x))]^{-1}$, the above definition yields the Anderson-Darling statistic. In the further analysis it is denoted as AD . Similarly to the Kolmogorov-Smirnov statistic there exist statistical tests that allow to test the proper distribution of examined data by using the CVM and AD statistics. More details can be found in [?, ?, ?]. The Cramer-von Mises test has better properties than the Kolmogorov-Smirnov test, but it is relatively insensitive to "tails" of the distribution. In order to eliminate this disadvantage the Anderson-Darling test was introduced. The Anderson-Darling test is a statistical test of whether a given sample of data is drawn from a given probability distribution. In our case the base distribution is normal. The test is one of the most powerful statistical tools for detecting deviations from normality.

4.2.3 Quantile-quantile plot-based selectors

Except of statistical tests with explicit hypothesis, there are some visual tests to compare two distributions, e.g. the theoretical distribution and the empirical one. One of the most famous examples is the quantile-quantile plot (QQplot), [?]. Plot of the theoretical distribution quantiles versus the underlying ones might be useful to recognize goodness-of-fit. Straight line on the QQplot means that compared distributions have the same shape. Straight line with

equal scales on the axes means equal distributions. If there is no straight line, then one can compare, for example, tail heaviness of both distributions. In most of numerical packages (MATLAB, R) there is an additional straight line plotted to make analysis easier. This line connects two points: first and third quartiles of both distributions. To make this test numerical, we propose to measure the horizontal distance between the QQplot markers and the additional straight line. One can note that statistics contained in this group require sorting, similar to the previous group. Nevertheless, the lack of explicit hypothesis of gaussianity test based on the QQplot tends us to classify them into an individual group.

For this test, we propose to compute mean and maximum of those distances. The formula for

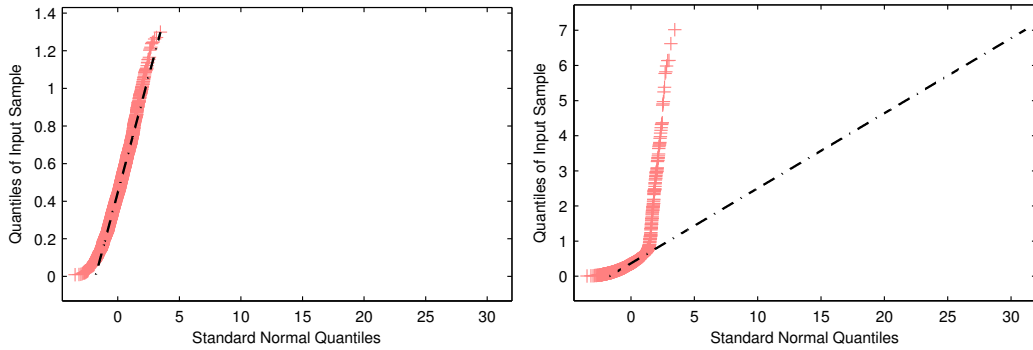


Figure 4.3: QQplot of the healthy (left panel) and unhealthy (right panel) sub-signal compared to the normal distribution. The black dashed line represents the reference quantile line for Gaussian distribution. Note that only horizontal distance between markers and line is quantified by H_{aver} and H_{max} .

the maximum distance between the Gaussian distribution and the sub-signal corresponding to the frequency band f is as follows:

$$H_{max}(f) = \max_{1 \leq k \leq \#T} \left| \Phi_f^{-1} \left(\frac{2k-1}{2\#T} \right) - aS(k, f) - b \right|, \quad (4.15)$$

where Φ_f^{-1} is the inverse of Φ_f defined in (4.12) for $\mu = 0$ and $\sigma = 1$, $S(k, f)$ is the k -th value of ascending sorted sub-signal $\{|STFT(t, f)|\}_{t \in T}$, $a = \frac{\Phi^{-1}(0.75) - \Phi^{-1}(0.25)}{q_f(0.75) - q_f(0.25)}$, $b = \Phi^{-1}(0.75) - aq_f(0.75)$ and $q_f(p)$ is a p -th order quantile of a sub-signal $\{|STFT(t, f)|\}_{t \in T}$.

The formula for the average distance is analogous with the max function substituted by the arithmetic mean. We denote the corresponding statistic as H_{aver} . The exemplary QQplots for real data examined in Sec. ?? of a healthy signal (for a given frequency bin) is presented in

Fig. 4.3 (left panel) while for the sub-signal with defect - in the right panel of Fig. 4.3. We observe the healthy signal is closer to Gaussian distribution than the unhealthy one. Both average and maximum horizontal distances between straight line and markers are significantly larger in the right panel.

4.2.4 Local maxima method-based selector

The last procedure that allows for construction of a selector for local damage detection is based on the local maxima method [?, ?]. For each frequency band (i.e. each sub-signal) we check the local maximum occurrence. We assume that local maximum occurs at a given time point when the modulus of STFT value therein is higher than the other values in its neighborhood of a length not less than a certain value - r . Then, for each frequency band we create a new binary vector which is a transformation of the original data into zero-one series. More precisely, we put 1 at a time point when the local maximum occurs and 0 otherwise. Let us point that the binary values obtained in this way minimize influence of insignificant signals for local damage detection as well as maximize influence of characteristic signals for locally damaged machinery. In our methodology for each time point we use the vector of weights (VoW), which is a vector of averaged maxima occurrence, i.e. VoW at point t is defined as follows:

$$W(t) = \frac{1}{\#F} \sum_{f \in F} M(t, f), \quad (4.16)$$

where $M(t, f)$ represents binary valued vector of the local maxima occurrence at the time point t and frequency f . After multiplying each previously computed binary value by the value of VoW at the corresponding time point we obtain an enhanced spectrogram. Therefore the enhanced spectrogram at point (t, f) is defined as follows:

$$ENH(t, f) = W(t)M(t, f). \quad (4.17)$$

More details of the procedure for the enhanced spectrogram construction for different applications one can find in [?, ?]. The selector based on the local maxima method for frequency band

f is constructed as follows:

$$LM(f) = \frac{1}{\#T} \sum_{t \in T} ENH(t, f). \quad (4.18)$$

4.3 Linear filter design based on selectors

In this section we present the whole methodology which leads to the raw vibration signal enhancement. It is composed of 4 steps (Fig. 4.4):

- decomposition of the signal into two-dimensional time-frequency plane,
- selector values calculations for informative band selection,
- estimation of thresholds for individual frequency bins,
- filtering of raw vibration signal and envelope analysis.

At first, the signal is decomposed into a time-frequency map (STFT), which is an estimate of energy fluctuation at particular frequency bins in time. Specifically, we process sub-signals, i.e. time series associated with a particular frequency bin. Each sub-signal is examined how far from Gaussian is its empirical distribution. In order to do this, we examine values of several selectors calculated for every sub-signal. The selectors are based on statistical moments, empirical quantiles and cumulative distribution function. As one of the selectors we use the spectral kurtosis.

For a given selector, we obtain a set of weights for the whole signal's spectrum. The weights are used to establish a linear filter similar to the Wiener filter based on the SK [?]. Filtering incorporates the discrete Fourier transform (DFT) and its inverse. In order to enhance filter's amplitude response we propose to cut-off the selector values using individual thresholds for each frequency bin. The thresholds are calculated upon reference signals, whose amplitude spectra are similar to the amplitude spectrum of the raw vibration signal. The reference signals are simulated using the Monte Carlo method and a procedure called inverse pre-whitening.

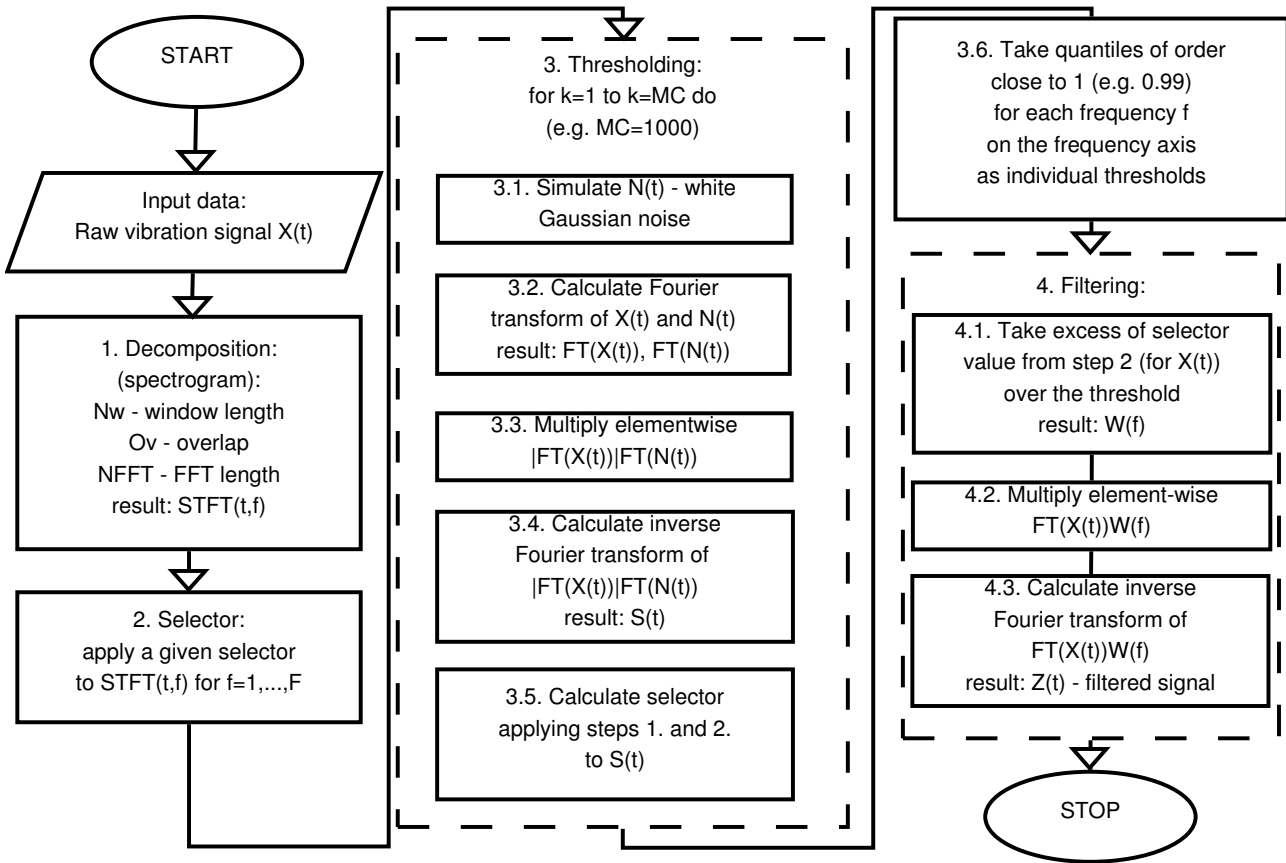


Figure 4.4: Block diagram of the filtering procedure.

After the thresholds are calculated and selector values are enhanced, we propose to filter the signal in frequency domain. Then, the signal's envelope spectrum is analyzed.

4.3.1 Decomposition

Decomposition is based on analysis of the discrete short-time Fourier transform (STFT) which for x_1, x_2, \dots, x_N , time point $t = \{1, \dots, T\}$ and frequency $f = \{1, \dots, F\}$ is defined as follows [?]:

$$STFT(t, f) = \sum_{k=0}^{N-1} x_k w(t-k) e^{-2j\pi fk/N}, \quad (4.19)$$

where $w(t-k)$ is the shifted window and x_k is the input signal. The window (length and shape) affects the final result in the similar manner as in the spectral kurtosis case. In this paper we present results obtained by using 80% overlapping.

4.3.2 Selectors

In this section we recall four selectors [?, ?], each of them could be a base for a linear filter. For comparison, one of the selectors is the classical spectral kurtosis. Recall, that the SK is based on the fourth-order statistic. The spectral kurtosis at the frequency bin f is defined as follows [?]:

$$SK(f) = T \frac{\sum_{t=1}^T |STFT(t, f)|^4}{(\sum_{t=1}^T |STFT(t, f)|^2)^2}. \quad (4.20)$$

Besides the ability of a pulse train detection, the SK is also very sensitive to a single non-informative impulse that might occur, for instance, during the signal acquisition. In the classical definition, the sum in (4.20) is reduced by 2 which stands for a cut-off threshold, i.e. only the values of $SK(f)$ larger than 2 are significant. In our approach such subtraction is not necessary - the thresholding procedure quantifies the significance of each selector's value and takes into account only the excess over the threshold.

The second selector is the Jarque-Bera statistic [?, ?]. It is based on both kurtosis and skewness. The JB at $f = 1, \dots, F$ is defined as follows:

$$JB(f) = \frac{T}{6} \left(S(f)^2 + \frac{(K(f) - 3)^2}{4} \right), \quad (4.21)$$

where $S(f)$ and $K(f)$ are the empirical skewness and kurtosis, respectively, calculated for a given sub-signal, corresponding to the frequency bin f . JB exploits not only the fourth, but the third moment as well, in order to examine gaussianity of the random sample. Thus, it might indicate asymmetry of distribution, which occurs in specific types of damage in rotating machines [?]. The higher value of JB , the more the distribution of the sample differs from the Gaussian distribution.

The next selector is based on a quantile-quantile plot (QQplot). Vertical and horizontal axes of the QQplot are here related to quantiles of empirical sub-signal's distribution and the standard Gaussian distribution, respectively. The selector quantifies the average distance between markers of QQplot and a reference line defined by first and third quartiles of both distributions [?].

The selector H_{aver} at $f = 1, \dots, F$ is defined as [?]:

$$H_{aver}(f) = \frac{1}{T} \sum_{k=1}^{k=T} \left| \tilde{\Phi}^{-1} \left(\frac{2k-1}{2T} \right) - aS(k, f) - b \right|, \quad (4.22)$$

where $\tilde{\Phi}^{-1}(\cdot)$ is the inverse of cumulative distribution function of the standard Gaussian distribution, i.e.

$$\tilde{\Phi}(x) = \int_{-\infty}^x \frac{1}{\sqrt{2\pi}} \exp \left(-\frac{x^2}{2} \right) dx,$$

$S(k, f)$ is the k -th value of ascending sorted sub-signal $\{|STFT(t, f)|\}_{t=1, \dots, T}$, $a = \frac{\tilde{\Phi}^{-1}(0.75) - \tilde{\Phi}^{-1}(0.25)}{q(f, 0.75) - q(f, 0.25)}$, $b = \tilde{\Phi}^{-1}(0.75) - aq(f, 0.75)$ and $q(f, p)$ is a p -th order quantile of a sub-signal $\{|STFT(t, f)|\}_{t=1, \dots, T}$.

In [?] it is shown that this selector distinguishes healthy from faulty bearing's signal as good as SK does, but H_{aver} defines a different order on the set of sub-signals than SK does. Recall that H_{aver} is scale-invariant, since the distance is measured on the axis corresponding to standard normal distribution. Due to the design of H_{aver} , one can notice its robustness to single outlying values. One can consider two signals of different lengths, the same statistical distribution and both of them contain a single outlier of similar level. Then H_{aver} is lower for the longer signal, since the appropriate quartiles and $S(k, f)$'s are similar and the denominator, namely T , distinguishes these signals.

The next selector incorporates the idea of quantifying the distance between the empirical cumulative distribution function (empirical CDF) of the sub-signal and the CDF of the fitted Gaussian distribution. Specifically, it is a Kolmogorov-Smirnov statistic which is defined as follows [?, ?, ?]:

$$KSS(f) = \sup_x |ECDF(f, x) - \Phi(f, x)|, \quad (4.23)$$

where $\Phi(f, \cdot)$ is the cumulative distribution function of the Gaussian distribution with mean and variance estimated from the sub-signal corresponding to the frequency bin f . Therefore this function is given by:

$$\Phi(f, x) = \int_{-\infty}^x \frac{1}{\sqrt{2\pi\hat{\sigma}^2(f)}} \exp \left(-\frac{(x - \hat{\mu}(f))^2}{2\hat{\sigma}^2(f)} \right) dx, \quad (4.24)$$

where $\widehat{\mu}(f)$ is the empirical mean of the sub-signal $\{|STFT(t, f)|\}_{t=1, \dots, T}$, and $\widehat{\sigma}(f)$ is the empirical standard deviation of $\{|STFT(t, f)|\}_{t=1, \dots, T}$. Moreover, $ECDF(f, x)$ is the empirical cumulative distribution function calculated for the sub-signal corresponding to the frequency bin f :

$$ECDF(f, x) = \frac{1}{T} \sum_{t=1}^T \mathbf{1}\{|STFT(t, f)| \leq x\}. \quad (4.25)$$

In the above definition $\mathbf{1}\{a \leq x\}$ denotes the indicator function, i.e. $\mathbf{1}\{a \leq x\} = 1$ if $a \leq x$ and 0 otherwise. This selector is also scale-invariant. Moreover, in opposite to the previous selectors, KSS is bounded since values of both cumulative distribution functions (i.e. $ECDF$ and Φ) are between 0 and 1.

The values of a particular selector for the entire spectrum constitute a ground for the amplitude response of the filter. The following sections provide a complete description how to obtain the final filter that might be used to obtain the informative part of the vibration signal.

4.3.3 Thresholding

Once the amplitude response of the filter is calculated, it has to be enhanced in order to take into account the significant values of the selector only. We propose to design significance thresholds for each frequency bin individually. This step is essential when energy contained in the informative frequency band is relatively low, i.e. the signal also contains high-energy components that do not carry information about the local damage. In order to illustrate this point, consider a vibration signal that consists of: a) high-energy low-frequency component (component related to normal operation of the machine), b) low-energy component located at the half of the frequency range (component related to local damage) and c) low-energy noise located at the highest frequency bands (non-informative from diagnostic point of view). Values of any selector (that indicates impulsivity) at low frequency bands (not related to damage) are significantly lower than selector values at middle frequency bands (related to local damage). Thus, the signal filtered using such selector might still be affected by the low-frequency component. In other words, high spectral amplitudes of low-frequency signal components multiplied

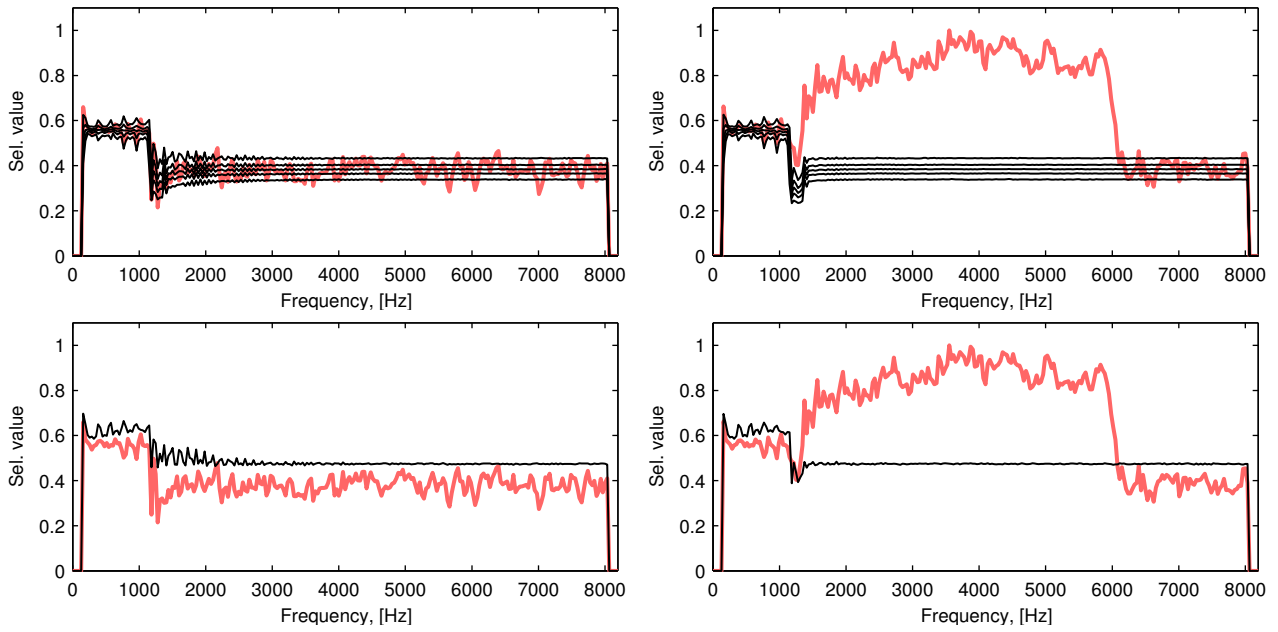


Figure 4.5: Selector values of reference signals. Faulty (right panels) and healthy machine (left panels). Red thick lines represent selector values based on H_{aver} . Top panels present quantile lines of orders: 0.1, 0.3, 0.5, 0.7 and 0.9 (black thin lines) obtained upon selector values of 1000 reference signals. Bottom panels present significance thresholds for the selector values, i.e. quantile of order 0.99. Note that only at a few frequency bins selector values for healthy machine exceeds the threshold and the threshold is significantly exceeded at 2000-7000 Hz for faulty machine.

by low selector values might be still larger than low amplitudes (located at informative, middle frequency bands) multiplied by a high values of the selector. Thus, the whole procedure might provide unsatisfactory results, i.e. energy of non-informative components will dominate in the filtered signal.

Another reason describing benefits of thresholding is derived from analysis of a signal that consists of the high-energy low-frequency component and the noise only. It might happen that selector values at low frequency bands, containing high-energy deterministic content, are different from values at frequency bands containing noise (with relatively low energy). Such case might be caused by specific windowing, e.g. when the STFT window length is not large enough to appropriately estimate energy flow at low frequency bands. Fig. 4.5 illustrates this point. The signals $r_1(t)$ and $r_2(t)$ presented therein are sums of 6 sine waves with frequencies $190n$ Hz, $n = 1, \dots, 6$ and a noise dependent on whether the signal from faulty or healthy machine is

simulated. The signals $\{r_k(t)\}$, $k = 1, 2$ are obtained using the following formula:

$$r_k(t) = \sum_{n=1}^N Aa_n \sin(2\pi f_n t) + \sigma m_k(t), \quad (4.26)$$

where $N = 6$, $A = 10$, $a_n = 0.75^{(n-1)}$, $f_n = 190n$, $\sigma = 0.1$ and $\{m_k(t)\}$, $k = 1, 2$ is the noise. The signal from a healthy machine corresponds to the noise $m_1(t)$, which basically is a zero-mean white Gaussian noise with standard deviation equal to 1. $m_2(t)$ is related to a faulty machine and structure of this signal is more complicated. In order to construct $m_2(t)$ we decompose the signal $m_1(t)$ by filtering into 3 components: a) $\{m_{1a}(t)\}$ - low-pass filtered $\{m_1(t)\}$ with cut-off frequency 2000 Hz, b) $\{m_{1b}(t)\}$ - bandpass filtered $\{m_1(t)\}$ with cut-off frequencies 2000 Hz and 7000 Hz and c) $\{m_{1c}(t)\}$ - high-pass filtered $\{m_1(t)\}$ with cut-off frequency 7000 Hz. We use ideal filters, i.e. filters with characteristics equal to 1 along the passed band and 0 elsewhere. Then, we modulate amplitude of $\{m_{1b}(t)\}$ using an impulsive signal - sum of 128 sine waves with frequencies that are multiples of the fault frequency - 13 Hz. As a result, the amplitude of the signal between impulses becomes similar to the corresponding amplitude of $\{m_1(t)\}$. Signal to noise ratio defined as $\text{SNR}_{\text{dB}} = 10 \log_{10} \left(\frac{P_{\text{signal}}}{P_{\text{noise}}} \right)$, where P_{signal} denotes power of $\sigma m_k(t)$ and P_{noise} - power of $\sum_{n=1}^N Aa_n \sin(2\pi f_n t)$, equals to -42.53 dB in healthy case ($m_1(t)$) and -36.21 dB in faulty case ($m_2(t)$). Frequency sampling is 16384 Hz and length of the signals is 2.5 s. The time-frequency map that provides sub-signals is calculated using 133-sample-long Kaiser windows ($\beta = 5$) and discrete Fourier transform calculated in 512 points. It can be noticed that values of H_{aver} at low frequency bands are different than values of H_{aver} at middle and high frequency bands. Thus, we claim that each single frequency bin should be thresholded individually.

The proposed thresholding procedure is inspired by so called "pre-whitening". Pre-whitening is a method that flattens frequency spectrum of the examined signal [?, ?, ?]. Formula for the pre-whitened version of a signal $x(t)$ is [?]:

$$y(t) = \text{IDFT} \left\{ \frac{\text{DFT}(x(t))}{|\text{DFT}(x(t))|} \right\}, \quad (4.27)$$

where DFT and $IDFT$ indicate the discrete Fourier transform and its inverse. Frequency spectrum of a signal processed using pre-whitening is flat, but the signal might still contain spikes related to local damage. When the damage signature is weak, the pre-whitened signal might be dominated by noise from frequency bands outside the informative frequency band. Thus, there is a need for enhancement of the pre-whitened signal.

We use an inverse of pre-whitening in order to simulate a large number of signals without transients (so called reference signals), but keeping the amplitude spectrum similar to the real data's frequency spectrum. Basically, we multiply absolute value of discrete Fourier transform of the examined signal (e.g. $r_k(t)$ or real data) element-wise by discrete Fourier transform of white noise, i.e. $DFT\{n(t)\}$, where $n(t)$ is a vector of independent identically distributed Gaussian random variables with mean $\mu = 0$ and variance $\sigma^2 = 1$. Length of $n(t)$ is the same as length of the examined signal. Then, we return to time domain using inverse discrete Fourier transform. The formula for a simulated signal without transients is:

$$s(t) = IDFT \{ |DFT(p(t))| DFT(n(t)) \}, \quad (4.28)$$

where $p(t)$ is the examined signal and the multiplication is performed element by element. Next, we calculate values of the selector for each reference signal $s(t)$.

The procedure is repeated with a lot (e.g. 1000) of different $n(t)$'s (so called Monte Carlo method), thus we obtain a significant number of selector values for each frequency bin. Finally, a certain quantile (e.g. 99%) is calculated individually for every f . If the selector value at f is lower than the quantile, it is said to be insignificant and set to 0. Otherwise, only the excess over the quantile is taken for final design of the filter.

Fig. ?? in Sec. ?? presents a spectrogram of a vibration signal from a locally damaged heavy rotating machine (a two-stage gearbox from a mining company) and a spectrogram of an exemplary realization of the simulated signal $s(t)$. One can see that both signals share similar content along frequency axis, but the simulated one has no wide-band excitations related to local damage.

4.3.4 Filtering

In the final step we propose to follow the approach presented in [?], where the optimal Wiener filter based on the SK is described. Recall, that the filter is proportional to the square root of the SK . We propose to follow this approach to the selectors proposed in Sec. 4.3.2 and replace square root of the SK by square root of selector values that remains after filter's amplitude response enhancement (thresholding). We also normalize these square roots by their maxima in order to make visual comparison of them easier.

Firstly, the discrete Fourier transform of the examined signal is calculated and the filter's amplitude response obtained in Sec. 4.3.3 is interpolated at all the frequency bins of the discrete Fourier transform. Next, the discrete Fourier transform is multiplied element-wise by the interpolated frequency characteristic. Finally, the inverse discrete Fourier transform is used in order to return to the time domain. The formula for the filtered signal $z(t)$ is as follows:

$$z(t) = IFT \{FT(x(t))W(f)\}, \quad (4.29)$$

where $W(f)$ is the amplitude response of the filter driven by a given selector (e.g. $SK(f)$, $KSS(f)$, $H_{aver}(f)$, etc.), i.e. square root of thresholded values of the selector, interpolated to make the size of $W(f)$ equal to the size of discrete Fourier transform of $x(t)$.

4.3.5 Discussion

In this section we discuss motivation and properties of the proposed methodology and compare it with existing methods. The novelty of the paper is contained mainly in the extension of SK-based filtering (including the thresholding procedure), thus we discuss other methods of one dimensional clustering that might be found in the literature. One dimensional methods of clustering are significantly different from multidimensional ones. The 1D real-valued data is only a special case of multidimensional data, but the difference is in natural ordering of real numbers. All of the discussed methods benefit from this property. The fundamental problem is to distinguish between significant and insignificant values of a particular selector. Thus, there

is a need for clustering values of the selector into two groups only.

The classical approach for filtering based on the spectral kurtosis (calculated from the STFT) is to subtract 2 from calculated fourth-order statistic and then take only excess over a given significance level α , which is proportional to the given quantile of the normal distribution [?, ?]. While applying other impulsivity criteria (selectors) to the signal, one can derive analogous thresholds for each single selector. On the other hand, one can simply exploit one of the existing 1D thresholding procedures. We recall and analyze only a few of them, because comparing thresholding methods is not the goal of this paper.

In 1979 N. Otsu proposed a method for finding the threshold that minimizes the variance within the group, namely a weighted sum of each group's variances, where weights are just the number of elements in a particular group divided by the number of all thresholded values [?]. In order to calculate this variance-minimizing threshold it is proposed to calculate firstly the variance within the group, taking as the threshold each element of the entire set in the sequence. Then, the final threshold is the argument which minimizes the variance within the group. In our case, where the entire set of selector values is denoted by $\{W(f), f \in \{1, \dots, F\}\}$ it is only needed to calculate, for each $f_i \in \{1, \dots, F\}$, the weighted average of variances of each of two groups - one constituted from elements of $\{W(f) \leq W(f_i), f \in \{1, \dots, F\}\}$ and $\{W(f) > W(f_i), f \in \{1, \dots, F\}\}$. Then, f_i that maximized the weighted sum of variances is the final threshold. Such method is known for setting the threshold close to the component with larger class probability or larger class variance [?], thus it might fail if only a small frequency band is non-informative (with low values of $W(f)$) and values of $W(f)$ at other frequency bands are much higher and scattered. Then, the threshold might be too high, what results in ignoring some of the informative frequency bins. Recently, a new method for such heavy-tailed 1D data classification called "head/tail breaks" has been proposed by B. Jiang [?]. In order to avoid the effect of threshold shifting through the right tail of the data, it is proposed to iteratively constitute breakpoints (thresholds). Each breakpoint divides a set into two subsets - one above and one below the breakpoint. These breakpoints are just arithmetic means of the considered set, thus in the first step the arithmetic mean μ_1 of all values in $\{W(f), f \in \{1, \dots, F\}\}$ is calculated. Then, the mean μ_2 of values above μ_1 is calculated, and so on. In our case,

where $\{W(f), f \in \{1, \dots, F\}\}$ has to be divided into two groups only, this method might provide unsatisfactory results when, for instance, there are just a few values of the selector at IFB much higher than others therein, and low values at non-informative frequency band are present, as usual. Arithmetic mean is known to be sensitive to outliers, thus, once again, some of informative components might be omitted. To sum up, both methods are interesting since they do not assume specific distribution of the data. However, they might omit some informative components, for which corresponding values of the selector are not the largest, but still are significant. This remark led us to invent the thresholding method described in Sec. 4.3.3. This one might be applied not only to the kurtosis calculated from the spectrogram, but also to other selectors, for which taking a given quantile of Gaussian distribution is not a method proved as efficient. The only thing we assume is that the reference signal which imitates the same signal as the investigated one, but without local damage, might be simulated using the inverse pre-whitening. Using a number of such simulated signals it can be examined, whether our investigated machine significantly differs from a healthy one or not. Additional advantage of this method is its insensitivity to windowing, i.e. when a particular STFT windowing method provides unlikely high values of a selector for some frequency bands, the method adapts and makes the threshold higher at these bands. One can also make the procedure closer to the reality, i.e. when an appropriate (large) number of signals representing the same measurement related to a healthy machine, might be acquired. Since this extension might be performed well in a laboratory, its application to an industrial case might be difficult.

4.4 Blind equalization

Consider an input signal $\varepsilon, n = 1, \dots, N$ (raw vibration signal). The classical version of the minimum entropy deconvolution is based on searching for coefficients $f_l, l = 1, \dots, L$ of a filter

which maximizes the following objective function of the filter's output y_n [?]:

$$O_4(f[l]) = \frac{\sum_{n=1}^N y^4[n]}{\left[\sum_{n=1}^N y^2[n] \right]^2}, \quad (4.30)$$

where $y_n = \sum_{l=1}^L f[l]\varepsilon[n-l]$. Optimal coefficients of the filter are calculated by solving

$$\frac{\partial(O_4(f[l]))}{\partial(f[l])} = 0. \quad (4.31)$$

Since $\frac{\partial y[n]}{\partial f[l]} = \varepsilon[n-l]$, Eq. (4.31) can be rewritten as:

$$\frac{\sum_{n=1}^N y^2[n]}{\sum_{n=1}^N y^4[n]} \sum_{n=1}^N y^3[n]\varepsilon[n-l] = \sum_{p=1}^L f[p] \sum_{n=1}^N \varepsilon[n-p]\varepsilon[n-l]. \quad (4.32)$$

Denoting the left side of Eq. (4.32) as b (cross correlation of the input and the output cubed) and the right side of Eq. (4.32) as multiplication of the vector f and the Toeplitz autocorrelation matrix A , Eq. (4.32) can be expressed as $b = fA$ (matrix form of Eq. (4.32)). This system might be solved iteratively. A clear description of the iterative procedure might be found in [?, ?]. In the literature one can find many different criteria that define the moment to stop iterations. For instance, the iterative procedure might be stopped while a minimum change in objective function of the filter's output is reached [?], while correlation coefficient between outputs related to two following iterations is close enough to 1 [?] or while difference between filter coefficients related to two following iterations is small enough [?]. In this paper we analyze behavior of several stopping criteria through a fixed number of iterations.

The combined skewness-kurtosis criterion that we analyze in this paper is based on the Jarque-Bera (JB) statistic. The JB statistic calculated for the output signal y_n , $n = 1, \dots, N$ is defined as [?]:

$$JB(y) = \frac{N}{6} \left(S(y)^2 + \frac{(K(y) - 3)^2}{4} \right), \quad (4.33)$$

where $S(y)$ and $K(y)$ are the skewness and kurtosis of the output, respectively. The JB statistic is sensitive to both skewness and excess kurtosis - any deviation from zero skewness and zero excess kurtosis increases the JB statistic. Such statistical properties are profitable especially when the blind equalization algorithm with JB statistic as the cost function is applied to a vibration signal which is leptokurtic, skew or both. The JB statistic is a special case of the LM (Lagrange multiplier) statistic used in the so-called “score test”, known also as the Lagrange multiplier test. The score test can be used for testing a general class of distributions with given density function. Under the H_0 hypothesis, namely the vector of observations constitutes sample from some specific distribution, the LM statistic has asymptotically χ^2 distribution with r degrees of freedom (r - number of parameters of this distribution). The JB statistic is a particular case of LM statistic for Gaussian distribution. In our case the asymptotic distribution of JB defined as in Eq. (4.33) is χ^2 with 2 degrees of freedom (as the number of parameters in Gaussian distribution). It is worth mentioning that the test based on skewness and kurtosis is locally most powerful when the test statistic has form as in Eq. (4.33). For more details see [?]. The asymptotic distribution of JB statistic (defined as in Eq. (4.33)) is also discussed in [?]. On the basis of the JB statistic we propose the following objective function for blind equalization algorithm:

$$O_{JB}(f[l]) = \left(\frac{\frac{1}{N} \sum_{n=1}^N y^3[n]}{\left[\frac{1}{N} \sum_{n=1}^N y^2[n] \right]^{\frac{3}{2}}} \right)^2 + \frac{1}{4} \left(\frac{\frac{1}{N} \sum_{n=1}^N y^4[n]}{\left[\frac{1}{N} \sum_{n=1}^N y^2[n] \right]^2} - 3 \right)^2. \quad (4.34)$$

Calculating f for which:

$$\frac{\partial(O_{JB}(f[l]))}{\partial(f[l])} = 0 \quad (4.35)$$

one can obtain filter coefficients for which the optimization criterion defined in Eq. (4.34) is maximized.

Thus, the analogous formula to Eq. (4.32) is:

$$\frac{C_1 \sum_{n=1}^N y^2[n] \varepsilon[n-l] + C_2 \sum_{n=1}^N y^3[n] \varepsilon[n-l]}{C_3} = \sum_{p=1}^L f[p] \sum_{n=1}^N \varepsilon[n-p] \varepsilon[n-l], \quad (4.36)$$

where:

$$\begin{aligned} C_1 &= 3 \frac{1}{N} \sum_{n=1}^N y^3 \left(\frac{1}{N} \sum_{n=1}^N y^2 \right)^2 \\ C_2 &= \frac{1}{N} \sum_{n=1}^N y^4 \frac{1}{N} \sum_{n=1}^N y^2 - 3 \left(\frac{1}{N} \sum_{n=1}^N y^2 \right)^3 \\ C_3 &= 3 \left(\frac{1}{N} \sum_{n=1}^N y^3 \right)^2 \frac{1}{N} \sum_{n=1}^N y^2 - 3 \frac{1}{N} \sum_{n=1}^N y^4 \left(\frac{1}{N} \sum_{n=1}^N y^2 \right)^2. \end{aligned} \quad (4.37)$$

Similarly as in Eq. (4.32), the left side of Eq. (4.36) consists of weighted cross correlations and the right side is a multiplication of the vector f and the Toeplitz autocorrelation matrix A . The filter f has to be normalized (by its Euclidean norm) in every iteration to control energy of the filter's output, thus Eq. (4.36) can be simplified. i.e. dividing by C_3 is not necessary. $\frac{1}{N} \sum_{n=1}^N y^k$ is the k -th order moment and $\sum_{n=1}^N y^k[n] \varepsilon[n - l]$ is the cross correlation of the input and the output to the power k . Eq. (4.36) might be solved for f using the standard iterative algorithm described in [?]. As it is mentioned in [?], the recommended way of calculating cross correlations is based on the Wiener-Khinchin theorem, i.e. using the Fast Fourier Transform (FFT) and its inverse (IFFT). Benefits from using FFT and IFFT are clearly perceptible when the order of the filter is large and the input signal is long.

In order to provide comprehensive analysis, we compare the results obtained using kurtosis and JB statistic as criteria with the blind deconvolution driven by one of Gray's variability norms, that incorporates normalized third statistical moment (skewness). The objective function is defined as [?]:

$$O_3(f[l]) = \frac{\sum_{n=1}^N y^3[n]}{\left[\sum_{n=1}^N y^2[n] \right]^{\frac{3}{2}}}, \quad (4.38)$$

where $y_n = \sum_{l=1}^L f[l] \varepsilon[n - l]$. Optimal coefficients of the filter are calculated by solving

$$\frac{\partial (O_3(f[l]))}{\partial (f[l])} = 0. \quad (4.39)$$

Eq. (4.39) can be rewritten as:

$$\frac{\sum_{n=1}^N y^2[n]}{\sum_{n=1}^N |y|^3[n]} \sum_{n=1}^N |y|^3[n] \varepsilon[n-l] = \sum_{p=1}^L f[p] \sum_{n=1}^N \varepsilon[n-p] \varepsilon[n-l]. \quad (4.40)$$

The left side of Eq. (4.40) consists of weighted cross correlation and the right side is a multiplication of the vector f and the Toeplitz autocorrelation matrix A . The iterative algorithm mentioned earlier solves Eq. (4.40) for f .

4.5 Autoregressive model in case of multiple damage

The proposed two-stage procedure is based on signal filtering. Here we use both autoregressive modeling and optimal frequency band selection. Sometimes, the raw vibration signal contains a strong deterministic contamination which is highly amplitude modulated. In such case of time varying signal-to-noise ratio the signal of interest is invisible in both time series and envelope spectrum. Then, signal filtering based on measures of dispersion (e.g. the spectral kurtosis) may indicate a wrong frequency band as informative. We propose to filter out the deterministic signal using autoregressive filtering. The next step is based on linear filtering using frequency characteristics of the filter obtained by measures of impulsiveness. We compare filters driven by the spectral kurtosis [?] and one of informative frequency band selectors presented in [?, ?, ?]. As it was mentioned, we use the autoregressive model to filter out highly amplitude modulated mesh harmonics. The AR model of order p is defined as follows:

$$\sum_{i=0}^p \phi(i) X(t-i) = \epsilon(t), \quad (4.41)$$

where $\phi(0) = 0$ and $\epsilon(t)$ stands for noise.

It is known, that the AR time series model is able to model noisy sinusoidal pattern if its characteristic polynomial has complex roots. In the case of a large number of harmonics a high-order AR model is expected with at least two complex roots corresponding to one mesh

harmonic. As the optimal order indicator we use the highest Kolmogorov-Smirnov criterion, i.e. $AR(p)$ is said to be optimal if the Kolmogorov-Smirnov (KS) test statistic of residuals is the highest [?]. According to the fact that the residual signal in case of local damage should be impulsive, it is expected that the distance between empirical distribution and Gaussian one is high – the higher KS statistic, the more impulsive signal. Recall the KS statistic for signal $X(t)$ is defined as follows [?]:

$$KS = \sup x \left| \hat{F}(x) - F(x) \right|, \quad (4.42)$$

where $\hat{F}(x)$ is the empirical cumulative distribution function for given signal while $F(x)$ is the cumulative distribution function of Gaussian distribution with parameters estimated from the signal.

Moreover, the results of AR filtering are also checked by comparing time-frequency maps of the residual signal with the raw signal. Parameters of the AR model are obtained by using Yule-Walker [?]. Fig. 4.6 Once mesh harmonics are suppressed during the previous step of the

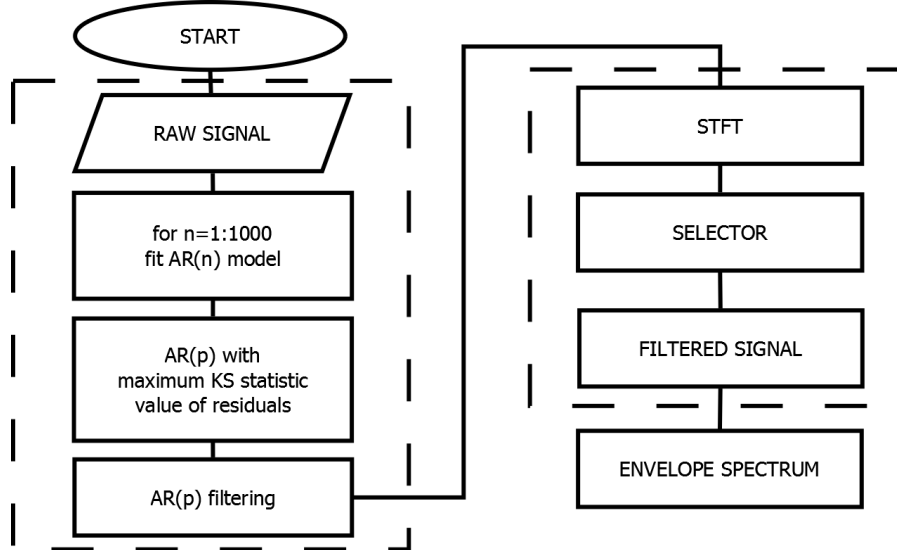


Figure 4.6: Block diagram of the two-stage procedure

procedure, the residual signal might be still noisy, e.g. when the SOI is relatively narrowband. We propose to select the informative frequency band using the average horizontal distance on quantile-quantile plot (QQplot) [?, ?, ?]. Namely, we quantify the average distance between markers and reference line on the QQplot. The QQplot we use here is a graphical goodness-of-fit

tool which compares quantiles of empirical distribution of the sample with the Gaussian distribution. The reference line connects first and third quartiles of both distributions. We compare it to the well-known spectral kurtosis. Both of them are based on analysis of narrowband slices of a time-frequency map. In this paper we design the filter using not only the characteristic given by a selector but we also enhance the characteristic by using individual thresholds of selector's value for a given frequency bin. Namely, we put 0 in the frequency characteristic of the filter if the value of the selector is lower than the threshold for a given frequency bin. The thresholds are obtained using the Monte Carlo method and inverse pre-whitening [?].

After designing the filter, we filter out the residual signal by computing Fourier transform of the signal, multiplying it by frequency response of the selector-based filter and, finally, using the inverse Fourier transform to return to the time domain. This method is an extension of the method presented in [?], where the filter is constructed using the spectral kurtosis.

A block diagram of our two-stage procedure is presented in Fig. 4.6.

4.6 Periodic autoregressive model for cyclic load of bucket wheel excavator

4.6.1 Influence of non-Gaussian noise to PAR estimation

The signals analyzed in this section represent vibration acceleration of a planetary gearbox used in a bucket wheel excavator [?]. - **NO TO TRZEBIA JAKOS INACZEJ UJAC** Such vibration signal might be simulated as a sum of several sinusoidal components with frequencies that meet the gear mesh frequency and its harmonics and a white noise. Due to the cyclic regime in which the excavator operates, the sinusoidal components are frequency and amplitude modulated with the period corresponding to the period of the bucket wheel operation [?]. Due to industrial environment, we decided to analyze white noises that follow the double Pareto distribution with parameters $\alpha_1 = 1.5$ (denoted later as Pareto1.5) and $\alpha_2 = 3.6$ (denoted as Pareto3.6) and compare result with the Gaussian case. Let us point out for α_2 the examined

Pareto distribution have finite second moment while for α_1 the second moment does not exists. This fact has important influence for the results.

Influence of non-Gaussian noise to PAR estimation is performed using the following algorithm. At first, a lot of signals related to each type of noise are simulated to preserve reliability of results. Energy of each noise sequence is normalized, i.e. time series are divided by its standard deviation to preserve fair comparison. Secondly, parameters of the PAR models are estimated for each signal. The procedure of estimation is based on the Yule-Walker method and is described in [?]. Order of the PAR model is chosen as 15 for every signal. This choice is motivated by the number of sinusoidal components and the fact, that the residual time series are satisfactory [?]. After that, we analyze amplitude response of the models at each $1 \leq t \leq T$, namely a surface of amplitude response. It is a natural extension of the amplitude response of an autoregressive model. The autoregressive model (AR) of order p and parameters $a = (a_i)_{i=1,\dots,p}$ is defined as follows:

$$X(t) - \sum_{i=1}^p a_i X(t-i) = Z(t), \quad (4.43)$$

where the sequence $Z(t)$ is a white noise time series.

Amplitude response of an autoregressive model with coefficients $a = (a_i)_{i=1,\dots,p}$ is defined as follows:

$$S(f) = \left| \frac{1}{FT(a)} \right|, \quad (4.44)$$

where $FT(a)$ is the discrete Fourier transform (DFT) of $a = (a_i)_{i=1,\dots,p}$. The amplitude response of an autoregressive model is a tool used for interpretation of its coefficients. It illustrates how the model applied to an input signal increases amplitudes of input's spectral components. For an autoregressive model with time-varying coefficients a natural extension of the amplitude response is a surface of amplitude response. Therefore it depends not only on the frequency f , but on the time instance t , as well. Thus, the surface of amplitude response is defined as:

$$S(t, f) = \left| \frac{1}{FT(a(t))} \right|, \quad (4.45)$$

Interpretation of the surface of amplitude response is similar to the classical, one dimensional amplitude response, i.e. $S(t, f)$ describes how the model applied to an input signal increases amplitudes of input's spectral components at the time instance t .

In order to examine influence of the considered distribution to PAR model estimation we calculate the mean square error (MSE) between estimated amplitude response and so called "perfect surface", described in Sec. 4.2. To preserve fair results, every surface (estimated and "perfect") is normalized by its average value, i.e. arithmetic mean of the whole surface is subtracted from the surface. Higher MSE means that the procedure gives worse results in the considered case.

4.6.2 Influence to PAR estimation for different number of period repetitions

In this section we analyze influence of the number of period repetitions on PAR parameters estimation procedure. Such analysis is motivated by the question how long the data acquisition should be to ensure appropriate results using the PAR model. In order to examine influence of different number of period replications we analyze MSE between PAR parameters $a_i(t)_i = 1, \dots, p, t = 1, \dots, T$ estimated from the noiseless signals and corresponding noisy signals of different numbers of period repetitions. The minimum number of period repetitions is set to 3 and the maximum - to 18. We compare boxplots and medians to clearly see how the estimation procedure is influenced by the number of period repetitions.

4.7 Conclusions

Podsumowanie algorytmow, co ktory wykorzystuje, ktory jest szybki, ktory odporny itd

Chapter 5

Description of the analyzed data

5.1 Simulated data

5.1.1 Dane do motywacji indywidualnych poziomow odciecia filtra dla kazdego delta f - bez AM i FM

5.1.2 Dane z FM do PAR

5.1.3 Dane z symulowanym impulsem

5.2 Real data

5.2.1 Lozysko i lozysko_b

5.2.2 Y2 i Y4

Chapter 6

Results

Tak jak w methodology, trzeba ustalic czy nazywac sekcje metodami (local maxima, odporne selektory, two-stage method, PAR) czy problemami (t-f map enhancement, selection of IFB, significance levels of selectors for filtering purposes, more than 1 damage, frequency modulation due to time-varying load)

W ponizszych sekcjach beda porownania z dotychczasowymi metodami

6.1 Time-frequency map enhancement - skompilowac z Ferrara

6.1.1 Simulated data analysis

To accurately illustrate the whole methodology we analyze simulated signals that represent acceleration of vibrations of both healthy and damaged bearing operating under industrial conditions where vibrations of a gearbox located nearby strongly contaminates the informative signal, i.e. the signal related to local damage. The raw signal is composed of deterministic components, i.e. high-energy sine waves related to vibrations of the gearbox and noise which in the case of damage is amplitude modulated with a frequency of 13 [Hz] (fault frequency).

Length of both signals is 2.5 [s], sampling frequency is 20000 [Hz]. The noise (amplitude

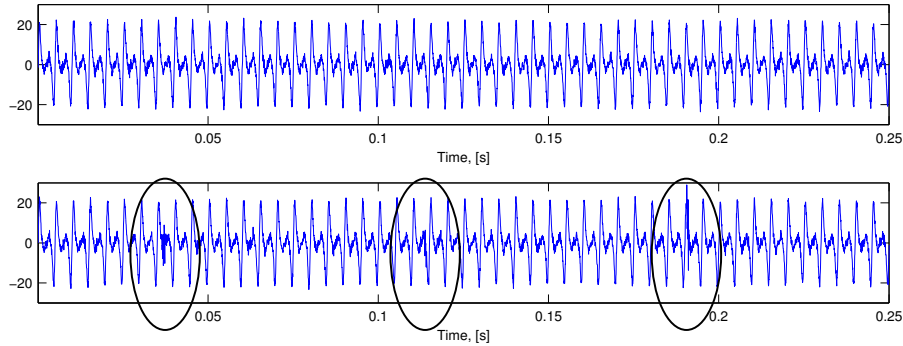


Figure 6.1: Time series of raw simulated data (first 0.25 [s]), healthy (top panel) and faulty (bottom panel) bearing. Note three marked time points with barely visible disturbances.

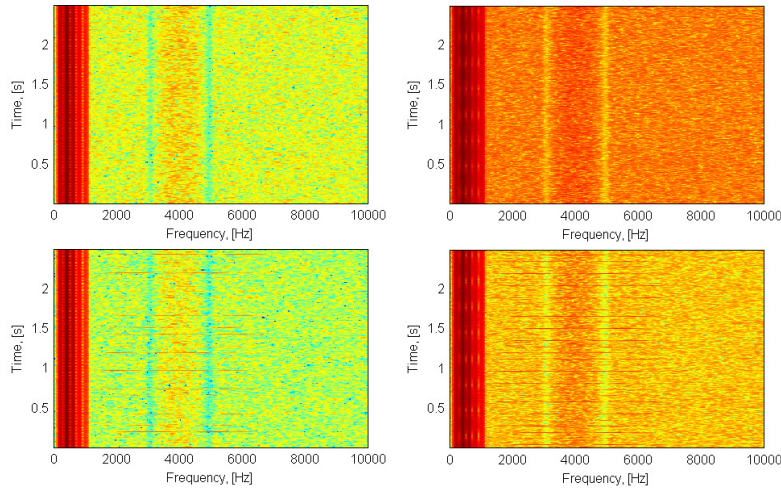


Figure 6.2: Time-frequency representations (spectrograms) of the signals, healthy (top panels) and faulty (bottom panels) bearing, 95% overlap case (right panels) and non-overlapping case (left panels).

modulated or not) is filtered at frequency range 3000-5000 Hz to imitate resonance effects. The signals are presented in Fig. 6.1 (time series) and Fig. 6.2 (spectrograms). For time-frequency representation a Kaiser window of length 230 was used and FFT was calculated at 512 points. In the overlapping case 95% of segments overlaps, i.e. 219 samples. Thus, non-overlapping case consists of 87 spectra per second and overlapping case – 1659 spectra per second. It can be seen that energy of deterministic components is much higher than energy of the signal related to damage, thus the latter is barely-visible in time series plot.

Fig. 6.3 presents binary spectrograms in all cases, including data representing healthy and

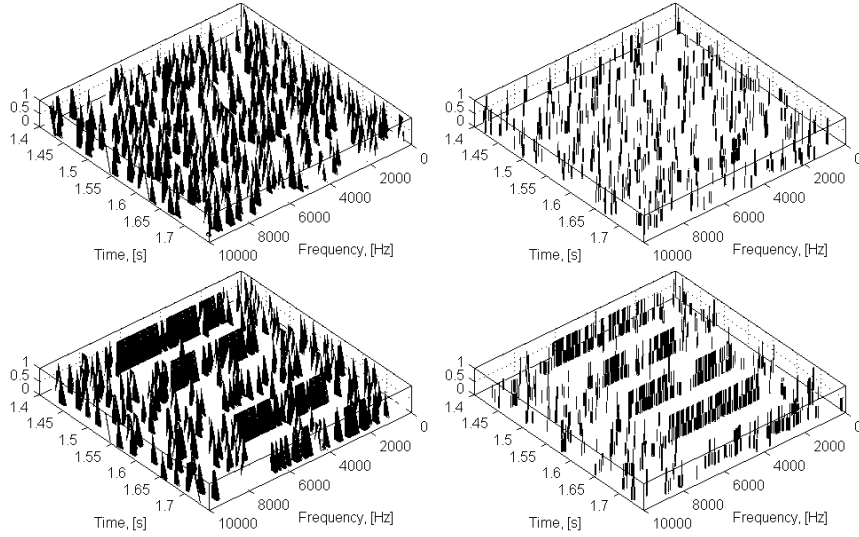


Figure 6.3: Binary spectrograms of the signals, healthy (top panels) and faulty (bottom panels) bearing, 95% overlap case (right panels) and non-overlapping case (left panels).

faulty bearing and both cases of overlapping. Here a theoretical ranges of local maxima were used, $r_0 = 5$ and $r_{95\%} = 113$. The case of healthy bearing plots looks totally random despite different content of each band that can be seen in Fig. 6.2. In the damaged bearing case we obtain some wide-band lines related to local damage, but there is still a large amount of local maxima that do not follow any of them. Applying formula (4.5) enhanced spectrograms are obtained (Fig. 6.5).

Basically, we multiply the vector of weights (Fig. 6.4) by the binary spectrogram (Fig. 6.3)

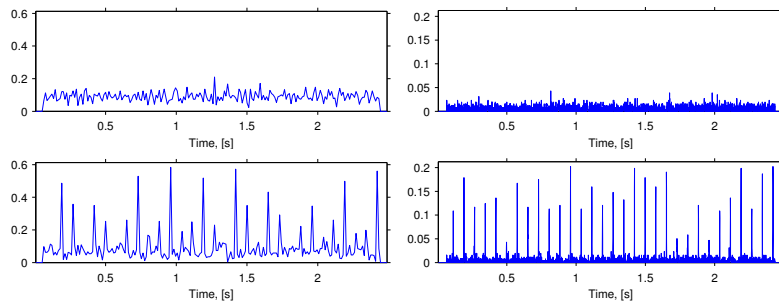


Figure 6.4: Vectors of weights of the signals, healthy (top panels) and faulty (bottom panels) bearing, 95% overlap case (right panels) and non-overlapping case (left panels).

.They share positive behavior of binary ones, because top panels in Fig. 6.5 still look randomly and bottom ones have clearly visible lines related to local damage. The biggest advantage of the local maxima method can be seen at non-informative frequency bands. Local maxima that

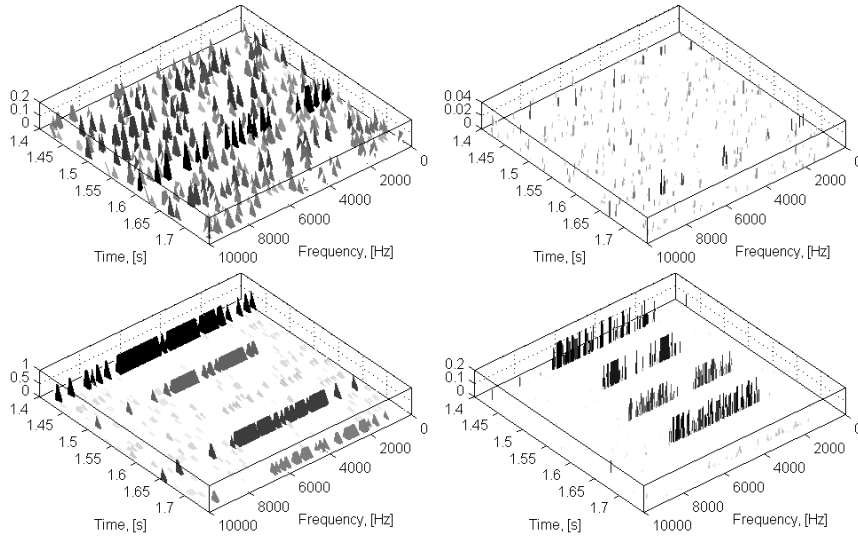


Figure 6.5: Enhanced spectrograms of the signals, healthy (top panels) and faulty (bottom panels) bearing, 95% overlap case (right panels) and non-overlapping case (left panels).

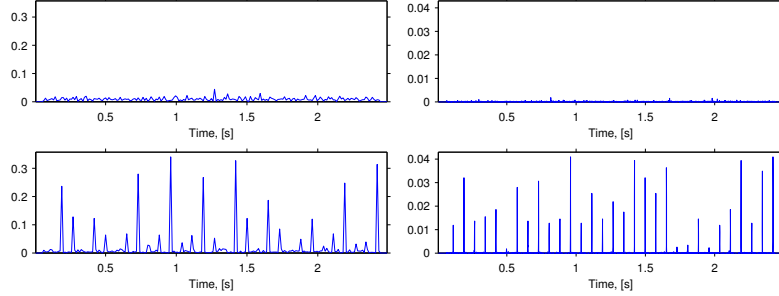


Figure 6.6: Enhanced vectors of weights., healthy (top panels) and faulty (bottom panels) bearing, 95% overlap case (right panels) and non-overlapping case (left panels).

do not follow any of wide-band excitations are reduced. In the overlapping case these local maxima almost completely disappeared. In this way, the informative frequency band is clearly visible.

After we have enhanced spectrograms in all of 4 cases analyzed here, one can estimate the frequency of cyclic disturbances in time domain related to contact of rolling bearing elements with the local damage. Recall that the fault frequency is 13 [Hz]. We have introduced enhanced vector of weights as an revised indicator of local maxima occurrence in time domain. Fig. 6.6 presents how the enhanced vectors of weights exhibit cyclic disturbances. Thus, we can use methods discussed in Sec. 4.1.

Envelope spectra of vectors presented in Fig. 6.6 are shown in Fig. 6.7. In the non-overlapping

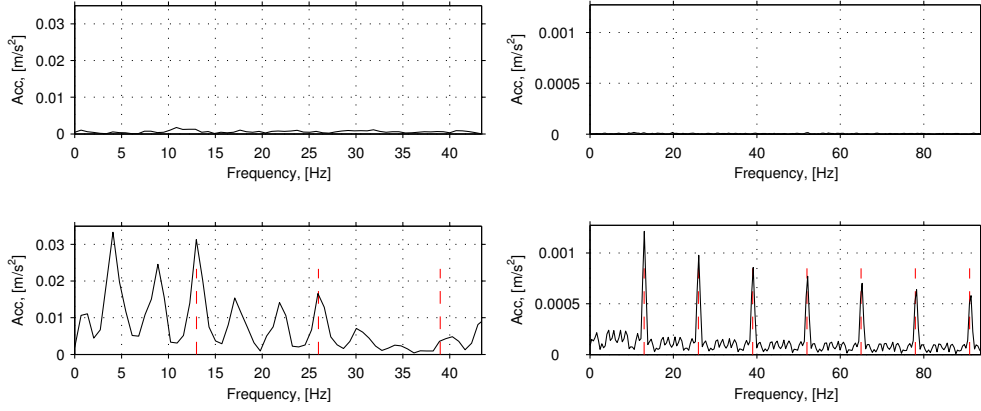


Figure 6.7: Envelope spectra of vectors of weights, healthy (top panels) and faulty (bottom panels) bearing, 95% overlap case (right panels) and non-overlapping case (left panels). Red dashed lines denote fault frequency and its harmonics.

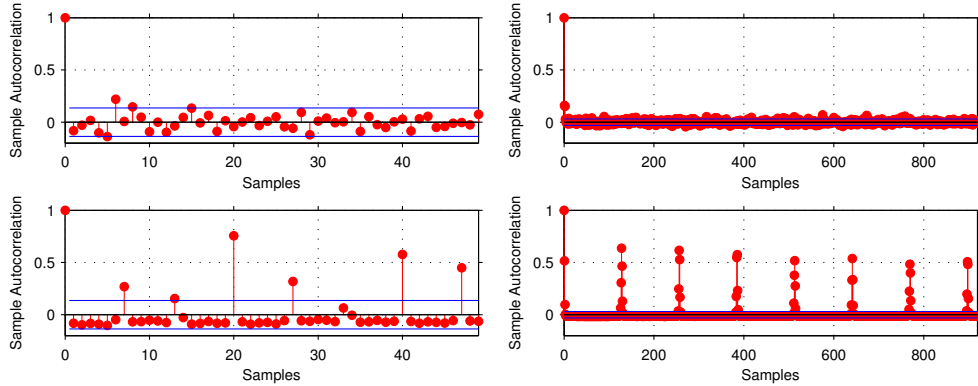


Figure 6.8: Sample autocorrelation functions, healthy (top panels) and faulty (bottom panels) bearing, 95% overlap case (right panels) and non-overlapping case (left panels).

case resolution of data is too small to clearly recognize the fault frequency. There are few similar peaks in the bottom left panel, but only two of them are related to the expected frequencies. Thus, estimation cannot provide satisfactory results. High overlap of segments in STFT results in much better resolution of data and envelope spectra analysis of the enhanced vector of weights gives clear information about fault frequency. Set of decreasing harmonics indicate impulsive character of noise modulation.

Since envelope spectra give unsatisfactory results in the non-overlapping case we analyze the sample autocorrelation function. In the healthy bearing case almost all of autocorrelations are inside the 95% confidence interval (Fig. 6.8, top left panel). In the opposite case (Fig. 6.8, bottom left panel) there are few lags at which the sample ACF significantly exceeds the confidence

interval. The expected fault frequency is 13 [Hz], so time interval between pulses is a multiple of about 0.0769 [s] ($\frac{1}{f_f}$). Recall that lag of 1 sample stands for 0.0115 [s], so lag of 7 samples stands for 0.0805 [s] and 12.42 [Hz]. One can observe that high values of autocorrelation at lags of 13, 20, 27, 40 and 47 samples are related to multiples of the expected time interval between pulses.

The sample ACF leads to useful results even in the case of high-overlapping windows in STFT. Here, 1 lag equals to 0.0006 [s], so the highest ACF should be manifested at lags of 128, 256, 385, 513, 641, 769 and 897 samples. Just a few high ACF values at first lags (Fig. 6.8, right panels) indicates a short in time dependency and might be associated with high overlap.

6.1.2 Real data processing results

Case A. In this section a real dataset described in the previous section is analyzed. Fig. ??

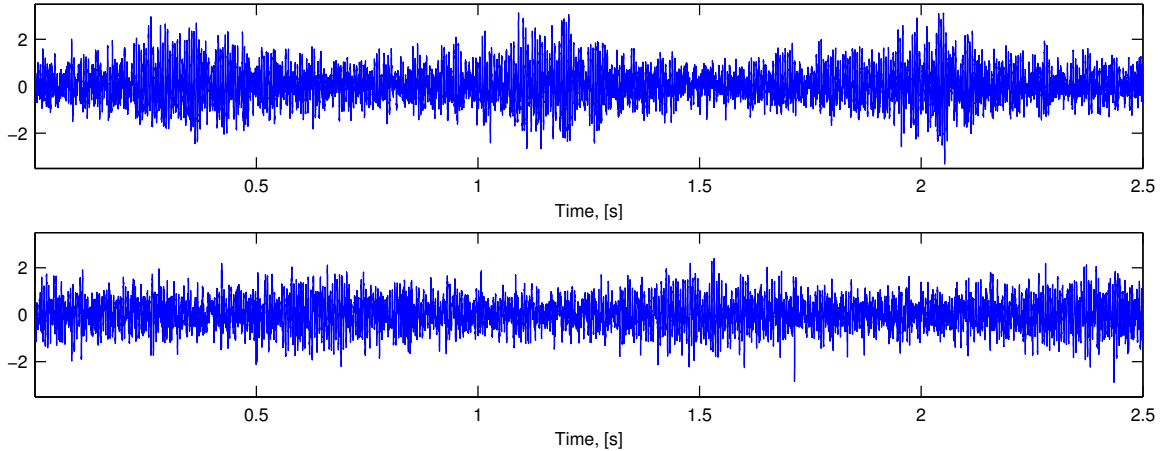


Figure 6.9: Time series of raw real data, healthy (top panel) and faulty (bottom panel) bearing.
KROPKI W NAZWACH PLIKOW DO USUNIECIA!!!

and Fig. ?? presents time series and spectrograms, respectively, of both (healthy and faulty) signals. Spectrograms were calculated with and without overlap. The Kaiser window of length 200 was used. In this case 95% overlap case stands for 190 samples. Fast Fourier transform is calculated in 512 points. These parameters result in 96 and 1912 spectra in non- and 95% overlapping case, respectively.

Both signals contain a high-energy contamination, but its frequency band is relatively narrow.

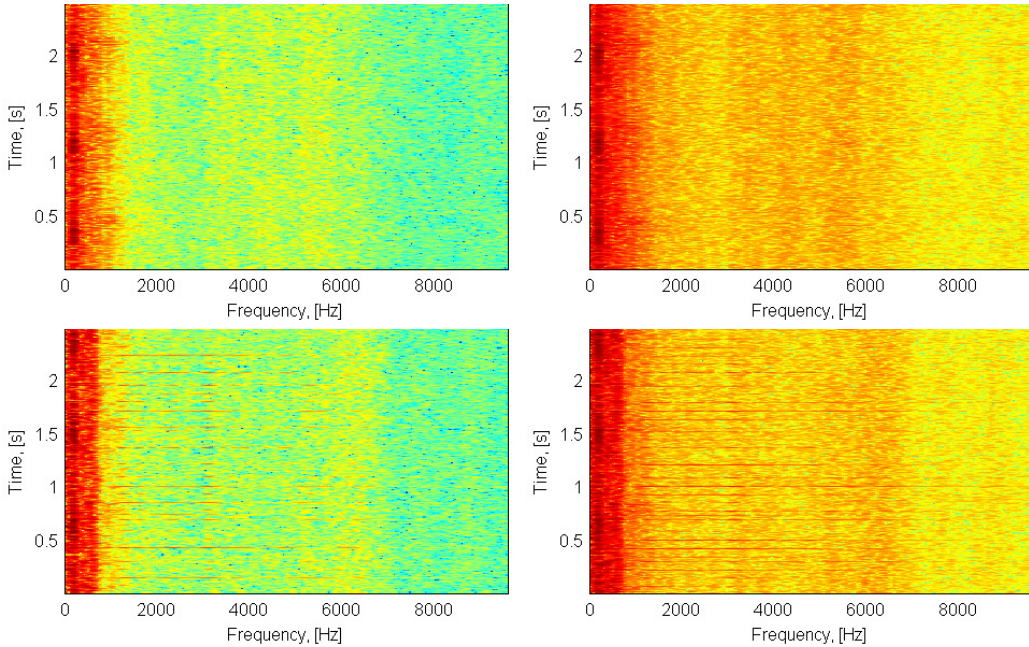


Figure 6.10: Time-frequency representations (spectrograms) of the signals, healthy (top panels) and faulty (bottom panels) bearing, 95% overlap case (right panels) and non-overlapping case (left panels).

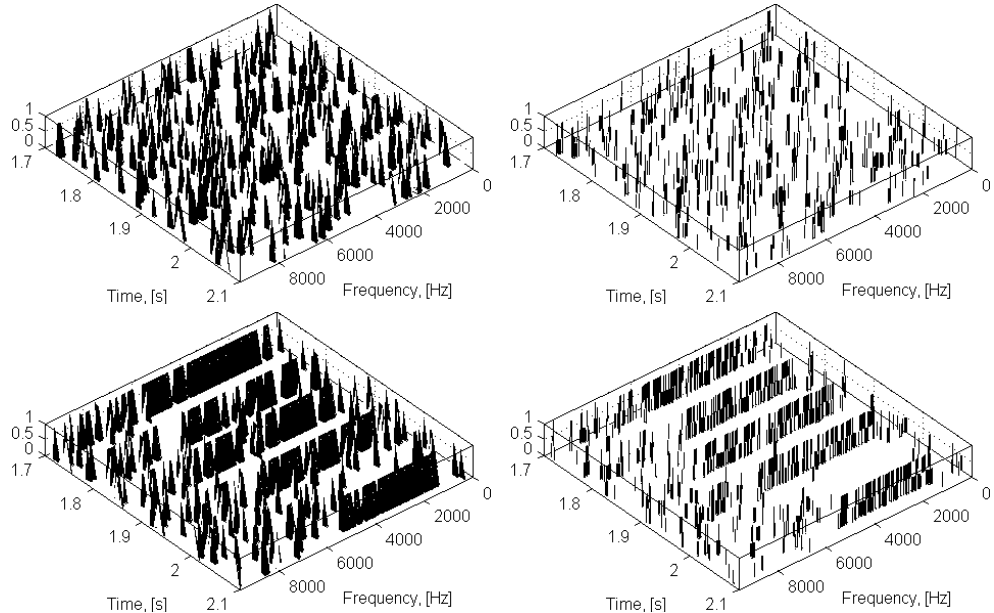


Figure 6.11: Binary spectrograms of the signals, healthy (top panels) and faulty (bottom panels) bearing, 95% overlap case (right panels) and non-overlapping case (left panels).

The informative frequency band, i.e. band, where wide-band excitations occurs, approximately starts at 1000 [Hz] and ends at 6000 [Hz], but there are few pulses whose bandwidth is wider. The ranges of local maxima we have chosen here are equal to the theoretical ones, $r_0 = 6$ and

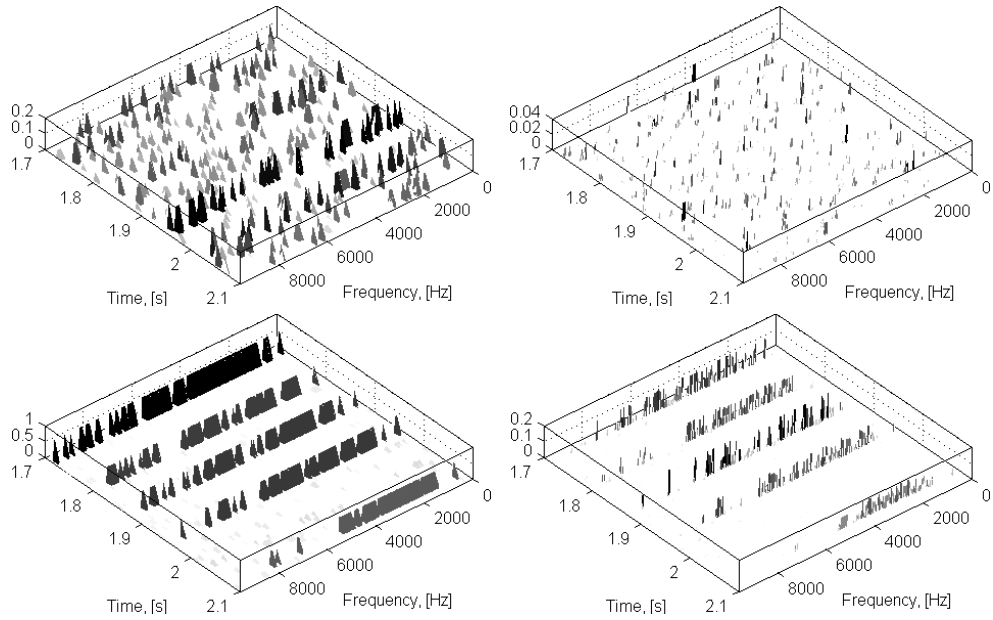


Figure 6.12: Enhanced spectrograms of the signals, healthy (top panels) and faulty (bottom panels) bearing, 95% overlap case (right panels) and non-overlapping case (left panels).

$r_{95\%} = 131$. Due to local character of damage the time of impulse relaxation is quite short and shortening the ranges is not necessary. Binary spectrograms (Fig. ??) for healthy bearing real data look randomly and (as in Sec. 6.1.1) none of frequency bands can be singled out. In the faulty bearing case almost continuous wide lines can be seen. They are a little bit longer than those presented in Fig. ??.

Enhanced spectrograms clearly present length of the informative frequency band with non-informative components removed (Fig. ??). While enhanced versions of time-frequency maps in healthy bearing case are still random, in the faulty case one can see almost only cyclically occurring wide lines.

Fig. ?? shows enhanced vectors of weights – result of application of formula (4.5). Their envelopes spectra are presented in Fig. ???. As it can be seen, higher resolution obtained by using 95% overlap enabled to estimate the fault frequency even using envelope spectrum. In this case, the estimated fault frequency is 12.69 [Hz] and is related to the frequency characteristic for outer race local damage.

As it was mentioned, one of the method that can be used to estimate the fault frequency is the sample ACF. Due to industrial origin of the data only few values of sample ACF exceeds the 95% confidence interval in the faulty bearing case (Fig. ??). Time interval between observations

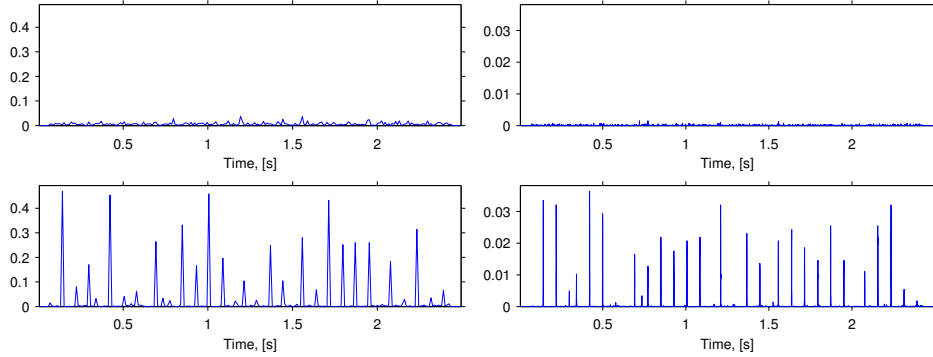


Figure 6.13: Enhanced vectors of weights, healthy (top panels) and faulty (bottom panels) bearing, 95% overlap case (right panels) and non-overlapping case (left panels).

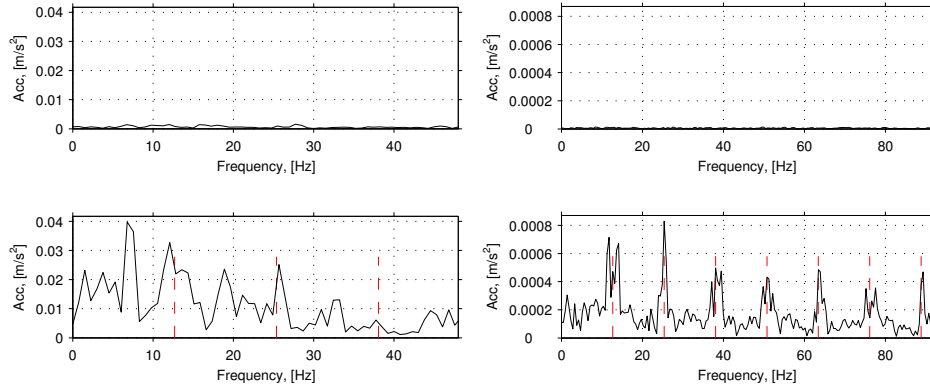


Figure 6.14: Envelope spectra of vectors of weights. Healthy (top panels) and faulty (bottom panels) bearing, 95% overlap case (right panels) and non-overlapping case (left panels). Red dashed lines denote fault frequency and its harmonics.

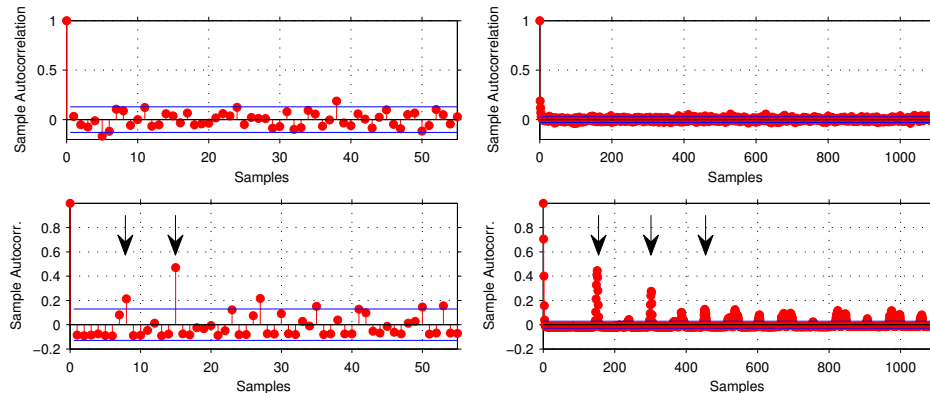


Figure 6.15: Sample autocorrelation functions, Healthy (top panels) and faulty (bottom panels) bearing, 95% overlap case (right panels) and non-overlapping case (left panels).

is 0.0104 [s] and 0.00052 [s] in non-overlapping and 95% overlapping case, respectively. Thus, in the first case fault frequency of 12.69 [Hz] stands for about 7.565 "samples", so high value

of the ACF at lag 7, 8 and 15 clearly confirms the fault frequency close to 12.8 [Hz]. In the second case the ACF should be significantly higher at lags that are multiples of 151 samples.

Case B. To complete analysis we present how the local maxima method deals with real dataset described in the previous section in Case B. Fig. ?? and Fig. ?? presents time series and spectrograms, respectively.

Here a Kaiser window of length 1000 samples is used with 95% overlap and without it ob-

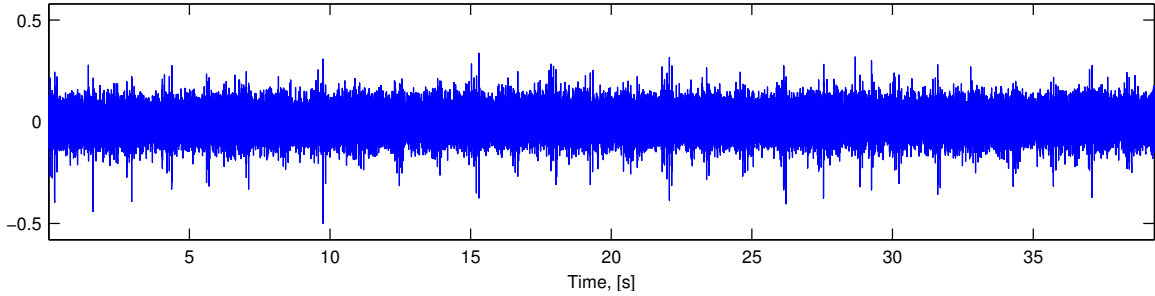


Figure 6.16: Time series of raw real data.

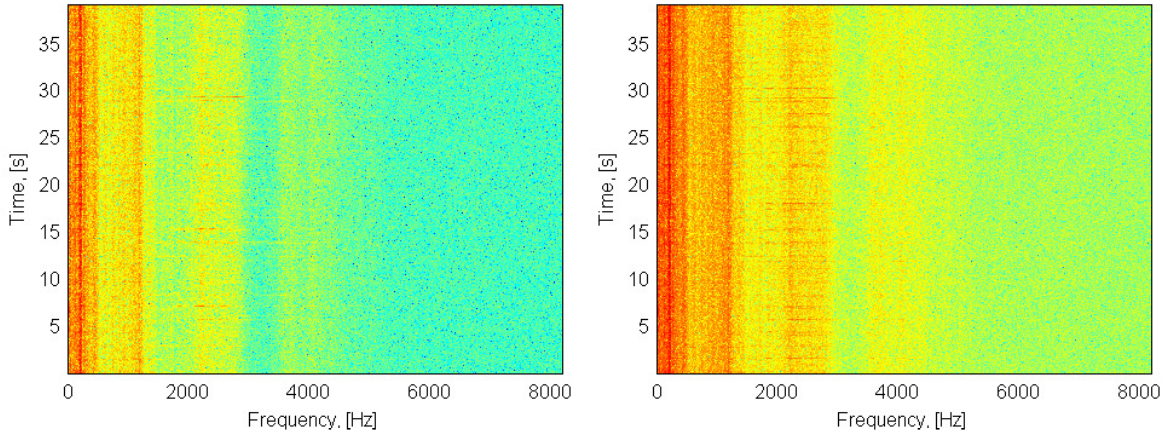


Figure 6.17: Time-frequency representations (spectrograms) of the signals, 95% overlap case (right panel) and non-overlapping case (left panel).

taining 16 and 327 spectra per second. Number of FFT points used for spectrograms is 1024. Few disturbances with low frequency are visible, but the informative frequency band is much shorter than in the case analyzed in Case A.

Binary spectrograms (Fig. ??) in both cases are very noisy and lines related to wide-band excitations are barely visible. After applying (4.4) the enhanced spectrograms look much clearer (Fig. ??). In the case of 95% overlap non-significant local maxima are almost completely re-

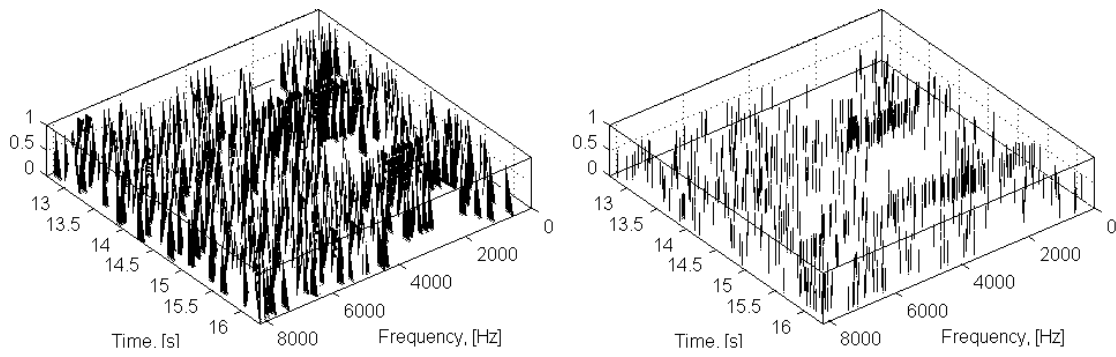


Figure 6.18: Binary spectrograms of the signals, 95% overlap case (right panel) and non-overlapping case (left panel).

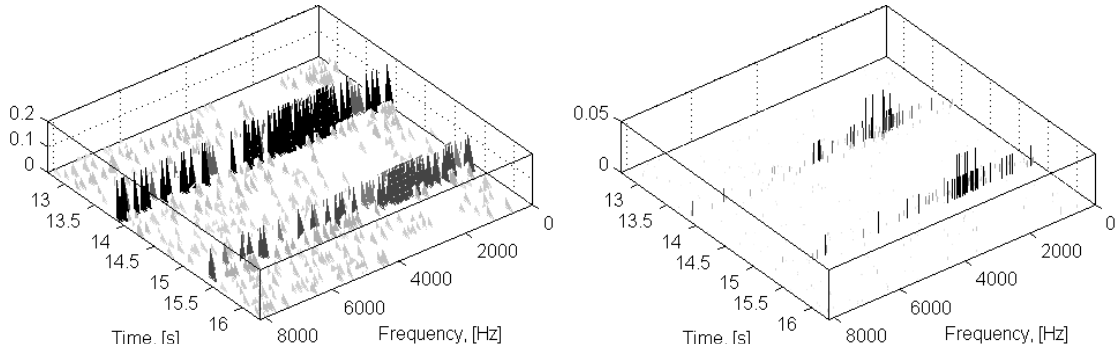


Figure 6.19: Enhanced spectrograms of the signals, 95% overlap case (right panel) and non-overlapping case (left panel).

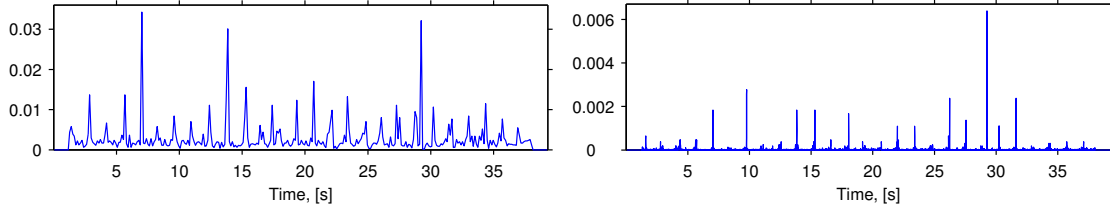


Figure 6.20: Enhanced vectors of weights, 95% overlap case (right panel) and non-overlapping case (left panel).

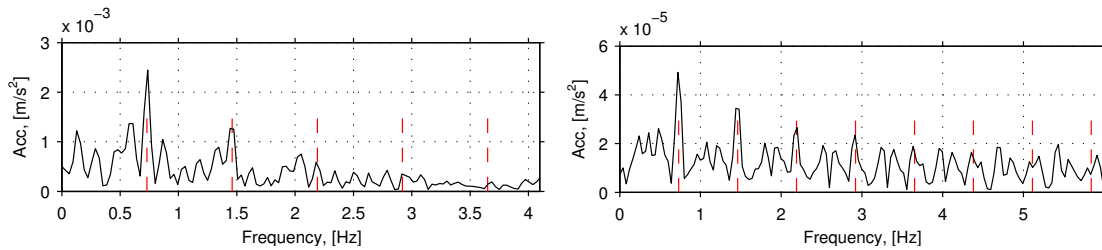


Figure 6.21: Envelope spectra of vectors of weights, 95% overlap case (right panel) and non-overlapping case (left panel). Red dashed lines denote fault frequency and its harmonics.

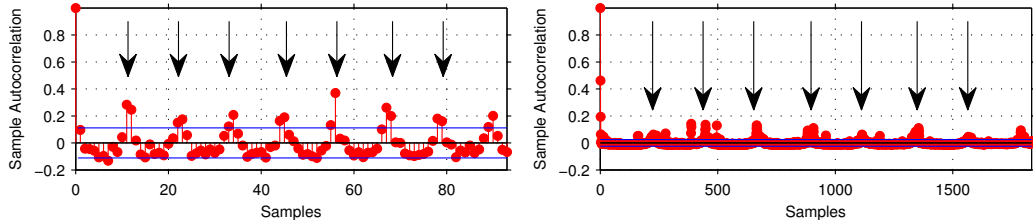


Figure 6.22: Sample autocorrelation functions, 95% overlap case (right panel) and non-overlapping case (left panel).

moved at the expense of visibility of desired results. Recall that in this dataset the expected fault frequency is very low (0.6 [Hz] - cage damage) comparing to the fault frequency in data analyzed in previous sections (13 [Hz]) because of different types of damage. It is worth mentioning that great resolution in time is presented even in non-overlapping case, so high overlapping is not necessary here. Nevertheless, it causes problems only in presentation of final enhanced spectrogram – wide-band lines are still visible, but there are thin, so they seem to be weaker than in non-overlapping case.

Fig. ??, ?? and ?? present enhanced vectors of weights, envelope spectra and sample ACF of them, respectively. Recall that the expected fault frequency is 0.6 [Hz]. From Fig. ?? it can be found that the fault frequency is 0.73 Hz. The difference between the expected and estimated frequency might be caused by different that assumed operating conditions. This frequency and its harmonics are much better visible when the STFT segments highly overlap each other. When the segments do not overlap there are some significant peaks in envelope spectrum, but their values are lower than first two harmonics of fault frequency.

Due to different kind of damage than in previous case shape of the sample autocorrelation functions is specific, but it is still a good estimator of fault frequency. Since one sample of enhanced vector of weights equals to 0.061 [s] while STFT do not overlap and 0.00305 [s] when they do (95% overlap) one can expect higher value of autocorrelation at lag that are multiples of 11 and 224 samples, respectively.

6.2 Selection of informative frequency band

6.2.1 Simulated data analysis

In this section we illustrate how the proposed selectors deal with simulated data set representing vibrations of hypothetical rotating machines, one of which is locally damaged and the second is in healthy condition. The signal $\{X(t)\}$ is obtained using the following formula:

$$X(t) = \sum_{i=1}^n Aa_i \sin(2\pi f_i t) + \sigma N(t), \quad (6.1)$$

where $n = 6$, $A = 10$, $a_i = 0.75^{(i-1)}$, $f_i = 190i$, $\sigma = 0.1$ and $\{N(t)\}$ is white standard Gaussian

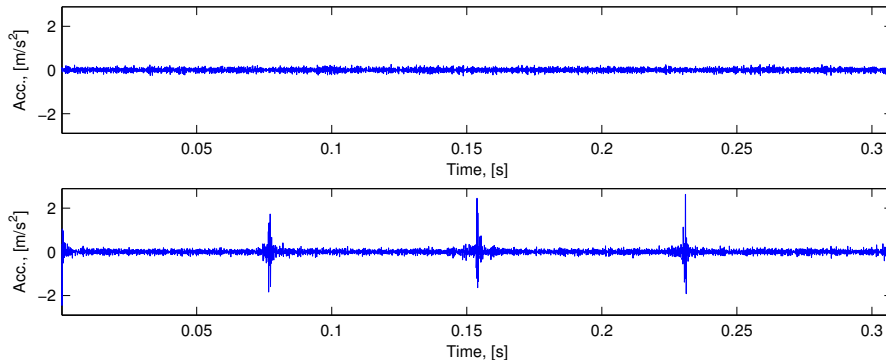


Figure 6.23: Signal of noise - $\{\sigma N(t)\}$ from healthy (top panel) and faulty (bottom panel) rotating machine. The whole signals last 2.5 s. Note some disturbances at 0.077, 0.15 and 0.23 s in bottom panel.

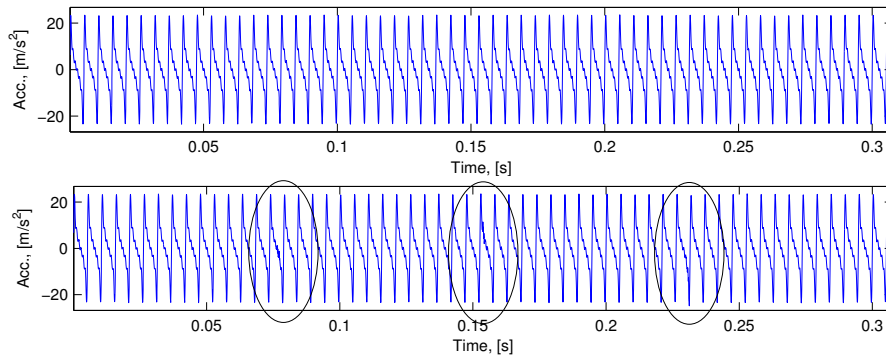


Figure 6.24: Raw vibration signal from healthy (top panel) and faulty (bottom panel) rotating machine. The whole signals last 2.5 s. Note some barely-visible disturbances at 0.077, 0.15 and 0.23 s marked by ellipses.

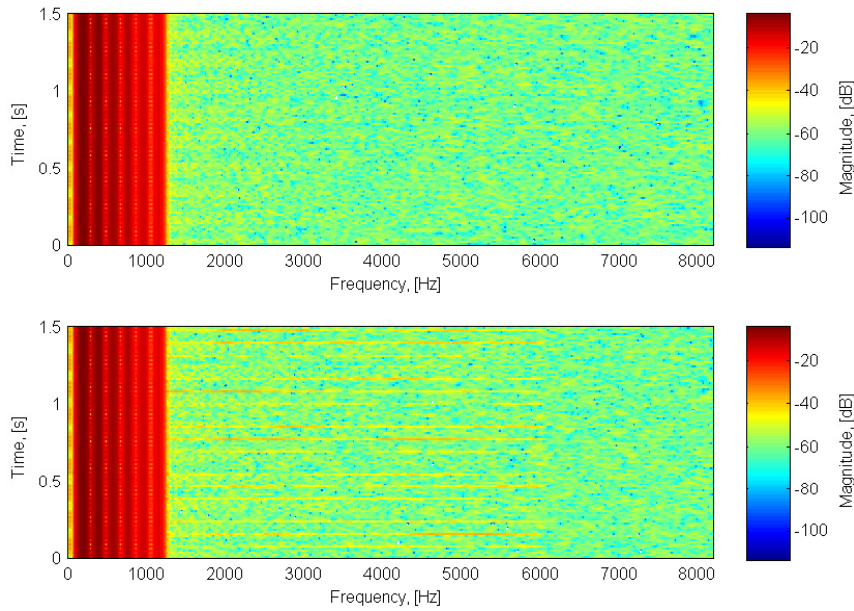


Figure 6.25: Spectrograms of raw vibration data from healthy (top panel) and faulty (bottom panel) rotating machine. The whole signals last 2.5 s. Note energy difference between low-frequency deterministic components and noise.

noise in case of healthy machine. In case of local damage $\{N(t)\}$ is divided by filtering into 3 groups: a) $\{N_1(t)\}$ - lowpass filtered $\{N(t)\}$ with cut-off frequency 1000 Hz, b) $\{N_2(t)\}$ - band-pass filtered $\{N(t)\}$ with cut-off frequencies 1000 Hz and 6000 Hz and c) $\{N_3(t)\}$ - highpass filtered $\{N(t)\}$ with cut-off frequency 6000 Hz. We use ideal filters, i.e. filters with characteristics equal to 1 along the passed band and 0 elsewhere. To simulate the pulse train we modulate amplitude of $\{N_2(t)\}$ using an impulsive signal - sum of a lot of sine waves with frequencies that are multiples of the fault frequency. Amplitude of the result is adjusted to make level of noise between pulses similar to the level of $\{N(t)\}$ in healthy case. Signal to noise ratio defined as $\text{SNR}_{\text{dB}} = 10 \log_{10} \left(\frac{P_{\text{signal}}}{P_{\text{noise}}} \right)$, where P_{signal} denotes power of $\sigma N(t)$ and P_{noise} - power of $Aa_i \sin(2\pi f_i t)$, equals to -42.5 in healthy case and -36.2 in faulty case. Frequency sampling is $f_s = 16384$ Hz and length of the signals is 2.5 s. The signal of interest occurs as an impulsive amplitude modulation of the noise with frequency 13 Hz. The resulting frequency band of the SOI is limited to 1000 – 6000 Hz. Frequencies of the 6 sine waves are successive multiplies of $f_h = 190$ Hz, so the band of SOI overlaps them at 1000 – 1140 Hz. Signal $\sigma \{N(t)\}$ (Gaussian noise in healthy case and amplitude modulated Gaussian noise in faulty case), raw signals and corresponding spectrograms are presented in Fig. ??, Fig. ?? and Fig. ??, respectively. Fig. ??

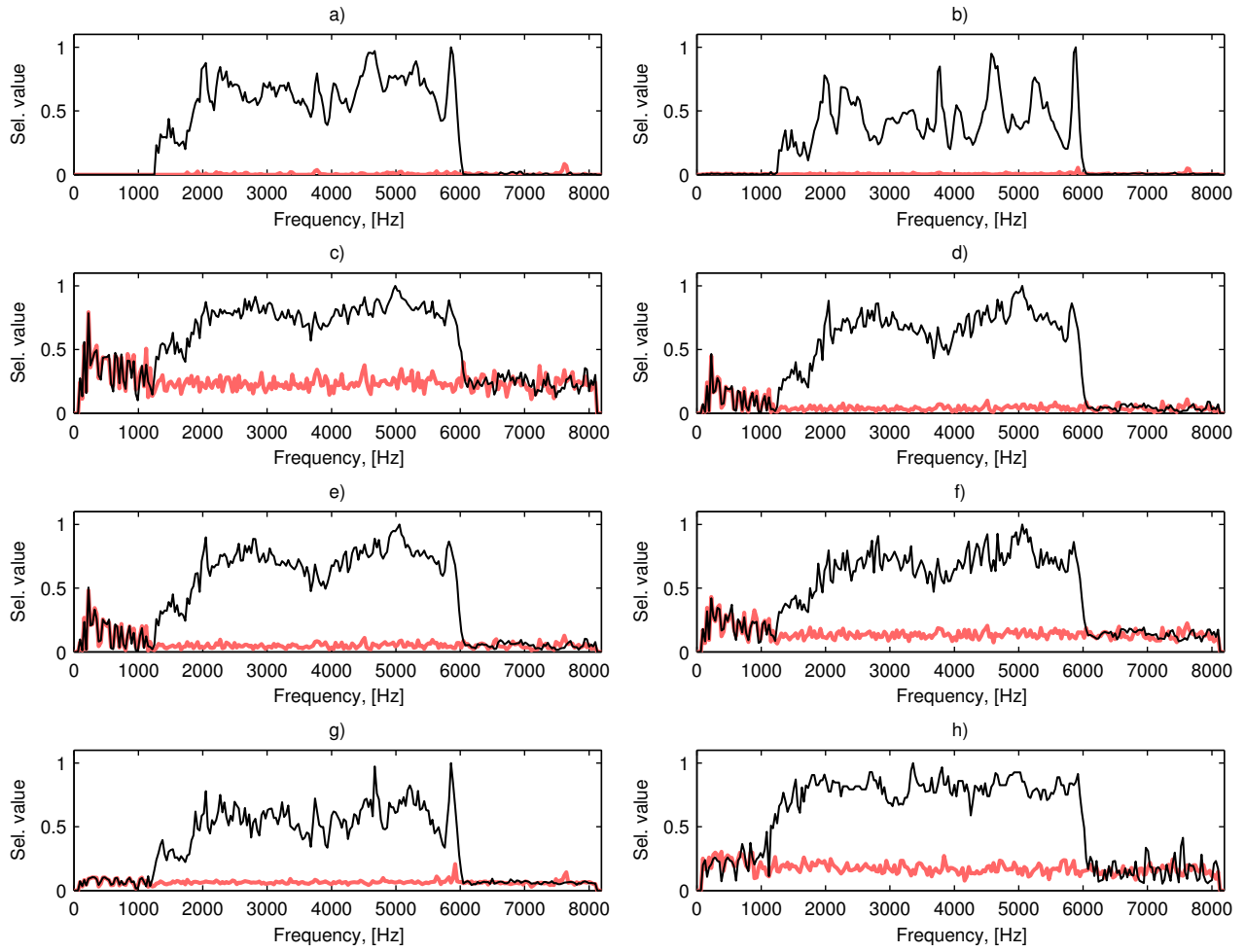


Figure 6.26: Selectors calculated for raw vibration data from faulty (thin black lines) and healthy (thick red lines) rotating machine: SK (a), JB (b), KSS (c), CVM (d), AD (e), H_{aver} (f), H_{max} (g) and LM (h). **UWAGA NA KOLEJNOSC RYSUNKOW I ODWOLANIA W TEKSCIE, MOZE BYC ZLA KOLEJNOSC**

present results of applying selectors described in Sec. 4.2 to the simulated data. Spectrograms used in Fig. ?? are obtained by using non-overlapping Kaiser windows of 219 samples and fast Fourier transform (FFT) calculated in 1024 points. In each of 8 cases the selectors are normalized by the maximum value to preserve possibility of comparison. One can note that in this simple case of simulated data all of the selectors indicated the informative frequency band correctly, but each one behaves in a different way.

Goodness of each of 8 selectors will be assessed with respect to few aspects. The ideal selector in the locally damaged rotating machine case should be close to 1 through the whole informative frequency band, i.e. from 1000 to 6000 Hz except band related to the 6th mesh harmonic (1140 Hz). Above 6000 Hz and below 1000 Hz the most valuable selector should be close to

0 and not distinguish between deterministic components and high-frequency noise. Transition from values close to 1 to values close to 0 should be as sharp as possible. While the machine is not damaged, no one of frequency bins should be indicated as informative, thus values close to 0 are expected through the whole spectrum.

Fig. ?? clearly shows that the selector value closest to 1 through the informative frequency band is owned by selector based on the *KSS* and the local maxima method (panels c) and h), respectively). Other selectors based on empirical cumulative distribution function share a behavior of value varying with the selector based on average horizontal distance on the QQplot (panels d), e) and f), respectively). The most varying behavior is presented by moment-based selectors (*SK* - a) and *JB* - b)) and the second selector based on QQplot (panel g)). No one selector clearly indicated the informative frequency band between 1000 and 1140 Hz, but this feature might depend on frequency resolution of the STFT used for calculating the selectors. To reveal such narrowband properties of the signal relatively high frequency resolution must be ensured.

While analyzing differences between behavior of the selectors in low frequency bands and the highest ones only in four of eight panels an acceptable result can be observed (panels a), b), g) and h)). Other selectors are more sensitive to rigid sine waves with a small amount of noise (amplitude modulated or not). The most sensitive one is the *KSS* (panel c)). One can see that the lower sensitivity to deterministic components, the lower dispersion of a selector value through the whole spectrum in a healthy machine case. Low dispersion is very important while setting a uniform threshold distinguishing selector related to the healthy machine from damaged one. Otherwise, individual thresholds for every frequency bin should be set.

The last aspect in respect to which we analyze goodness of selector is sharpness of transition from values indicating information related to local damage to the non-informative ones. Every selector owns this feature at frequency close to 6000 Hz. On the left edge of the informative frequency band only the local maxima based selector behaves acceptably. Slope of other selectors at the left edge of IFB is less sharp. Rigid transition between informative and non-informative components is important when a rigid frequency band must be specified for further processing, e.g. a band-pass filter.

To sum up, every new selector recognized the IFB comparably to the *SK*. There are some differences in behavior of each one but they are important only in particular further processing methods. Nevertheless, the differences are not significantly large and they might disappear by improving further processing methods (e.g. individual thresholds instead of a uniform one for filter design). It might be said that the new selectors provide similar information as *SK* in the simple signal case.

6.2.2 Real data analysis

To prove efficacy of the proposed methodology we will show results of application of selectors to real vibration data from complex mechanical system operating in mining industry. To provide

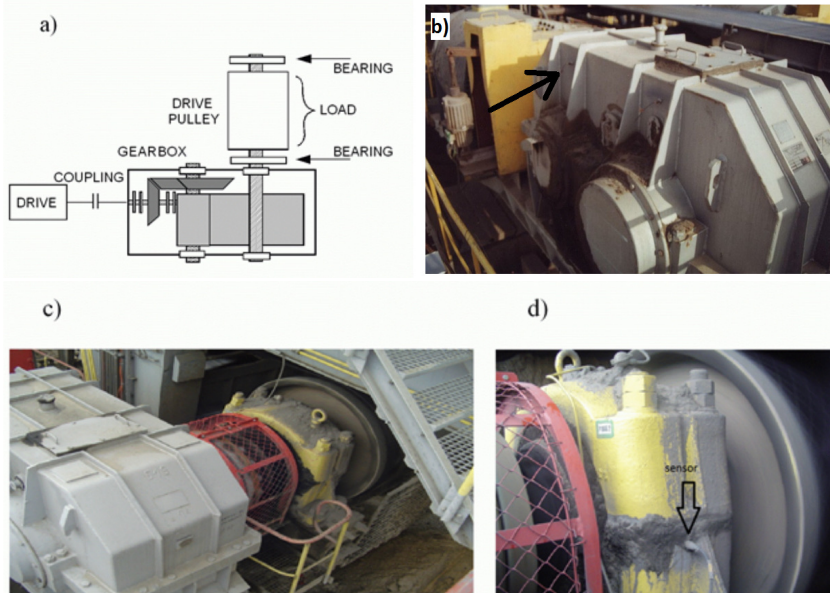


Figure 6.27: a) - scheme of the investigated machinery, b) - sensor location in gearbox case, c) - coupling between gearbox and pulley, d) - sensor location in pulley case.

"good condition" reference, two vibration signals representing a healthy rotating machine and a damaged one are considered. The first set represents vibrations of bearings and the second one - gearboxes' vibrations. Different sets of data are related to different types of damage. In Case A, there is an outer race damage in bearings pulley. In Case B, tooth local damage in gear-wheel mounted on second (middle) shaft in the gearbox. Both components (bearings from pulley, gearwheel from two stage gearbox) come from driving system used in belt conveyor,

very popular technology for transporting of bulk materials in mining industry. In fact signal from bearings and gearbox come from different driving stations, however design of drive unit is the same as presented in Fig. ???. Measurements have been performed using Brüel Kjaer Pulse system. Parameters of data acquisition depends on the investigated object. Details (duration of signal, sampling frequency, location of the sensor) are provided in subsections below.

In both cases, due to high amplitudes of mesh components, cyclic and impulsive nature of the signal can be hardly seen. For gearbox vibration, there are some barely visible disturbances in the vibration signal, however, any diagnose without performing detailed analysis might lead to misinterpretation of the results. In case of acquisition of vibration from pulleys bearing, the level of contamination is very high and mask signal of interest completely. In both cases, there are serious differences in amplitudes of selectors between good and bad conditions.

Bearing with a two-stage gearbox located nearby

Here we analyze signals related to two bearings. As mentioned, one is healthy and the

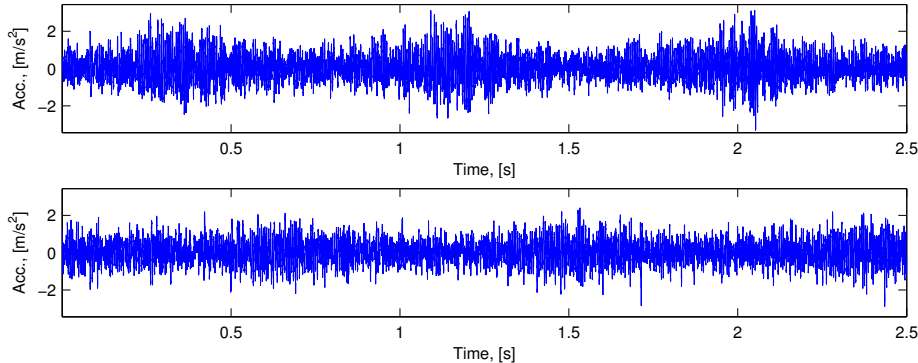


Figure 6.28: Raw vibration signal from healthy (top panel) and faulty (bottom panel) bearing. Note deep amplitude modulation present in both signals

second is locally damaged (outer race problem). Data were acquired using commercial system. Parameters of vibration acquisition are: sensor located in horizontal direction (see Fig. ??d), sampling frequency 19200 Hz, duration of signal 2.5 s and the expected fault frequency 12.69 Hz. Fig. ?? and Fig. ?? present raw signals and corresponding spectrograms, respectively. As one can see, both signals are strongly amplitude modulated. Cycle of modulation is related to pulley's shaft rotation, it does not indicate local nature of the problem. Impulses related to

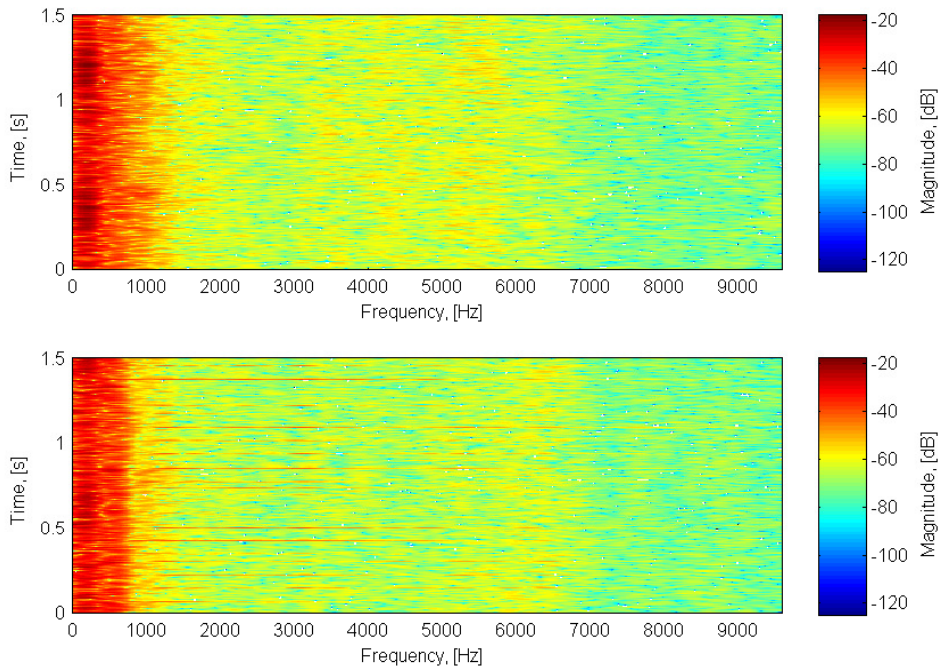


Figure 6.29: Spectrograms of raw vibration data from healthy (top panel) and faulty (bottom panel) bearing. The whole signals last 2.5 s. Note three energy-different bands: high-energy contamination from a gearbox, middle-energy informative components and low energy noise.

the damage are not visible in time domain, wideband excitations in the spectrogram are not so clear due to high energy band at approx. 0-1000 Hz.

Thus, the proposed selectors might be reasonable to apply in order to distinguish informative frequency band from uninformative. To obtain the spectrograms we use non-overlapping Kaiser windows of length 129 samples and calculate FFT in 1024 points. Relatively short window preserve a proper size of samples used for calculating the selectors and good time resolution at the expense of frequency resolution.

Recall that in Sec. ?? a model-driven analysis was performed. Since the whole structure of the signals was known, selectors were examined if they are sensitive to individual properties of the signals. While a real signal is analyzed, only a limited information about the data is given. Thus, we do not analyze selectors for a rigid informative frequency band detection here. In our analysis we focus on similarities between shape of the selectors at particular frequency bands, sensitivity to high-energy amplitude modulated components and low-energy noise, bandwidth indicated as informative and possibilities of performing future analyzes, e.g. band-pass filtering. The differences are also assessed beside their basis, i.e. the group to which they belong.

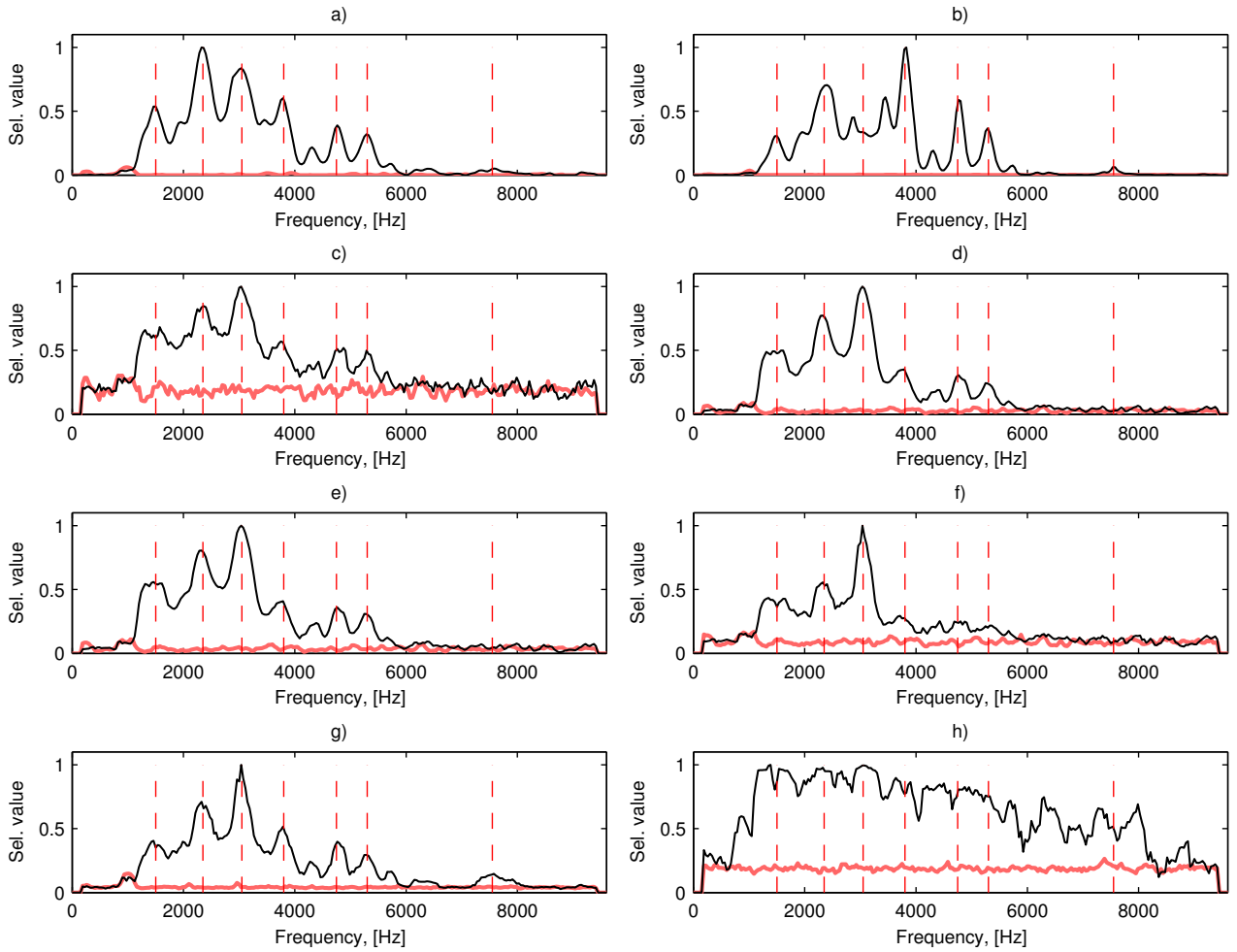


Figure 6.30: Selectors calculated for raw vibration data from faulty (thin black lines) and healthy (thick red lines) bearing: *SK* (a), *JB* (b), *KSS* (c), *CVM* (d), *AD* (e), H_{aver} (f), H_{max} (g) and *LM* (h). Frequencies marked with vertical red dashed lines corresponds to 1500, 2350, 3050, 3800, 4750, 5300, 7550 Hz.

From a theoretical point of view selectors are grouped into four sets. The first is a set of moment-based selectors and consists of the *SK* and *JB*. The second set consists of selectors based on empirical cumulative distribution function (*KSS*, *CVM* and *AD*). Selectors that quantify average and maximum horizontal distance in QQplots form the third set. The last one consist the last selector - based on the local maxima method. In Sec. ?? it was observed that selectors contained within the first set share similar behavior. Also selectors within the second group behave in a similar way. Only QQplot-based selectors are different from each other, especially in the lowest frequency bands. Here, as it can be observed in Fig. ??, shapes presented in panels c), d) and e) looks very similar, excluding higher values in *KSS* case for both healthy and damaged data outside the indicated IFB. In the case of locally damaged bearing three

large peaks at about 1500, 2350 and 3050 Hz with increasing height and three small peaks near 3800, 4750 and 5300 Hz with decreasing height are observed (panels c)-(e)). No other significant peaks are visible in both damaged and healthy cases. Maximum horizontal distance behaves similar them, but the damaged bearing is characterized by additional small peak at frequency of 7550 Hz (panel g). This single peak is also shared by moment-based selectors (panels a) and b)). Moreover, *SK* and *JB* are more dispersed than other selectors. Contrary to them, *LM* is the least scattered selector. All of the selectors that require sorting indicate frequency of 3050 Hz as the most informative. The most distinctive selector is the one based on the local maxima method. It indicates almost whole frequency band as informative except low-frequency contamination from the gearbox and high-frequency noise at band higher than 8000 Hz. Inside the indicated informative frequency band it can be observed that the curve related to damaged bearing slowly decreases with increasing frequency. All of the selectors behave similarly in the healthy bearing case. The only difference is visible in level of selectors, but all of them do not distinguish between low, middle and high frequency bands. In every case, band-bass filter design procedure should decide which choose leads to the best result: 1500-4000 Hz, 1500-6000 Hz or 1500-8000 Hz. In the case of more complicated linear filtering procedure exploiting *KSS*, the problem of relatively high scatter of the selector must be solved. In further work an interesting result obtained by using the local maxima method for IFB selection must be validated. Before performing filtering procedure it cannot be said if such wide indicated IFB leads to better enhancement of the raw signal or not.

To sum up, the new selectors might provide similar information as *SK* about informativeness of each frequency bin in the simple real data case. *JB* might provide more selective filter characteristic (passing only set of narrow band around the indicated ones), preserving clear difference between signal from healthy and damaged machine. Selectors based on ECDF and QQplot indicated the same frequency bin as the most informative. While performing further analyzes one can decrease the number of selectors contained in this groups. Surprising result obtained by *LM* is difficult to interpret and it must be examined if such wide IFB is better (e.g. other selectors does not indicate crucial frequency bins) or just leads to more noisy filtered signal.

Two stage gearbox

In this section we present how the selectors deal with another real data set. The signals rep-

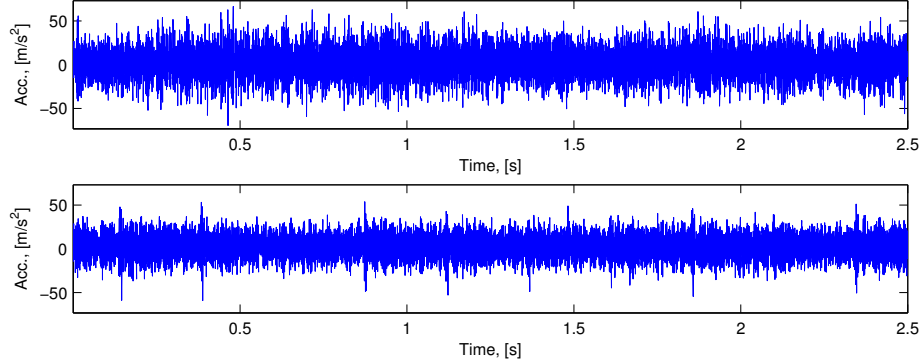


Figure 6.31: Raw vibration signal from healthy (top panel) and faulty (bottom panel) gearbox. Note barely-visible impulses related to the fault frequency (bottom panel).

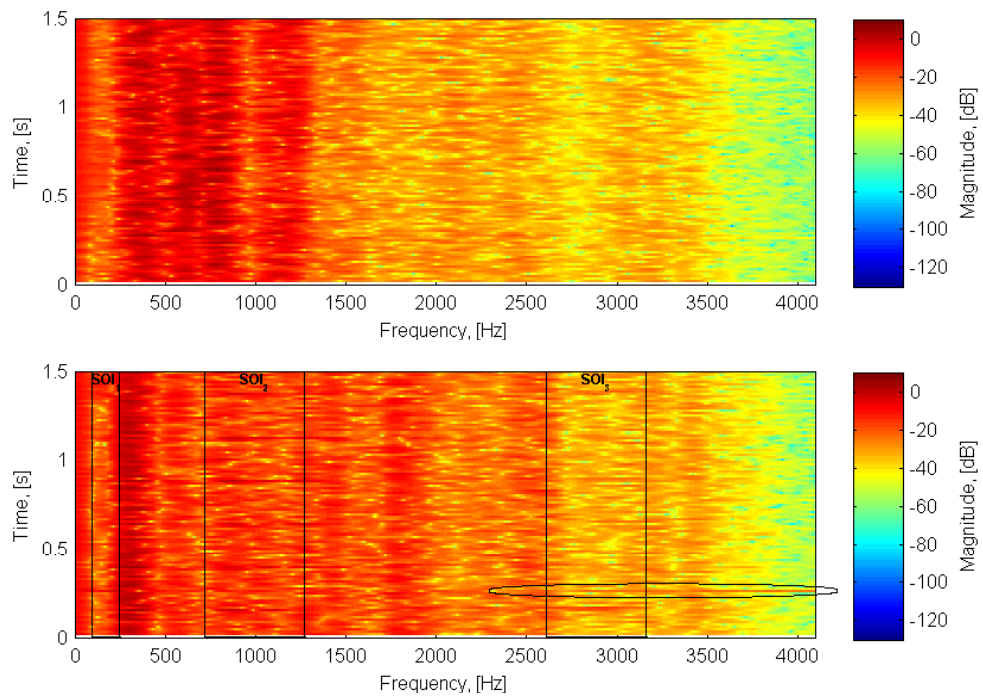


Figure 6.32: Spectrograms of raw vibration data from healthy (top panel) and faulty (bottom panel) gearbox. Note the artifact at 0.25 s occurred during data acquisition. Note 3 informative frequency bands (SOI_{text1} , SOI_{text2} , SOI_{text3}) and the artifact marked with an ellipse.

resent vibration of two gearboxes, one healthy and one which is damaged. Parameters of signal acquisition are: duration 2.5 s, sampling frequency 8192 Hz and the extepcted fault frequency 4.1 Hz. Several channels were used. Location of sensor associated with the signal used here is

pointed by arrow in Fig. ??b.

Raw signals and corresponding time-frequency maps are presented in Fig. ?? and ??, respectively. Spectrograms are obtained by STFT with non-overlapping Kaiser windows of length 111 samples and FFT calculated in 1024 points. As it can be seen, both impulses in time domain and horizontal lines in time-frequency domain are barely-visible. Moreover, there is an artifact, i.e. undesirable disturbance occurred during data acquisition. It can be seen in Fig. ?? (bottom panel) at frequencies lower than 250 Hz and higher than 3500 Hz, at 0.25 s.

We propose to analyze the selectors presented in Fig. ?? in two main aspects. Since the fre-

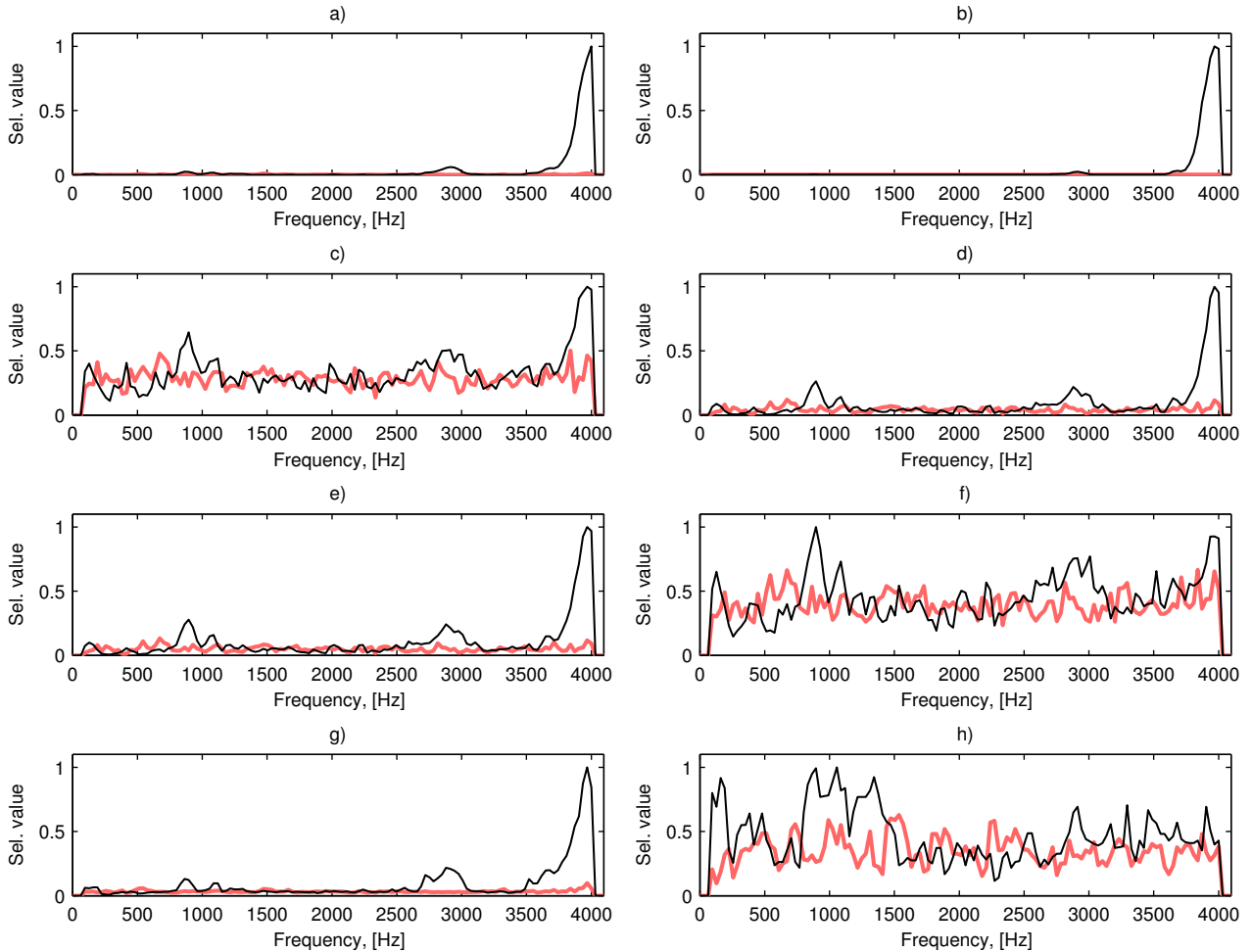


Figure 6.33: Selectors calculated for raw vibration data from faulty (thin black lines) and healthy (thick red lines) gearbox: *SK* (a), *JB* (b), *KSS* (c), *CVM* (d), *AD* (e), *H_{aver}* (f), *H_{max}* (g) and *LM* (h).

frequency band related to damage is narrow and it overlaps with a lot of high-energy components, the best selector should at first accurately distinguish the damaged gearbox from a healthy one.

It is a real challenge because high-energy components differ in the two analyzed signals. The second feature which the best selector should deal with is the artifact. While its whole energy is relatively low, its energy contained in high-frequency bands is relatively high, so selectors have to deal with an outlier present in spectrogram slices above 3000 Hz.

The artifact affected the Jarque-Bera statistic based selector the most and the spectral kurtosis is also very large at highest frequencies (panels b) and a), respectively). Thus, other frequency bands are relatively barely-indicated. One can see a little higher values at SOI_{text2} (800-1200 Hz) and SOI_{text3} (2700-3100 Hz) in SK but JB presents slightly higher values only at SOI_{text3} (except frequency bins related to the artifact). Among other selectors, the artifact affected also selectors in panels c), d), e) and g) but peaks SOI_{text2} and SOI_{text3} are clearly visible. The least affected selector is LM (panel h)). Sensitivity of H_{aver} to single excitations is average (panel f)).

As it can be observed in Fig. ?? the informative frequency band is composed of three parts. The first is narrow and is located near 200 Hz (SOI_{text1}). Two other are relatively wide and are located close to 1000 Hz (SOI_{text2}) and 3000 Hz (SOI_{text3}). The only selectors that indicated the first part are presented in panels f) (H_{aver}) and h) (LM) but the latter one is better visible. Most of other selectors also has higher levels at about 200 Hz (SOI_{text1}), but in these cases values of selectors for the healthy gearbox is on the same level. Thus it disappears while a uniform threshold of selector value is established to distinguish damaged from a healthy one. The SOI_{text2} is indicated by all the selectors but JB . The highest relative indication of it is presented in panels d), e), f) (ECDF-based selectors) and h) (LM).

The last aspect with respect of which we analyze the selectors is the artifact above 3000 Hz. The best behavior here is shared by CVM , AD and both average and maximum distances in QQplot (panels d), e), f) and g), respectively).

To sum up, the artifact is a serious challenge for informative band selectors. Since both moment-based selectors fail, the other ones are promising with a view to further processing. One might greatly benefit from a procedure that establishes thresholds for every frequency bin individually, because every selector that decreases influence of the artifact is very scattered. It can be said that the lower sensitivity to the artifact the larger dispersion of a selector's values. Thus, in

such case LM and H_{aver} might be the most effective selectors. While a uniform threshold has to be designed to distinguish between data from healthy and damaged machine the best choice must be a compromise between relatively low influence of the artifact and small dispersion of the data.

6.3 Linear filter design based on selectors

6.3.1 Application to industrial data

The signal analyzed in this section has been acquired using an accelerometer and represents 2.5 s of the system's operation. Sampling frequency is 8192 Hz.

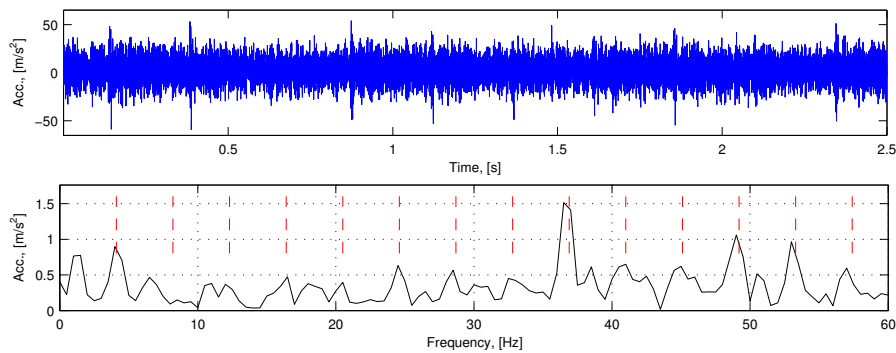


Figure 6.34: Time series (top panel) and envelope spectrum (bottom panel) of the real raw vibration signal from the two-stage gearbox. Red dashed lines denote 14 first multiplies of fault frequency (4.1 Hz).

Time series and its envelope spectrum are presented in Fig. ???. Impulses related to the local damage are barely visible in time domain due to high-energy low frequency components that do not carry impacts related to damage. The envelope spectrum does not indicate any of multiplies of the fault frequency (4.1 Hz). Spectrogram of the signal is presented in Fig. ?? (top panel). Bottom panel of Fig. ?? presents an exemplary reference signal. Recall, that this signal is basically a white Gaussian noise with amplitude spectrum multiplied by the spectrum of real data. Parameters of the STFT are: Kaiser window of length 329 samples, 80% overlapping and the discrete Fourier transform is calculated in 1024 points. Time-frequency map of the real data

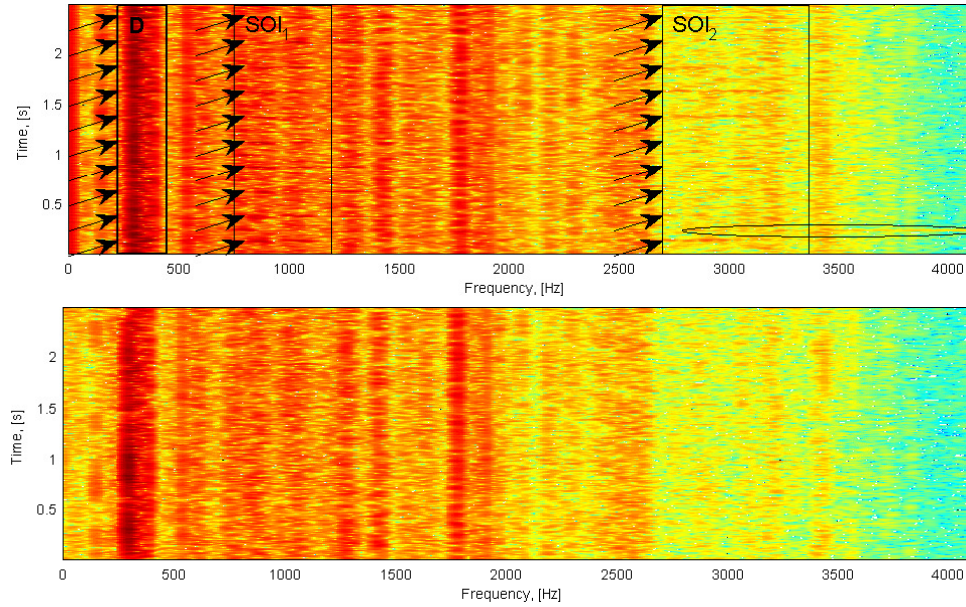


Figure 6.35: Spectrograms of the raw real (top panel) and one of the reference signals obtained by using the method based on inverse pre-whitening (bottom panel). Note similar frequency content of both signals (e.g. area labeled D). The difference can be noticed in terms of presence of wide-band excitations related to local damage (e.g. labeled SOI₁, SOI₂).

exhibits a few wide-band excitations, a single artifact which is invisible in time domain and high-energy low-frequency components. The artifact can be easily noticed in the spectrogram at highest frequency bands, i.e. over 3500 Hz. One can see that the most informative frequency band is located around 1000 Hz, but some wide-band excitations can be also seen close to 250 Hz and 2800 Hz (Fig. ??). This behavior is a result of the resonance effect - informative frequency band consists of two or more separated informative frequency sub-bands.

Selector values and significance thresholds corresponding to each of four selectors are compared in Fig. ???. One can notice that the artifact has the most significant influence on *JB* and *SK*, but the rest of the selectors are also slightly influenced. Thus, signal processing methods based on finding frequency band with the highest kurtosis or, in general, highest value of a given selector will definitely fail, since it will result in a signal with the artifact and low-energy noise. This is the reason why all of the frequency bins with significantly high selector values have to be taken into account in the signal filtering procedure. Otherwise, a bandpass filter with center frequency corresponding to the maximum of the selector's values might omit remaining features, assessed as significant. Characteristics of the filters based on *KSS* and *H_{aver}* are the

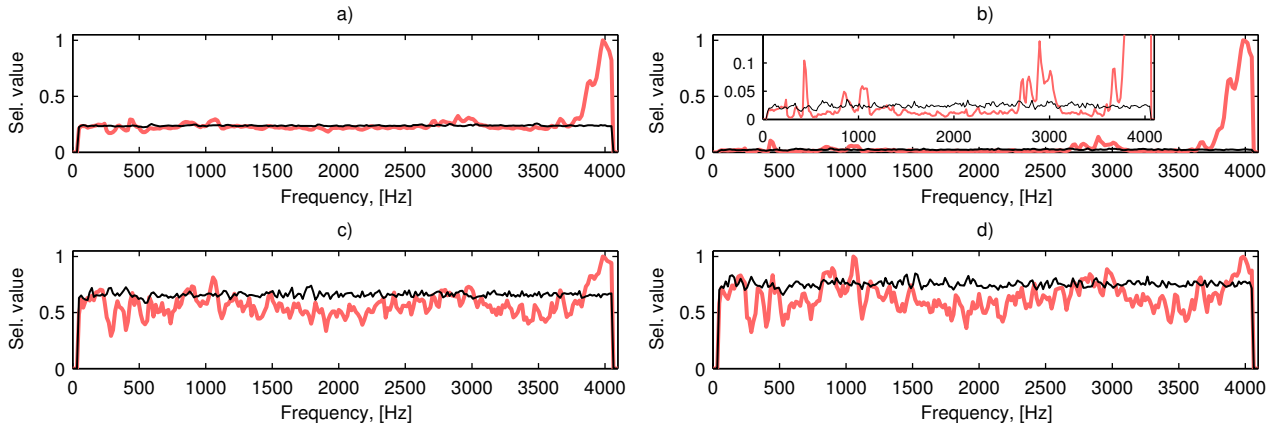


Figure 6.36: Filter characteristics before thresholding (red thick lines) and significance thresholds (black thin lines), a) SK , b) JB , c) KSS , d) H_{aver} .

least sensitive to the single disturbance. Moreover, values of H_{aver} at highest frequency bands are close to values at middle-low bands (about 1000 Hz) (Fig. ??). The plots also illustrate the relevance of individual significance thresholds for each frequency bin. At several frequency bins related to frequencies lower than 1000 Hz, the thresholds significantly differ. Thus, it cannot be said that a flat threshold (i.e. the same for each f) is appropriate. Higher values of selectors at the lowest frequency bins might have the same cause as in the simulated signals presented in 4.5. The problem of alternative methods for assessment of significance (thresholding) is investigated in Sec. 4.3.5.

Time series of filtered signals are presented in Fig. ???. It can be noticed that the artifact occurred only in case of SK and JB . Recall, that both of them are based on statistical moments. Other selectors, based on sample quantiles (H_{aver}) and empirical cumulative distribution function (KSS), suppressed the artifact to the level of noise. In all of 4 selectors, spikes related to local damage are now clearly visible in time domain.

Envelope spectra of filtered signals are presented in Fig. ???. It is shown that the relatively low-energy artifact that occurred during the experiment has affected characteristics of filters. However, the amplitude of the artifact is not high enough to affect envelope spectra of filtered signals. In all cases the fault frequency is properly recognized as 4.1 Hz. Lots of multiples of the fault frequency can be noticed.

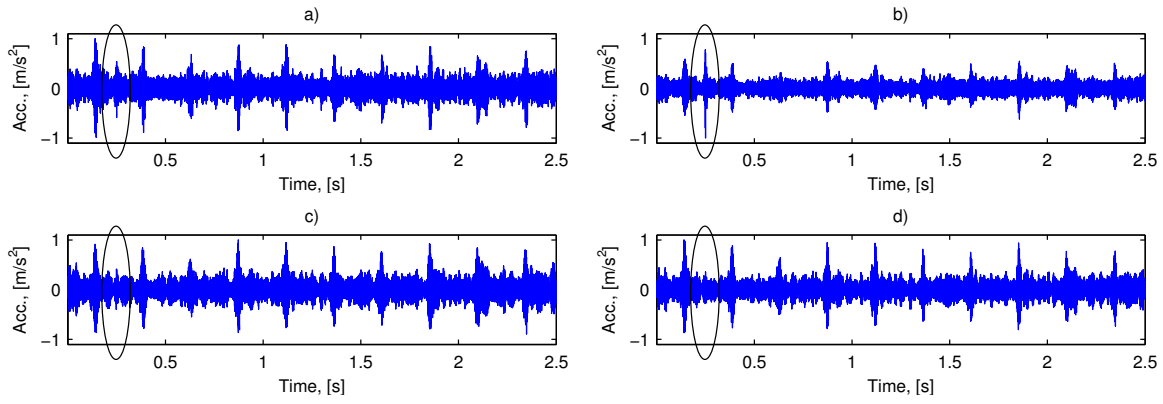


Figure 6.37: Time series of filtered vibration signals, a) SK , b) JB , c) KSS , d) H_{aver} . Time point at which the artifact occurs is marked by ellipse.

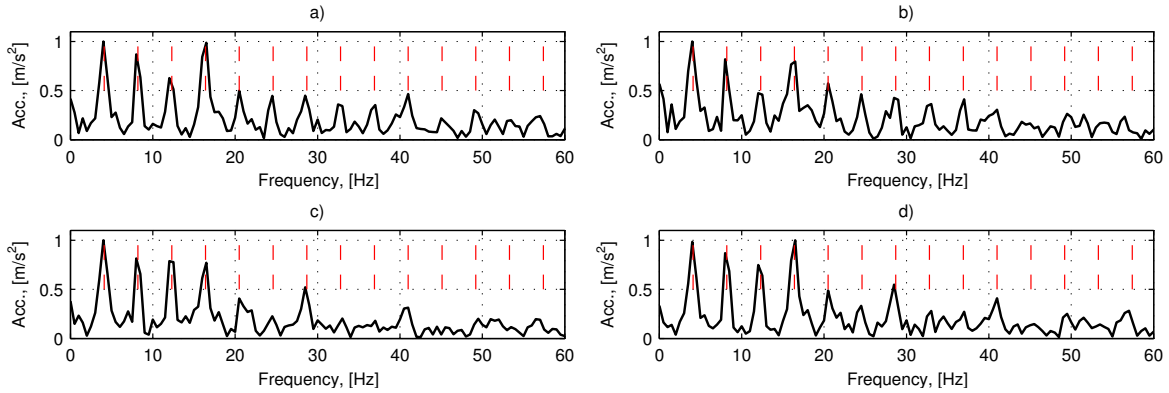


Figure 6.38: Envelope spectra of filtered vibration signals, a) SK , b) JB , c) KSS , d) H_{aver} . Red dashed lines correspond to first 14 multiplies of fault frequency (4.1 Hz).

6.3.2 Influence of larger artifact on filtered signal

Here we present how our procedure deals with a simulated signal with a larger artifact. The signal is obtained by compiling frequency structure from a signal that represents vibrations of a healthy heavy rotating machine, simulated signal of interest and the artifact. The machine is of the same kind as in the previous section (two-stage gearbox operating in the driving station for belt conveyor), but the sensor (accelerometer) is located on a different place on the housing. Thus, frequency structures of both signals are different. Moreover, sampling frequency of the signal is now 16384 Hz and duration is 2.5 s. The simulated signal of interest is an amplitude modulated Gaussian noise and it imitates a pulse train related to a local damage of the first shaft. Moreover, the pulse train is band-passed using an ideal filter to obtain relatively narrow informative frequency band, i.e. 3800-4200 Hz, which is typical for the local damage in early

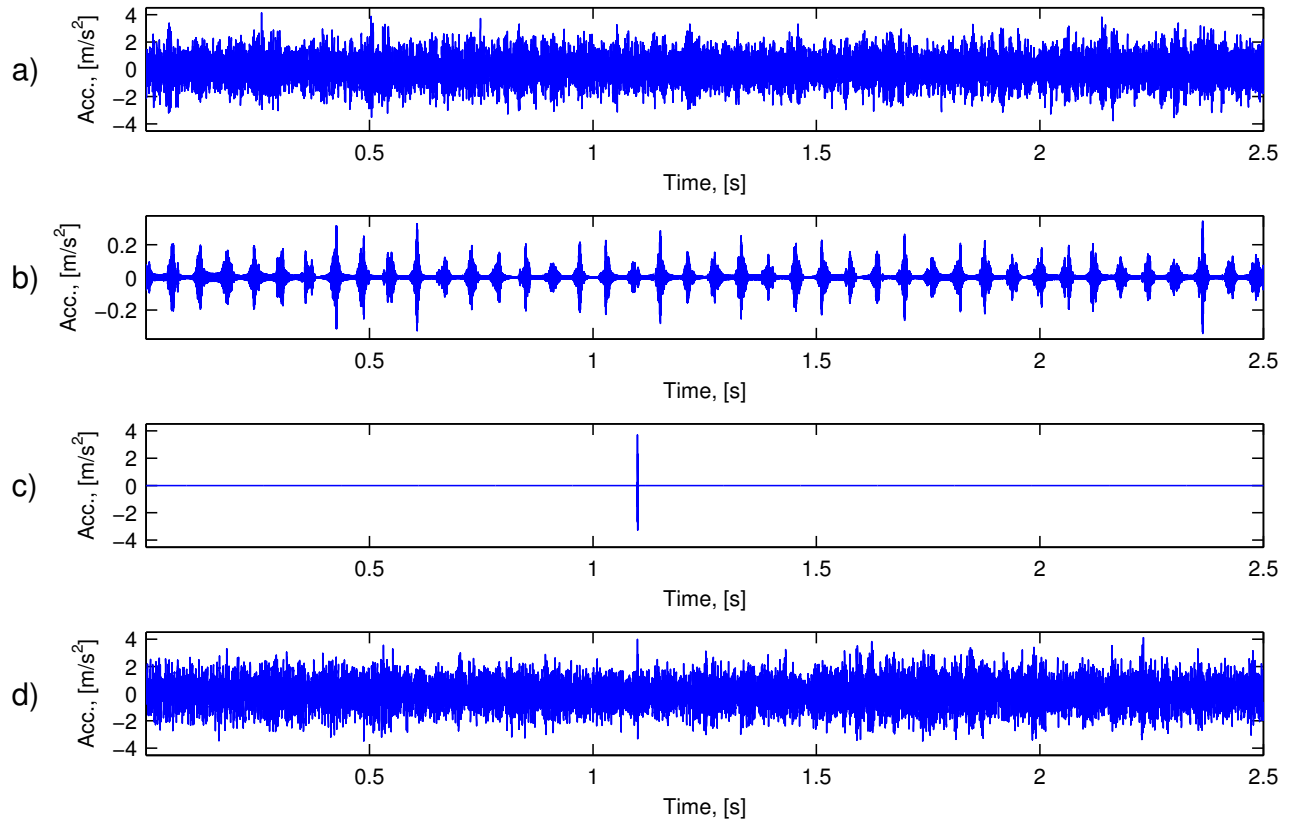


Figure 6.39: Time series of: a) the raw real vibration signal, b) simulated impulsive signal, c) artifact, d) sum of above signals.

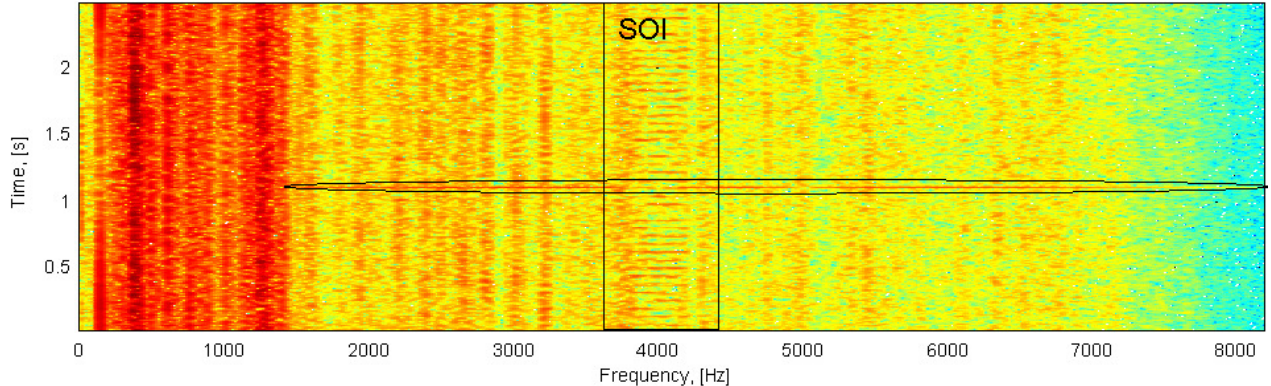


Figure 6.40: Spectrogram of the raw signal. Informative frequency band (3800-4200 Hz) and the artifact are marked by rectangle labeled "SOI" and marked by ellipse, respectively.

stage. Fault frequency is equal to 16.5 Hz. Also a single impulse is added in order to simulate an artifact. The impulse is short-lasting, but its amplitude is relatively high. We simulated the impulse as a Gaussian-modulated sinusoidal pulse. Its bandwidth completely covers the bandwidth of the SOI. Moreover, it covers almost the entire frequency range. The finally

analyzed signal is a sum of these 3 signals.

Time series of all components of the signal are presented in Fig. ???. The spectrogram of the analyzed signal is presented in Fig. ???. The spectrogram is obtained by using Kaiser windows of length 223 samples, 80% of overlapping and the discrete Fourier transform is calculated in 512 points.

The signal is designed to clearly illustrate how relevant it is to minimize the influence of a single artifact on frequency characteristic of a filter. In the previous case the artifact was too small to illustrate this statement, thus the analysis of the simulated signal is performed.

Fig. ?? presents characteristics of filters based on SK , JB , KSS and H_{aver} . It can be seen

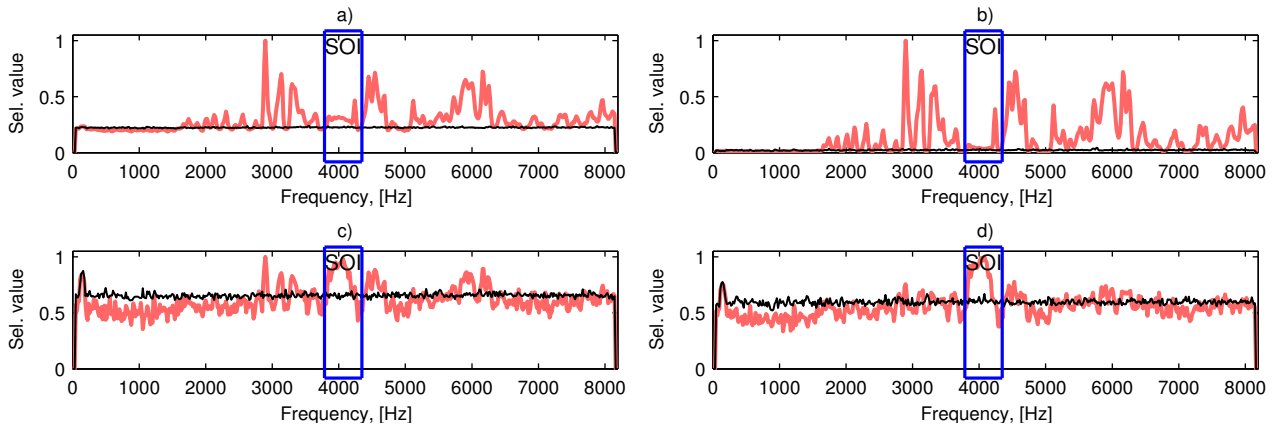


Figure 6.41: Filter characteristics before cut-off (red thick lines) and thresholds (black thin lines), a) SK , b) JB , c) KSS , d) H_{aver} .

that the artifact influenced all of the selectors. Similar to the previous case (real data, Sec. ??), the artifact influenced frequency characteristic driven by JB the most, the next is SK (both of them are based on statistical moments). KSS and H_{aver} are barely influenced. It is worth pointing out that the idea of individual significance thresholds for each frequency bin has been proved as important. There is a peak in the lowest frequency bands, clearly visible in Fig. ???, panels c) and d), but also in panel a). Any amount of this low-frequency high-energy part of the signal not suppressed by the filter might result in worsening of quality of the filtered signal.

Time series of the filtered signals are presented in Fig. ???. It can be easily noticed that the artifact is present in every plot, but its amplitude depends on a particular selector. The frequency bands of SOI are completely covered by the frequency band of the artifact. Thus, it is

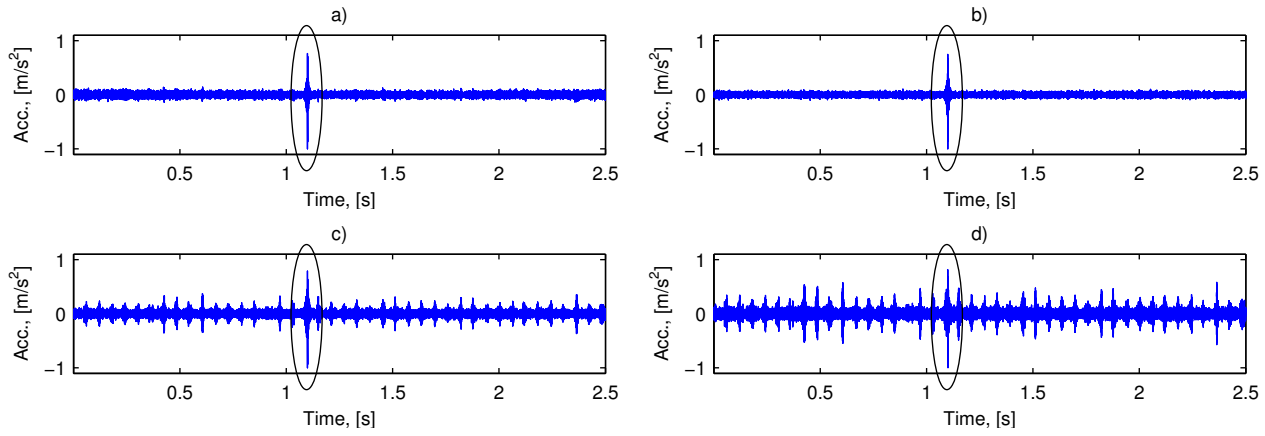


Figure 6.42: Time series of filtered simulated signals, a) SK , b) JB , c) KSS , d) H_{aver} . Time point at which the artifact occurs is marked by ellipse.

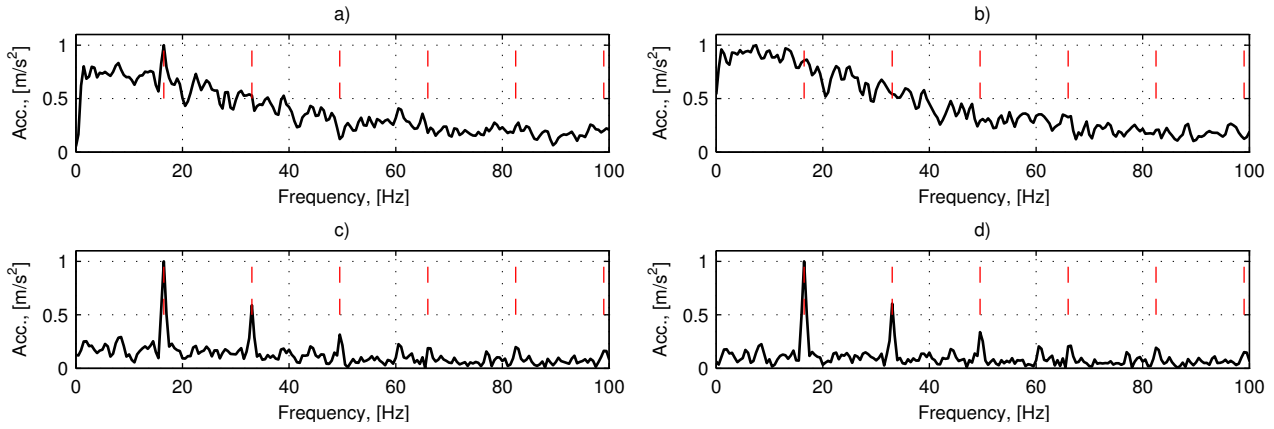


Figure 6.43: Envelope spectra of filtered simulated signals, a) SK , b) JB , c) KSS , d) H_{aver} . Red dashed lines denote 7 first harmonics of the fault frequency (16.5 Hz).

impossible to completely remove the artifact from the filtered signal, using a linear filter based on suppressing selected frequency bins. One can only design a filter that minimizes amplitude of the accidental impulse by suppressing energy of all other frequency bins that do not contain the SOI. In Fig. ?? one can observe that in panel a) impulses related to the signal of interest are barely visible and in panel b) they are completely invisible. On the other hand, impulses might be clearly seen in panels c) and d) of Fig. ?? and amplitude of the artifact is comparable to the amplitude of impulses that constitutes the SOI. KSS and H_{aver} indicated almost only the frequency band of the SOI, thus the noise at frequency bands under 3800 Hz and above 4200 Hz is minimized. Therefore, the resultant signals are close to the SOI presented in panel b) of Fig. ???. Bandwidth of the artifact is highly reduced, thus its amplitude is diminished as well.

As it was expected after the analysis presented in the previous section, single spike influenced envelope spectra the most in two of four cases (*SK* and *JB* - Fig. ??, panels a) and b), respectively). The envelope of the *SK*-filtered signal contains one peak corresponding to the fault frequency (16.5 Hz) with large amount of noise (Fig. ??). Panel b) of Fig. ??, which represents the result of filtration using *JB*, contains only a noise - none of fault frequency harmonics is presented. On the other hand, filters based on *KSS* and H_{aver} (Fig. ??, panels c) and d), respectively) recognized the true fault frequency, showing three clear harmonics related to first 3 multiples of the fault frequency. Also, the level of the noise is much lower in these two cases.

To sum up, the best results are obtained by filtering using selectors based on quantiles and empirical cumulative distribution function, i.e. H_{aver} and *KSS*, respectively. Signals filtered using selectors based on statistical moments are very sensitive to accidental impulses, thus they fail in case of the artifact.

6.3.3 Simulated data analysis

In this section we analyze performance of blind equalizers on simulated signals, providing a motivation to incorporate a combined skewness-kurtosis criterion.

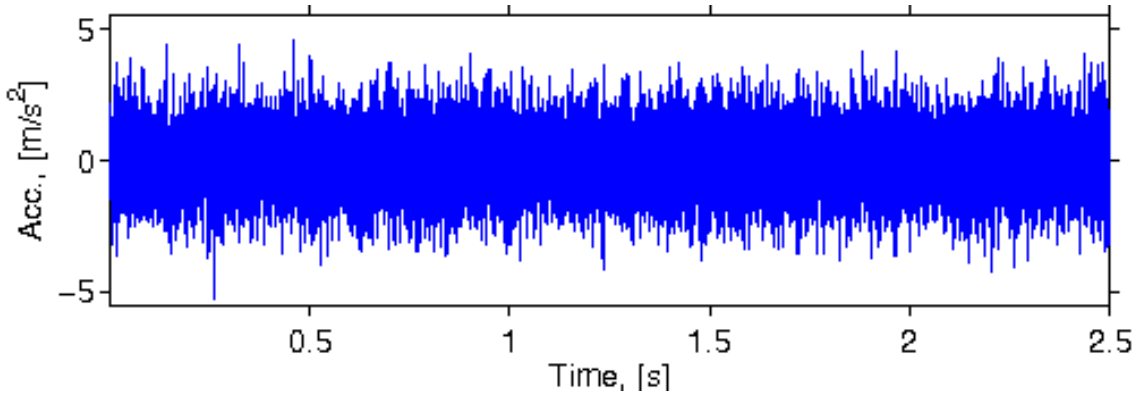


Figure 6.44: Time series of simulated signal related to gear fault (case K1).

The signals we analyze are sums of response of a linear time-invariant system to an asymmetric pulse train and an additive Gaussian noise [?]. The system is characterised by its impulse

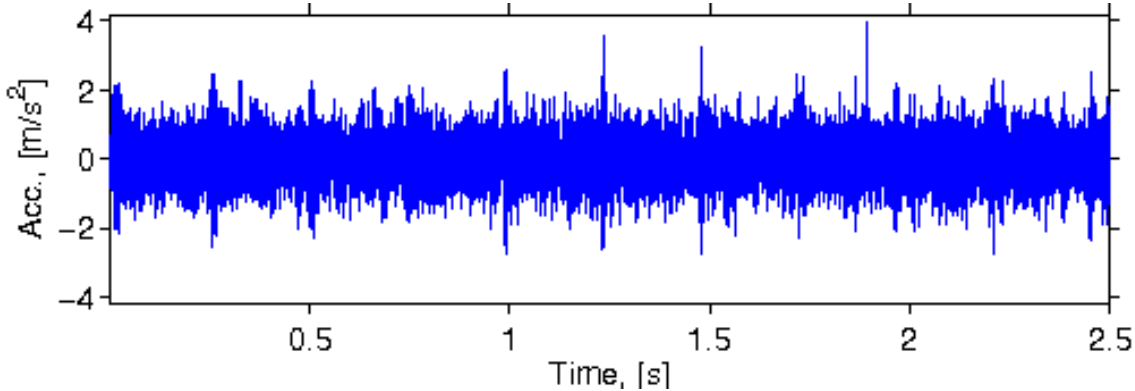


Figure 6.45: Time series of simulated signal related to gear fault (case K2).

response designed in order to follow properties observed in a real vibration signal from a two-stage gearbox. The asymmetric pulse train corresponds to a signal that arises in case of local damage. Duration of both signals is 2.5 s, sampling frequency is 8192 Hz and the fault frequency is 4.1 Hz. One of the signals is characterized by high level of background noise (Fig. ??, case K1) and the other one - by relatively high variability of impulses amplitudes related to local damage (Fig. ??, case K2). The noisy pulse train represents the signal that originates in a faulty gear. The linear time-invariant system represents the transmission path between the faulty gear and the accelerometer. Since the real signal related to gear fault analyzed in Sec. ?? is associated with more than one resonance frequency band, the linear time-invariant system is desired to consider this feature (resonance areas at 800-1200 Hz and 2500-3000 Hz). The simulated fault signal (excitation signal) is a noisy pulse train, i.e. it is a sum of a low-amplitude zero-mean white Gaussian noise and a scaled Kronecker comb function with period $P = 1998$ samples. Such period stands for fault frequency 4.1 Hz and sampling frequency 8192 Hz. The sum of Kronecker comb and a zero-mean Gaussian noise is a both asymmetric and impulsive signal. In case presented in Fig. ?? the impulses related to fault are barely-visible.

We analyze two signals related to different properties of skewness and kurtosis as criteria for blind deconvolution. The first signal (K1) is designed in order to illustrate how beneficial it could be to incorporate kurtosis in the deconvolution criterion in case of high level of background noise. This signal reveals two resonance frequency bands, although only the second band (2500-3000 Hz) is visible due to high level of noise (Fig. ??). The second signal (K2) is designed in order to present how the kurtosis-only driven deconvolution might converge to a single impulse

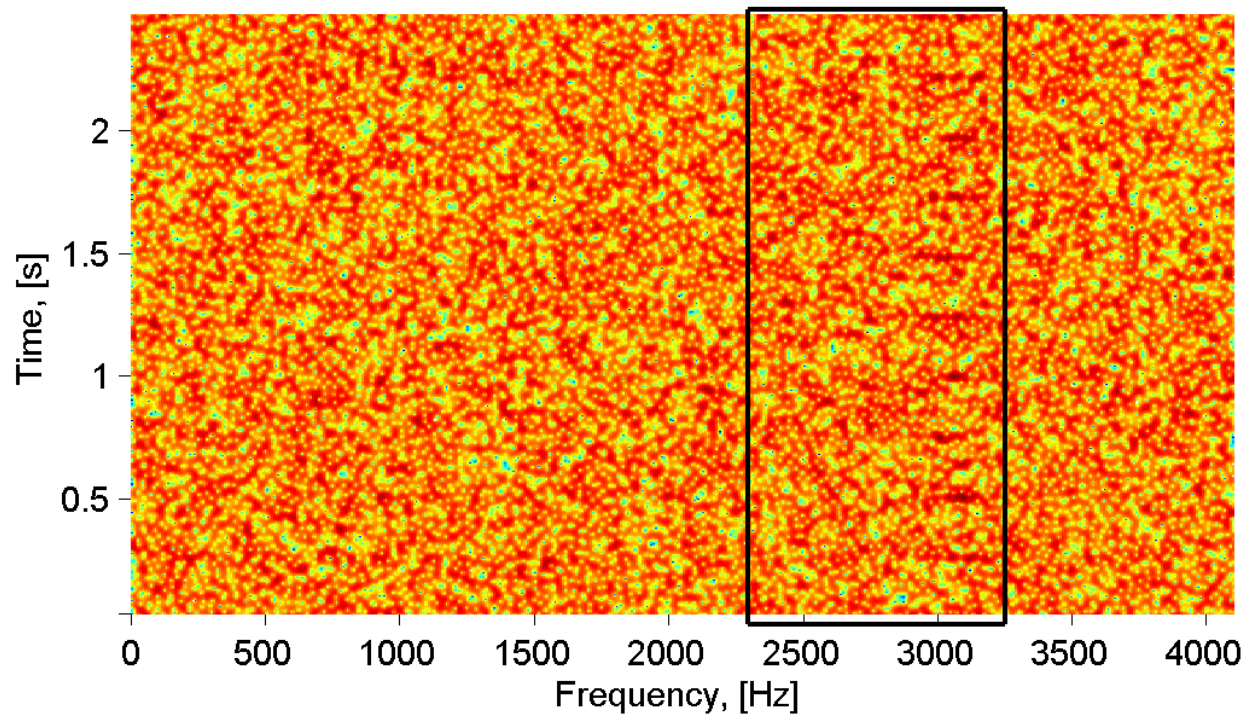


Figure 6.46: Spectrogram of simulated signal related to gear fault (case K1).

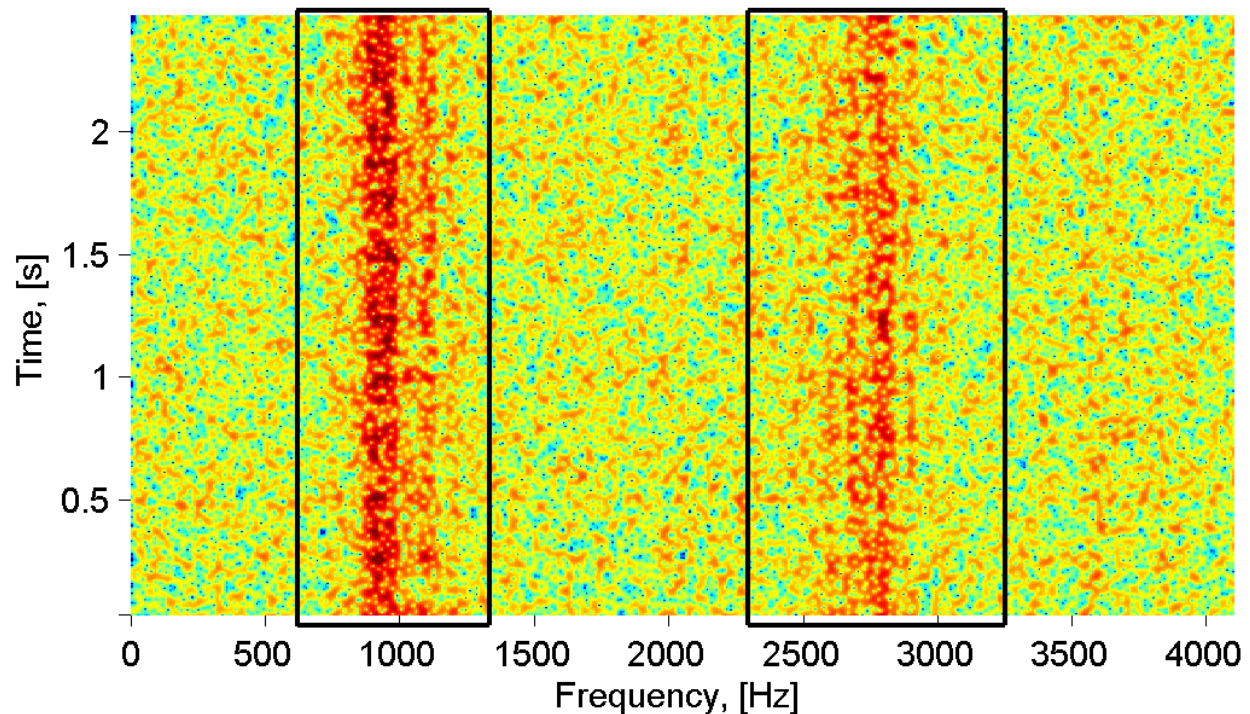


Figure 6.47: Spectrogram of simulated signal related to gear fault (case K2).

due to relatively high variability of excitation impulses amplitudes and low level of noise. One can notice that two resonance frequency bands are clearly seen in the time-frequency map (Fig. ??).

In order to demonstrate properties of the novel deconvolution criterion we stop the iterative procedure after 160 iterations and present results of several intermediate steps, i.e. deconvolved signals after 1, 2, 3, 4, 5, 10, 20, 30, 40, 50, 100, 160 iterations. Length of the filter is set to 300 in each case. The initial filter is set as a one-sample shifted pulse. Fig. ?? illustrates how beneficial it could be to incorporate a high-order statistic (order higher than 3) in a deconvolution criterion. Recall that the occurrence of the pulse train is somehow manifested only in one of two resonance frequency bands. In this case the skewness-based equalizer could not indicate an asymmetric excitation signal even after 50 iterations (Fig. ??b). After that it tends to a single positive spike. Outputs of two other deconvolution criteria successfully deal with a signal with high level of background noise. Both of them indicate the pulse train starting from 10 iterations and do not converge to a single pulse even after 160 iterations (Figs. ??a, ??c). In Fig. ?? it is demonstrated that the deconvolution driven by kurtosis tends to indicate a single spike in the deconvolved signal, beginning from the 40th iteration (Fig. ??a). This single spike is related to the second Kronecker delta of the excitation signal. Other two criteria (Figs. ??b, ??c) preserve the entire pulse train, even after 160 iterations. It is worth to notice that the JB-driven deconvolution converges to the pulse train faster than the skewness-based equalizer. This proves that the JB-driven equalizer could manage to indicate the pulse train properly even when one of two other analyzed criteria fail.

6.4 Real data analysis

In this section we analyze data that represents vibration acceleration of a two-stage gearbox operating in an open-pit mine. The gearbox transmits power from an engine to the belt conveyor driving pulley. Scheme of the gearbox and location of the accelerometer are presented in Fig. ???. Duration of the signal and sampling frequency are 2.5 s and 8192 Hz, respectively. During the measurement, rotational speed of the gearbox was almost constant, small fluctua-

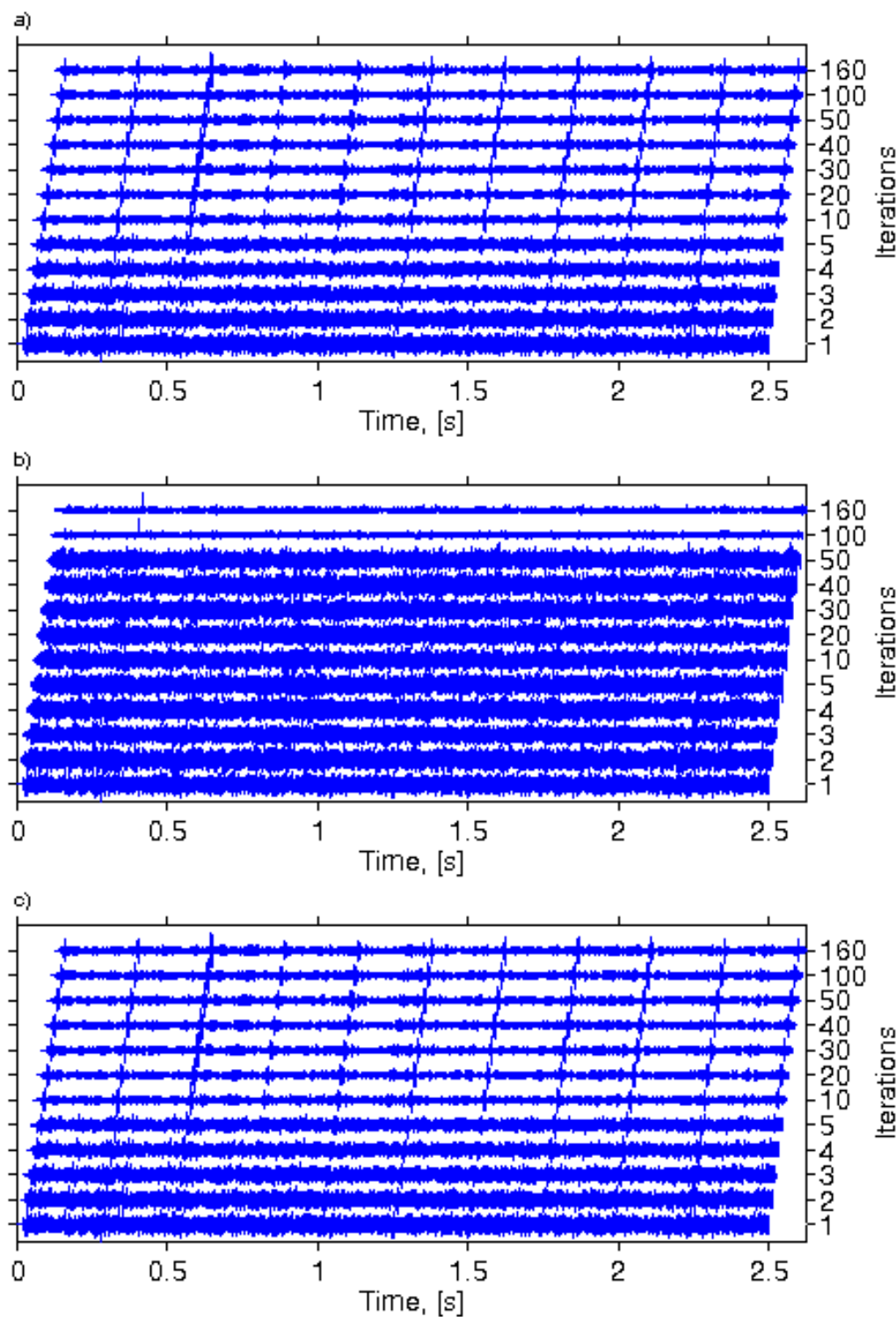


Figure 6.48: Outputs of the three analyzed blind equalizers against the number of iterations. The classical MED (a), skewness-driven equalizer (b) and JB-driven equalizer (c). Case K1.

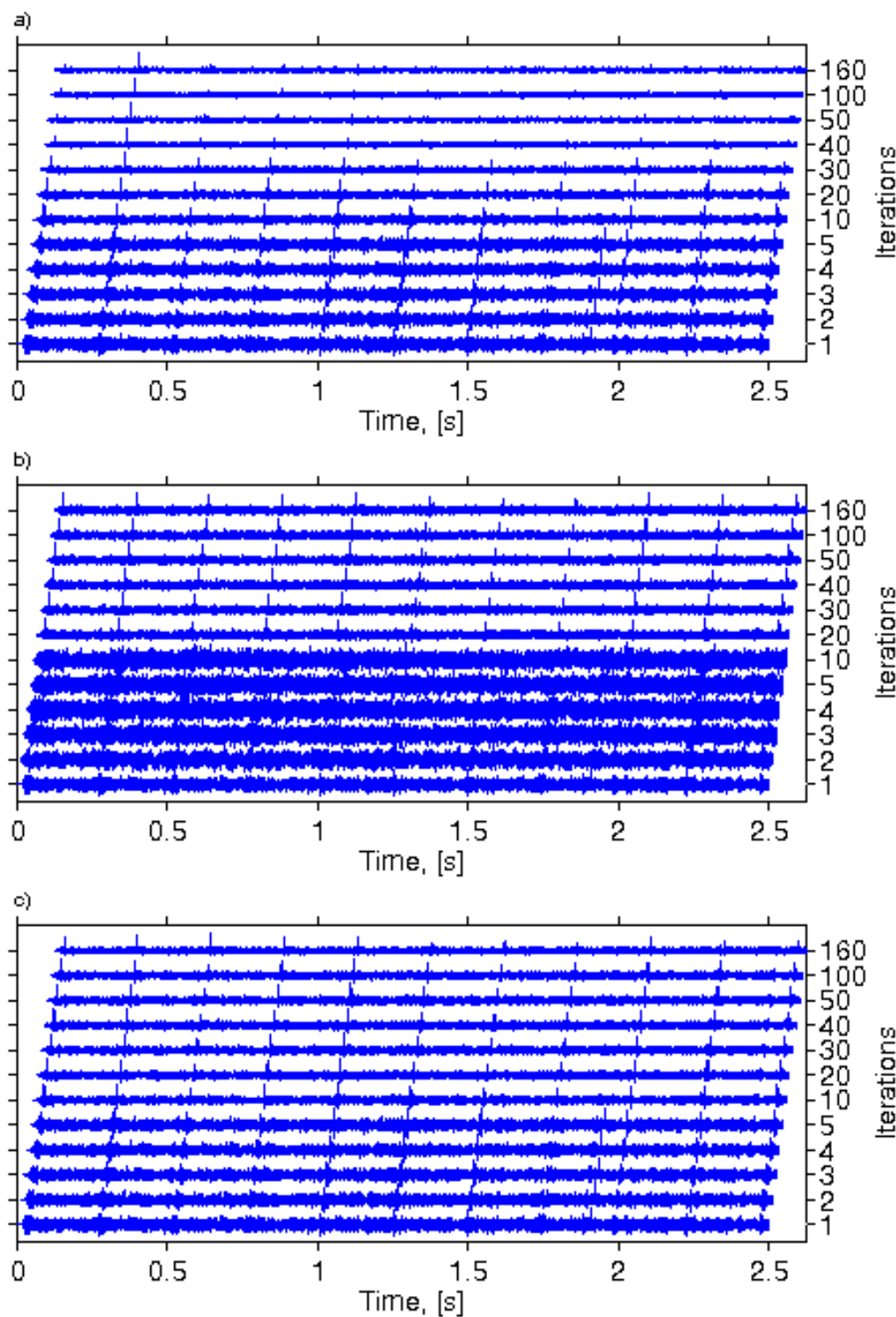


Figure 6.49: Outputs of the three analyzed blind equalizers against the number of iterations. The classical MED (a), skewness-driven equalizer (b) and JB-driven equalizer (c). Case K2.

tions from the average value are negligible. Characteristic frequencies related to the damage of the first and second shaft are 16.5 Hz and 4.1 Hz, respectively. The gearbox possesses a local damage of the second shaft.

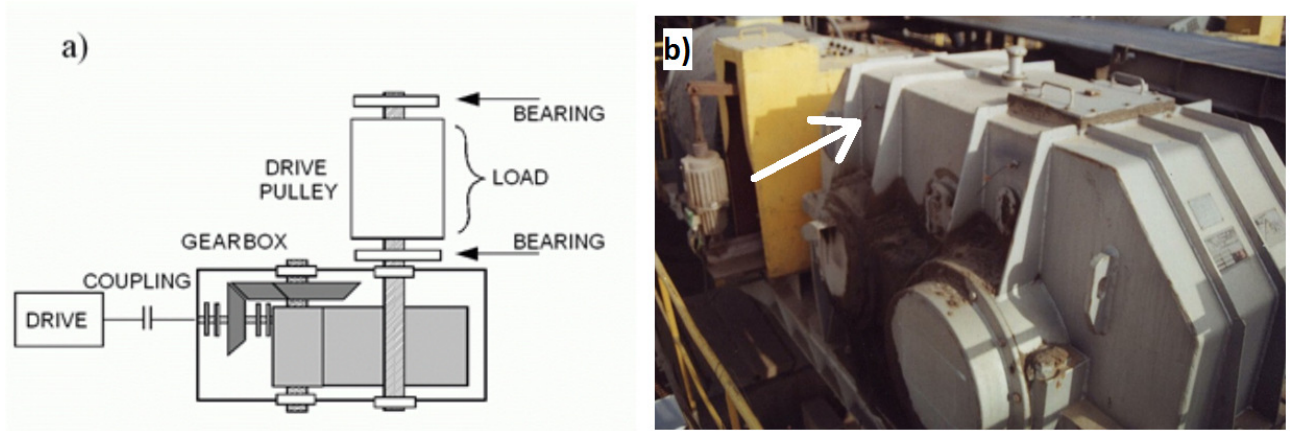


Figure 6.50: Two-stage gearbox: (a) - scheme, (b) location of the accelerometer.

The raw vibration signal, its spectrogram and the power spectral density estimate (peri-

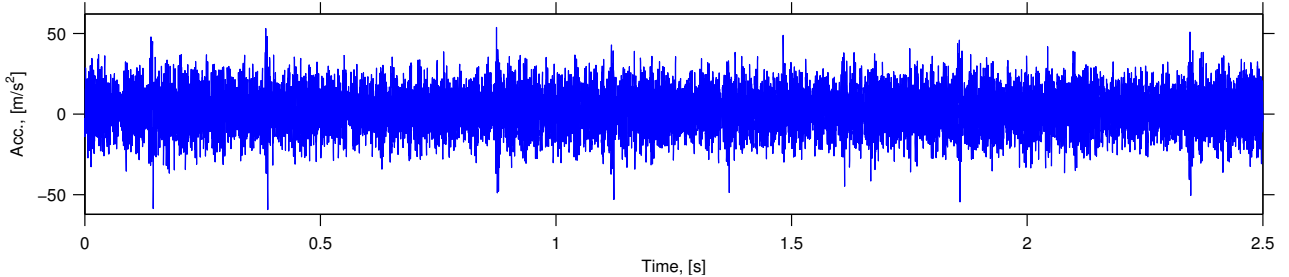


Figure 6.51: Raw vibration signal from the gearbox.

odogram) are presented in Figs. ?? and ??, respectively. The signal has been also analyzed in previous works of the Authors [?, ?]. One can see that majority of the power is contained in the low frequency bands, i.e. 300-400 Hz. Such energy content is related to the normal operation of the machine. The spectrogram (Fig. ??a) presents that there are cyclic impulses and they occur in 3 main frequency bands: below 300 Hz, 800-1200 Hz and 2800-3200 Hz. Such distribution of the informative frequency band might be caused by the resonance effect. While two first frequency bands contain almost every impulse that occurred during the measurement, the third one contains only a few impulses. This might be caused by random changes of the

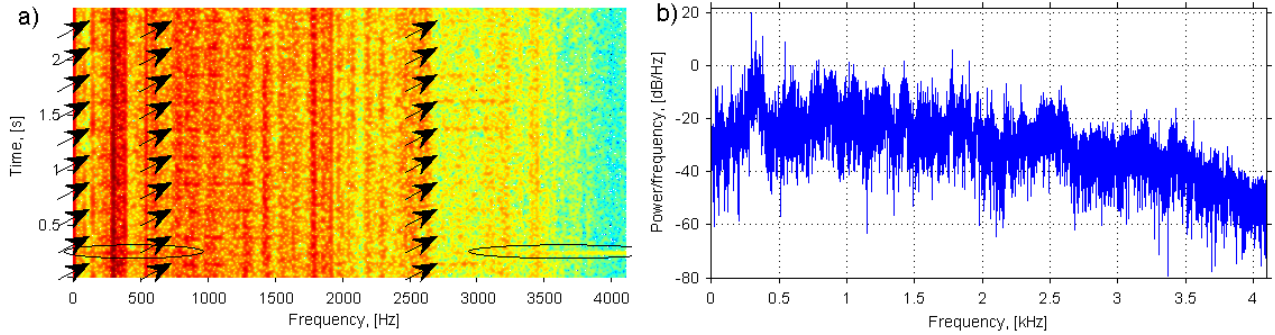


Figure 6.52: Spectrogram (left panel) and periodogram (right panel) of the raw vibration signal.

transmission path from the gear to the sensor and by small fluctuations of load. In order to make the visual analysis easier, the impulses are marked with arrows. There is also an artifact (at 0.25 s; marked with ellipses) which might affect results of methods based on quantifying impulsivity of the sub-signals from the spectrogram, i.e. the spectral kurtosis and a few of its generalizations presented in [?, ?].

Fig. ?? presents values of maximized criteria as functions of the filter length and number of

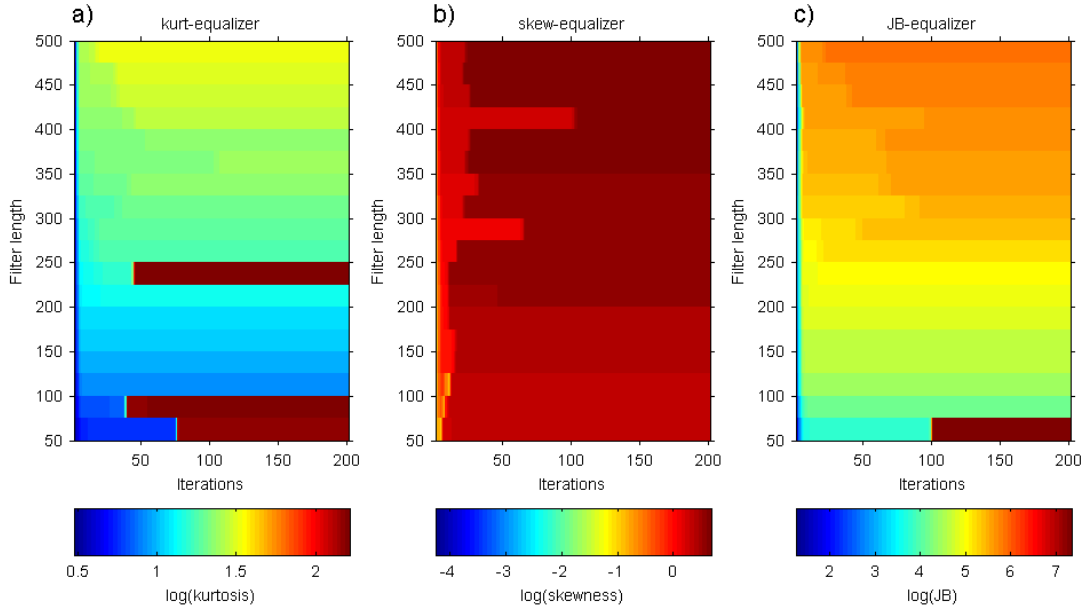


Figure 6.53: Values of the criteria maximized by blind equalizers through 200 iterations versus different filter lengths (log scale): kurtosis (a), skewness (b), JB statistic (c).

iterations. Note, that the log-scale is used here. Analysis of simulated signals revealed that the maximized criteria often rapidly grow through a few first iterations. Any next quick gain of a criterion value might indicate a large change of filter characteristics and thus, large change of

the filtered signal. It can be noticed that in every case the maximized criterion rapidly grows through a few first iterations. One can observe that every blind equalizer fails for a certain length of the filter. Although, the JB statistic-driven equalizer reveals second rapid grow less often than MED and skewness-based equalizer. This indicates that the JB statistic is a better criterion for different filter lengths and it deals better with the signal contaminated with the artifact. Skewness combined with kurtosis (in JB statistic) seems to share advantages of both skewness and kurtosis.

In order to illustrate how the considered criteria perform for a given length of the filter, we analyze waterfall plots and values of maximized criteria obtained by using the filter length L equal to 80. The key results of this paper are presented in Fig. ???. The results are obtained using criteria for blind equalization described in Section 4.4, i.e. kurtosis (Fig. ??a), skewness (Fig. ??b) and Jarque-Bera statistic (Fig. ??c). The iterative procedure has been stopped after 200 iterations. Note that the output after first iteration is only a shifted version of the input signal, because of the initial filter f (it is a shifted pulse in time domain). It can be noticed that the outputs of blind equalization driven by kurtosis and skewness (Figs. ??a and ??b) converge to the artifact (at 0.25 s). Although, output of MED from 3rd to 50th is the desired pulse train related to the local damage of the gearbox. Also, a few first iterations of the algorithm based on skewness indicate the desired pulse train. Then, both of the algorithms indicate only the single pulse. In this case, the limit behavior of JB statistic-driven equalizer is significantly better, because its output converges to the pulse train - not only to the single impulse like kurtosis- or skewness-driven equalizer.

Here, we stop the algorithm after 200 iterations, in order to show how the criteria behave through certain number of iterations and to present the approximation of the limit outputs of equalizers, i.e. output signals after a large number (200) of iterations.

Fig. ?? presents that the values of the criteria might not converge monotonically or, after fast grow and temporary stabilization they might grow once again. In order to illustrate this point, we calculated values of two common criteria that define the moment to stop the iterative procedure. The first is the value of the maximized criterion (Figs. ??a, ??b and ??c) and the second is the correlation coefficient between output signals of two following iterations (Fig. ??d). It

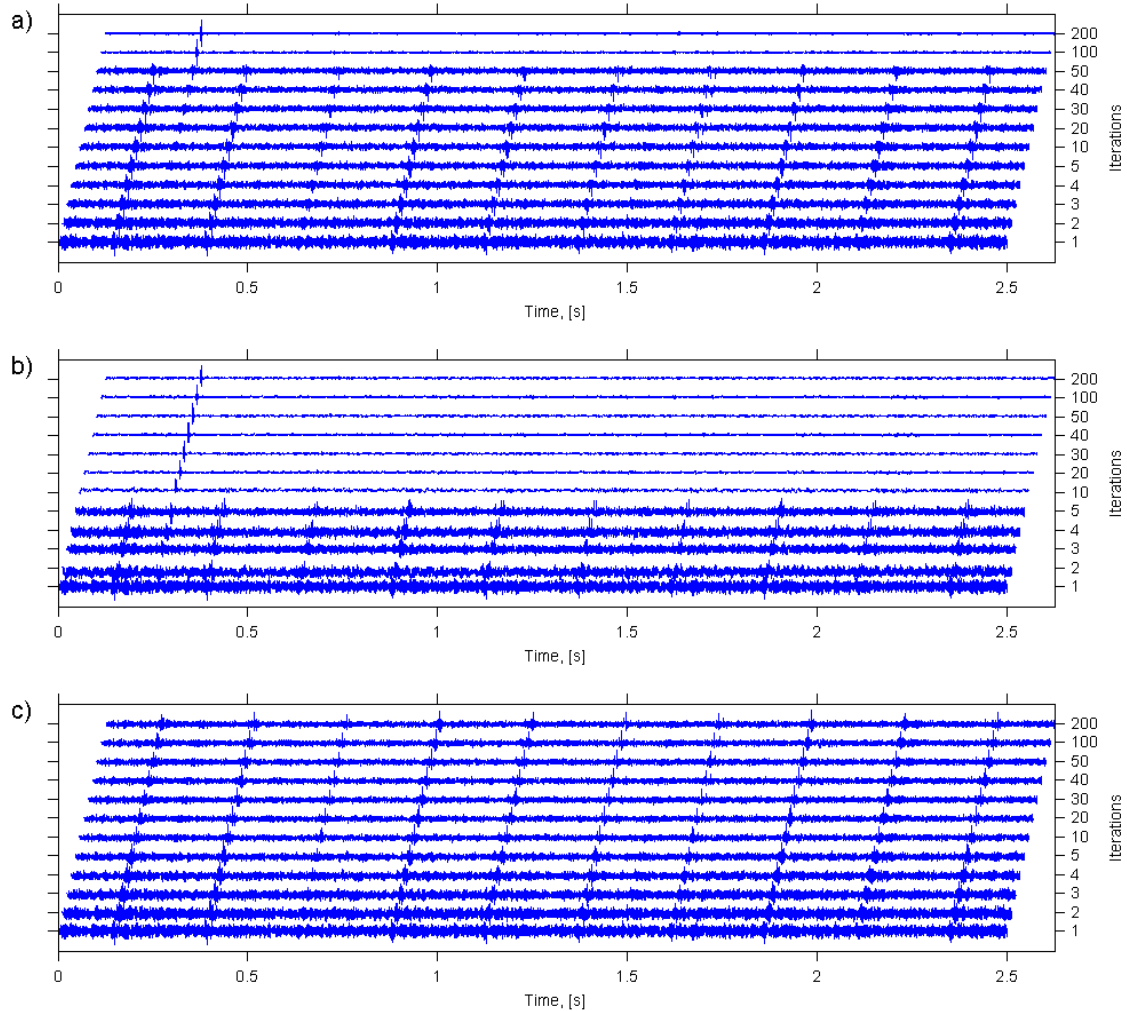


Figure 6.54: Outputs of the three analyzed blind equalizers versus the number of iterations.
MED (a), skewness-drive equalizer (b), JB statistic-driven equalizer (c).

is shown that the kurtosis of kurtosis-driven equalizer output signal grows rapidly and then it is stable from the 7th to 51th iteration. Next, it rapidly grows once again, which is related to convergence to the artifact. On one hand, increase of kurtosis through the iterations is an appropriate behavior of the iterative algorithm, since it has to find a filter that maximizes kurtosis value of the output signal. On the other hand, such indefinite maximization might be undesirable from the diagnostic point of view. The skewness-driven equalizer shares similar behavior. Skewness of the skewness-driven equalizer output grows up to the 5th iteration. This corresponds to the appropriate waterfall plot (Fig. ??b), where outputs of a few first iterations are the desired pulse train related to local damage. It cannot be said that the skewness-based filter coefficients stabilize through a certain number of iterations. Immediately after the 5th iteration, value of skewness drops till the 8th and then it rapidly gains. These inconveniences are overcome by the JB statistic-driven equalizer.

In Fig. ??c a monotonic grow and stabilization (after 10th iteration) of the maximized criterion might be observed. The stopping criterion based on the correlation coefficient indicates fast grow, drop and the next grow of correlation for skewness-based equalizer. The correlation for MED rapidly grows up to the 7th iteration, grows slowly between 8th and 51rd, then rapidly drops (local minimum at 54th iteration), grows once again and stabilizes, beginning from the 55th iteration. Behavior of JB statistic-driven equalizer is much better, i.e. it grows rapidly and stabilizes from 10th iteration. Although, a small decrease of the correlation coefficient might be observed from 3rd to 4th. Thus, this stopping criterion might provide significantly different results depending on the stopping condition. Let us denote the value of correlation coefficient at k th iteration as $C_{JB}(k)$. Firstly, while the algorithm is stopped while the C_{JB} reaches a value lower than $C_{JB}(3)$ (here, $C_{JB}(3) = 0.978$), then the output reveals barely indicated impulses (Fig. ??b). Thus, the benefit from blind equalization algorithm is minor. While a value larger than $C_{JB}(3)$ is chosen in order to stop the algorithm, then the resulting signal is the desired pulse train. On the other hand, such large threshold of the correlation coefficient would stop the skewness-based equalizer when it results in a single spike (Fig. ??b). If the iterative procedure is stopped after the first decrease of the correlation coefficient, then kurtosis- and skewness-based equalizer result in a pulse train, but then the benefit from the JB

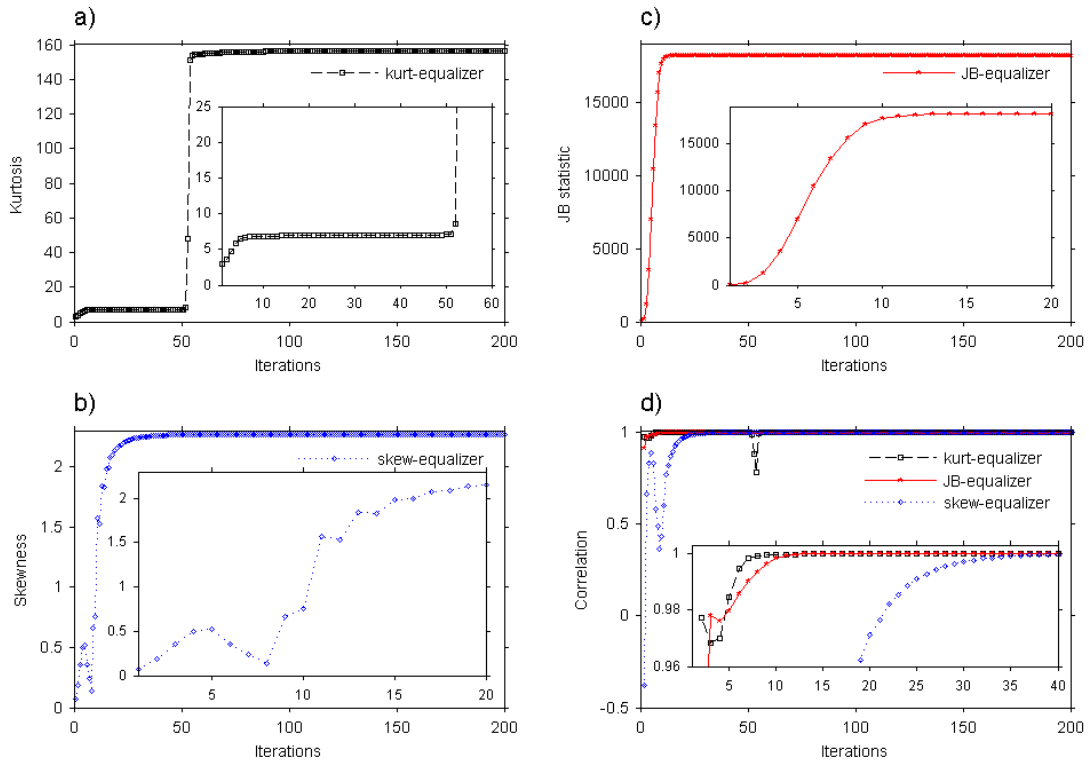


Figure 6.55: Values of the criteria maximized by blind equalizers through 200 iterations (linear scale): kurtosis (a), skewness (b), JB statistic (c). Correlation coefficient between signals from two following iterations (d). Black squares (dashed line), red triangles (solid line) and blue diamonds (dotted line) are related to 3 different equalizers: MED, JB statistic-driven equalizer and skewness-driven equalizer, respectively. Analyzed signal - real data.

statistic-driven algorithm is minor. Thus, considering the correlation coefficient as the stopping criterion might not provide appropriate results.

Finally, we investigate the results of both equalizers after a lot (200) of iterations, what might

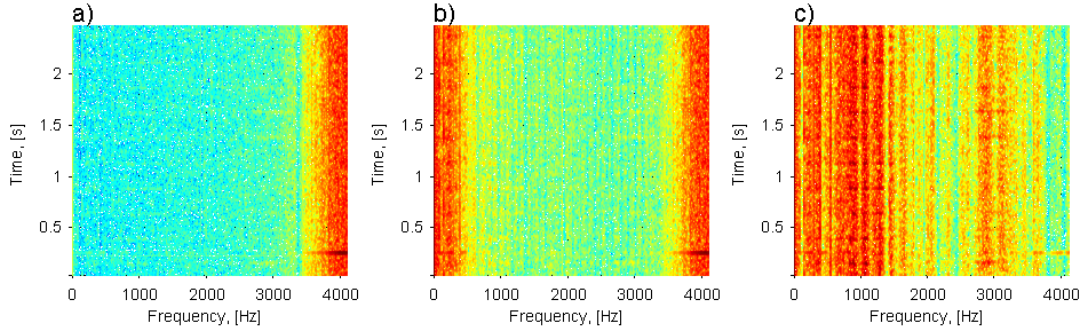


Figure 6.56: Time-frequency representations (spectrograms) of signals obtained after 200 iterations of the blind equalizers based on kurtosis (a), skewness (b) and JB statistic (c).

be considered as a limit behavior. As it can be noticed in Fig. ??, the classical MED indicates the informative frequency band located above 3700 Hz. Recall, that in this band only a single impulse appears and it is not related to condition of the machine. Likewise, the skewness-based equalizer indicate the frequency band related to the artifact. Additionally, it indicates also the lowest frequency bins (up to 500 Hz), where the artifact occurs as well. On the other hand, the JB statistic-driven equalizer indicates frequency bands related to the desired pulse train. The main energy of the resulting signal is contained between 800 and 1200 Hz. The frequency band between 2800 and 3200 Hz is also significantly indicated, but the energy is lower therein.

6.5 Autoregressive model in case of multiple damage

In this section we present analysis of the data that led us to establish the two-stage filtering procedure. The time series that we analyze is a raw vibration signal of a two-stage gearbox that operates in an open-pit mine and transfer torque from an engine to a belt conveyor pulley. The gearbox reveals two kinds of damage. They are related to a local damage of first and rather distributed one for second shaft (fault frequencies 16.5 Hz and 4.1, respectively). Length of the signal is 2.5 s and sampling frequency 16384 Hz.

Fig. ?? presents the raw vibration signal (time series, envelope spectra and spectrogram). Time-frequency map of the signal shows that there are three interesting features of the signal. One is a strongly amplitude modulated high-energy component that affects the shape of the signal (denoted by A). The second is consisted of two informative frequency bands (B, C) with visible horizontal lines corresponding to cyclic wideband excitations related to damage. The third is an artifact (single, non-cyclic wideband excitation), denoted by an ellipse. Perturbations like this should not be associated with any kind of damage. As it can be seen on the envelope spectrum,

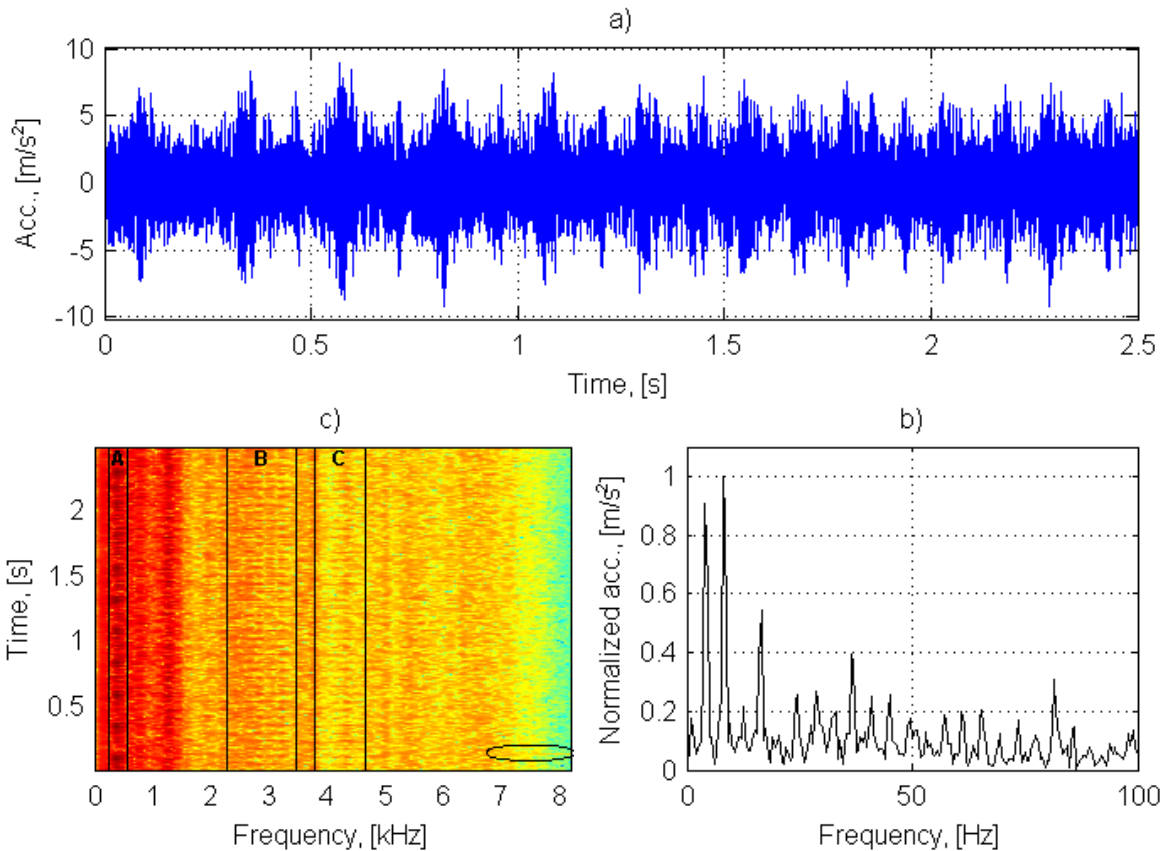


Figure 6.57: Raw time series (a), normalized envelope spectrum (b) and time-frequency map (c) of the raw vibration signal

amplitude modulation frequency equals to 4.1 Hz and the first and second harmonic are clearly visible. Single stage procedures based on informative frequency band selection do not work properly, due to high-energy amplitude modulated components (Fig. ??). Harmonics being multiples of 4.1 Hz are dominating. To suppress components related to 4.1 Hz amplitude modulation we fit an AR model to the raw time series. The highest Kolmogorov-Smirnov statistic criterion recommends AR(45) as the most suitable model (Fig. ??).

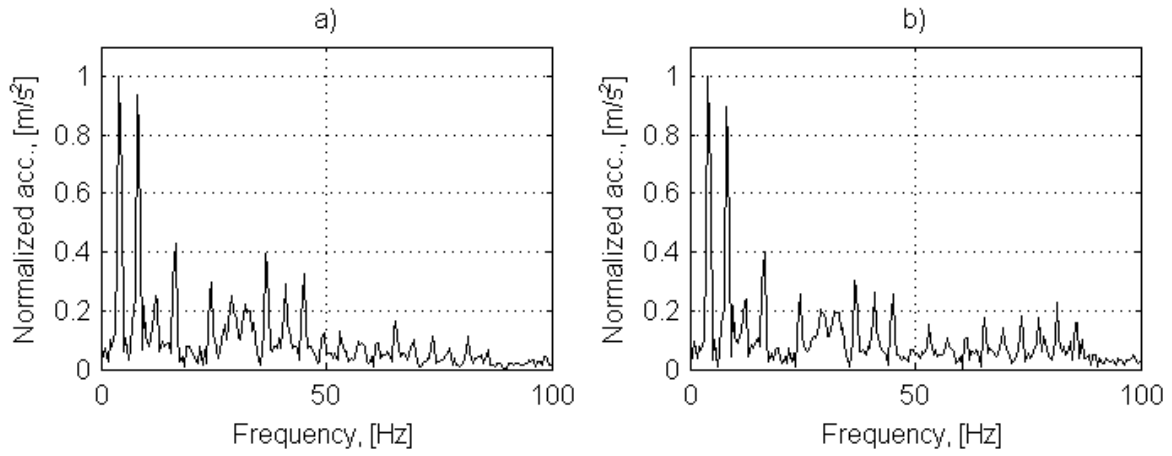


Figure 6.58: Normalized envelope spectra of the raw vibration signal filtered using the spectral kurtosis (a) and the horizontal QQplot distance (b)

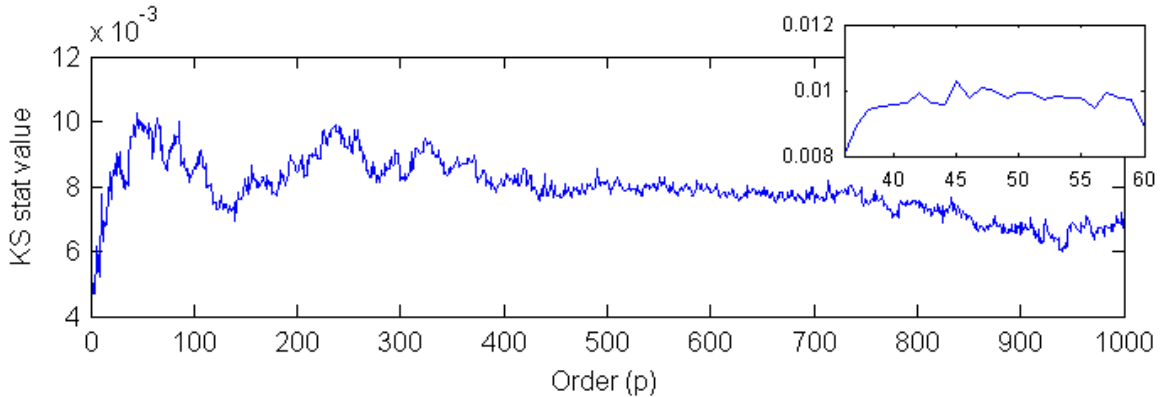


Figure 6.59: Kolmogorov-Smirnov test statistic value versus order of autoregressive model. The highest value is obtained at $p = 45$

The residual signal obtained using AR filtering is presented in Fig. ???. Plot of time series presents the artifact and a barely visible cyclic pattern. The signal is too noisy to see a clear pulse train related to the local damage of the first shaft. The envelope spectrum shows that the frequency of excitations barely visible in time series equals to 16.5 Hz and the second harmonic is present. However, there is still quite large amount of noise that can be seen in the envelope spectrum. The time-frequency map presents two informative frequency bands (B and C, Fig. ???, panel c)). These bands are relatively narrow which is consistent with large amount of noise in the time series plot. To extract only the SOI we decided to filter this signal using linear filters with frequency responses obtained by both the SK and QQplot average distance described in [9,10,11,12]. The thresholds are obtained using 1000 Monte Carlo repetitions and

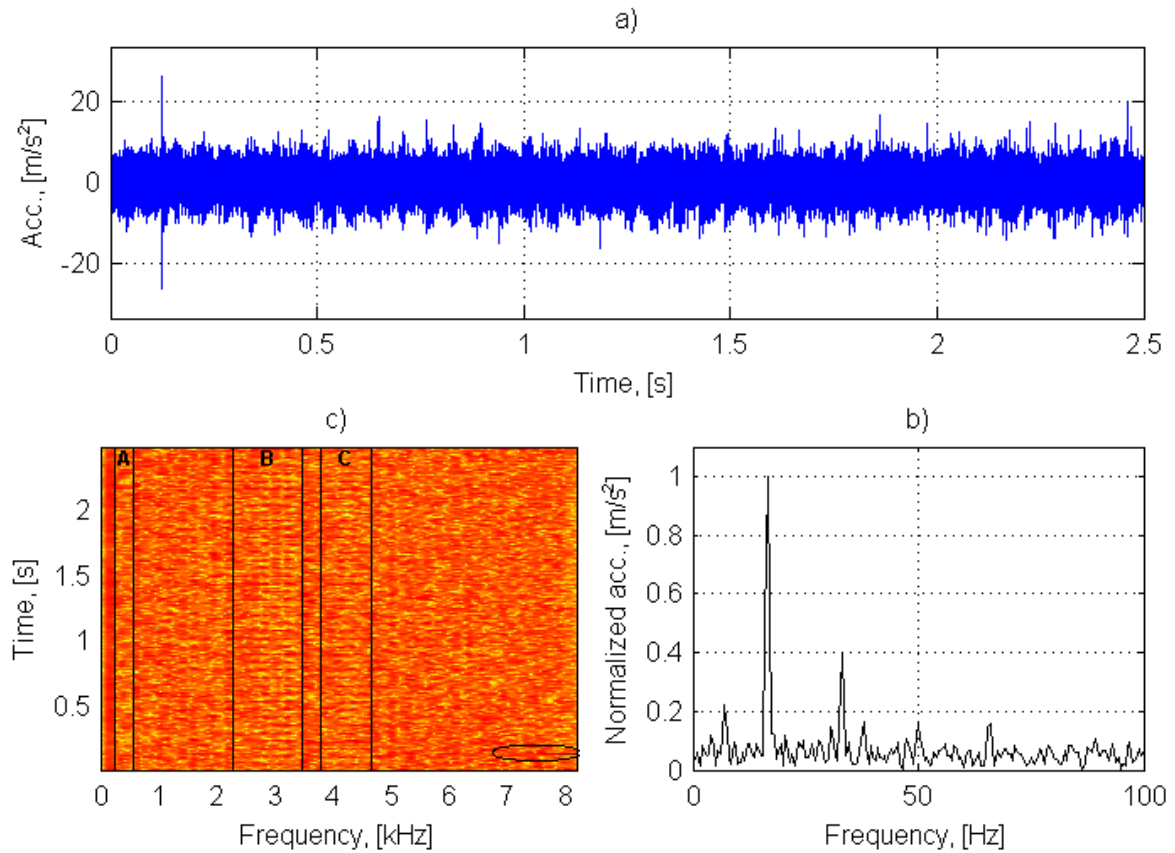


Figure 6.60: Time series (a), normalized envelope spectrum (b) and time-frequency map (c) of the signal after AR(45) filtering

quantiles of order 99% are taken as individual thresholds for each narrowband frequency bin. Fig. ?? shows that the accidental impulse has great influence on the SK and the filtered signal is consisted mainly of high-frequency component which includes the artifact. As it can be seen on spectrogram (Fig. ??d)), the SK also detected the in-formative frequency band, but values of frequency response at the highest bands are very large. Such structure of the signal results in noise in the envelope spectrum, Fig. ??c). i.e. none of the harmonics related to the fault frequency are indicated. In the presence of artifact the result obtained by only AR filtering is much more efficient. The filter driven by the selector that is a result of quantifying average horizontal distance on the quantile-quantile plot also indicated the high-frequency artifact, but its influence on the filtered signal is much lower (Fig. ??). Amplitude of the arti-fact is just a little bit higher than average amplitude of the pulse train (Fig. ??a)). Moreover, the pulse train is clearly indicated. The frequency characteristic of the filter shows that the selector based on average QQplot horizontal distance indicated frequency bands B and C as the most informative

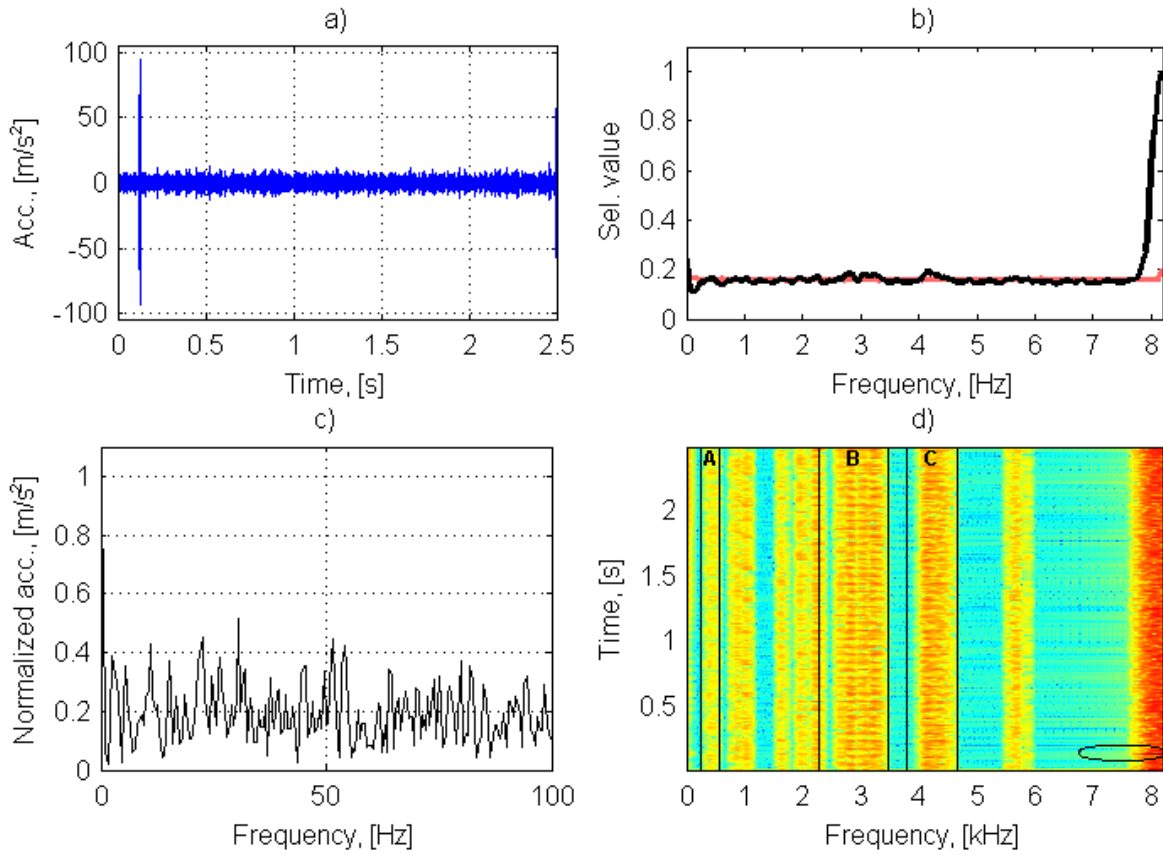


Figure 6.61: Time series (a), frequency response of the filter based on the SK (b), normalized envelope spectrum (c) and time-frequency map (d) of the AR-residual signal after applying the filter based on the SK

ones (Fig. ??b)). Envelope spectrum of the filtered signal clearly shows that the artifact has no influence on the fault frequency recognition (Fig. ??c)). This is the most valuable advantage of incorporating a different selector than the SK. Comparing the result of the two-stage filtering procedure to the signal filtered only by AR filter one can observe that our method results in a signal with significantly decreased amount of non-informative noise. Amplitude modulation of the signal of interest is clearly visible and several harmonics of the fault frequency are visible. The indicated frequency is related to the local damage of the second shaft, i.e. 16.5 Hz.

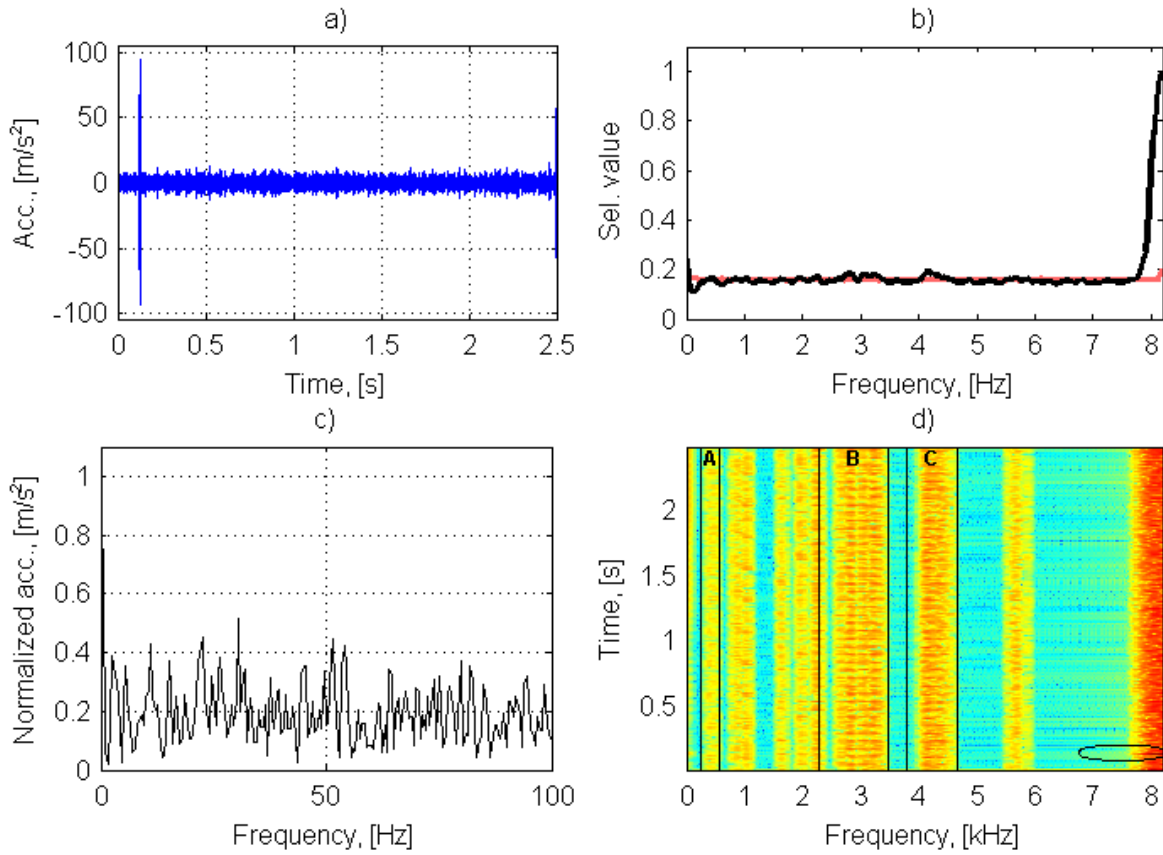


Figure 6.62: Time series (a), frequency response of the filter based on the average QQplot horizontal distance (b), normalized envelope spectrum (c) and time-frequency map (d) of the AR-residual signal after applying the filter based on the average horizontal QQplot distance

6.6 Periodic autoregressive model for cyclic load of bucket wheel excavator

6.6.1 Influence of non-Gaussian noise to PAR estimation

The results are obtained using 50 simulated signals for one noise distribution each, i.e. 150 signals overall. Length of each signal is 4 s and sampling frequency is 8192 Hz. Each signal is consisted of 4 sine waves of frequencies 900, 1800, 2700 and 3600 Hz, respectively. Frequency modulation type is a saw-tooth, modulation depth - 15% and modulation frequency is 6 Hz. Fig. ?? presents fragment of time series of the noise-less signal, i.e. noise consisted of a signal equal to 0 at every time t (top panel), fragment of the spectrogram of this signal containing only one period (bottom, left panel) and amplitude response surface of the fitted PAR model

of order 15 (so called "perfect surface"), see bottom, right panel. The term "perfect surface" is related to the specific signal consisted of frequency modulated sine waves only, i.e. amplitude of the noise is 0 at every time t . Noiseless signal is treated as an ideal ("perfect") one. In Fig. ??

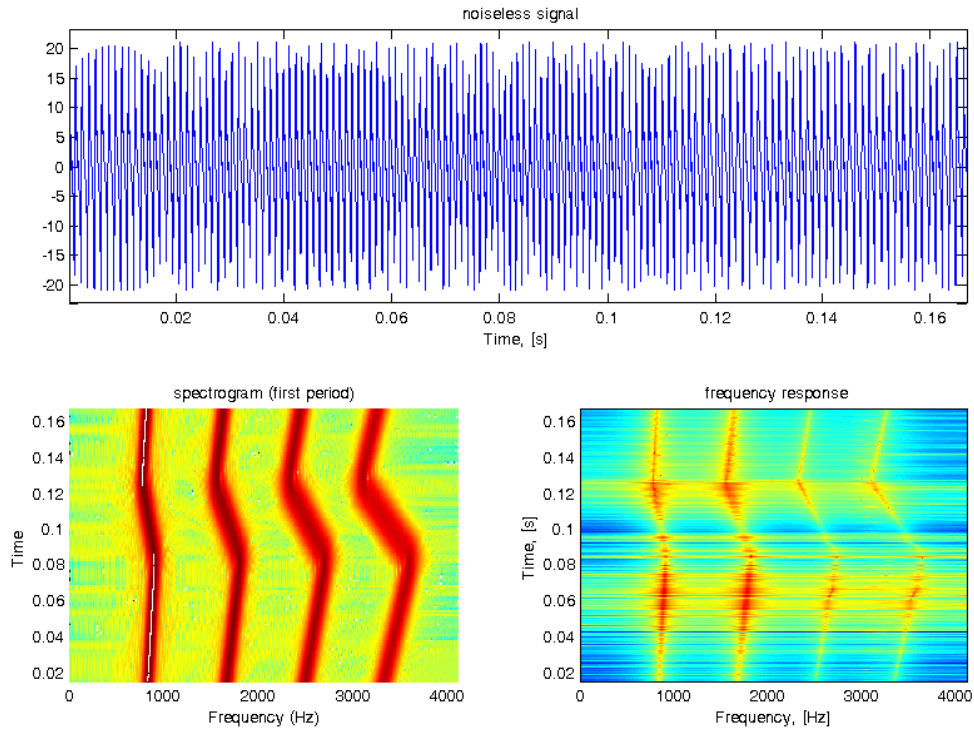


Figure 6.63: Noiseless signal (time series, spectrogram, frequency response of fitted PAR filter

one can compare the "perfect surface" and exemplary estimated surfaces obtained for three considered distributions of noise (two Pareto with different shape parameters and Gaussian). It can be seen that the Gaussian noise seems to provide the surface which is the closest one to the "perfect" one. The property of heavy tails of the Pareto distribution might be seen in Fig. ?? (top panels). It is easy to verify that the Pareto distribution with the shape parameter 1.5 gives the highest amplitudes of noise whereas energy of each signal is the same. In Fig. ?? we present the boxplots of MSE for three considered distributions of noise. More precisely, in each case we simulated 50 signals and for each of them we calculate the MSE of frequency responses. The boxplots are calculated on the basis of obtained measures. Boxplots in Fig. ?? clearly presents, that the MSE related to Gaussian noise is the lowest and MSE related to the Pareto distribution with $\alpha = 1.5$ is the highest. This result means that the heavier tail of the

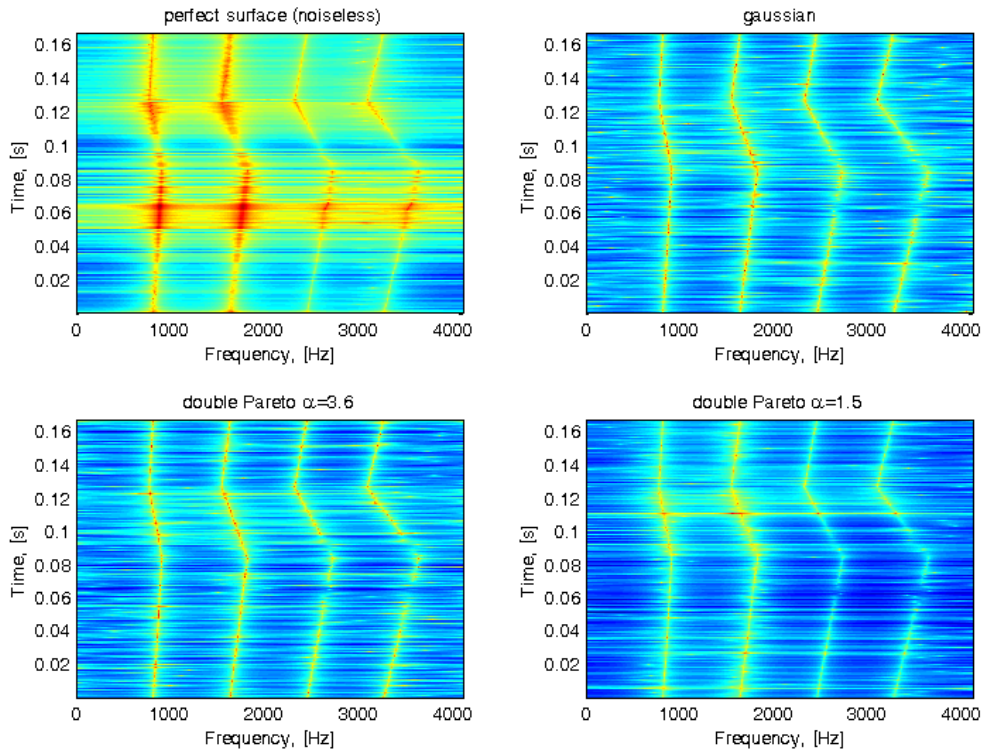


Figure 6.64: Exemplary frequency responses (surfaces) for noiseless (top left), Gaussian (top right), Pareto3.6 (bottom left), Pareto1.5 (bottom right)

noise the worse results of PAR model estimation. Thus heavy tail of the noise distribution has a huge impact on the estimation procedure.

6.6.2 Influence to PAR estimation for different number of period repetitions

In order to be consistent with Sec. 4 we analyze here signal of the same kind, i.e. sum of 4 frequency modulated (saw tooth modulation type) sine waves with modulation frequency 6 Hz and modulation depth 15% and noise. We consider 2 different kinds of noise - a white Gaussian noise and an amplitude modulated Gaussian noise, i.e. a white noise multiplied by a periodic impulsive function which reproduces impulses that might appear while the investigated machine is damaged. Fig. ?? presents boxplots of MSE mentioned in Sec. 5.1 in log scale. Each boxplot is obtained using 1000 signals of the given length. One can see, that results obtained for signals

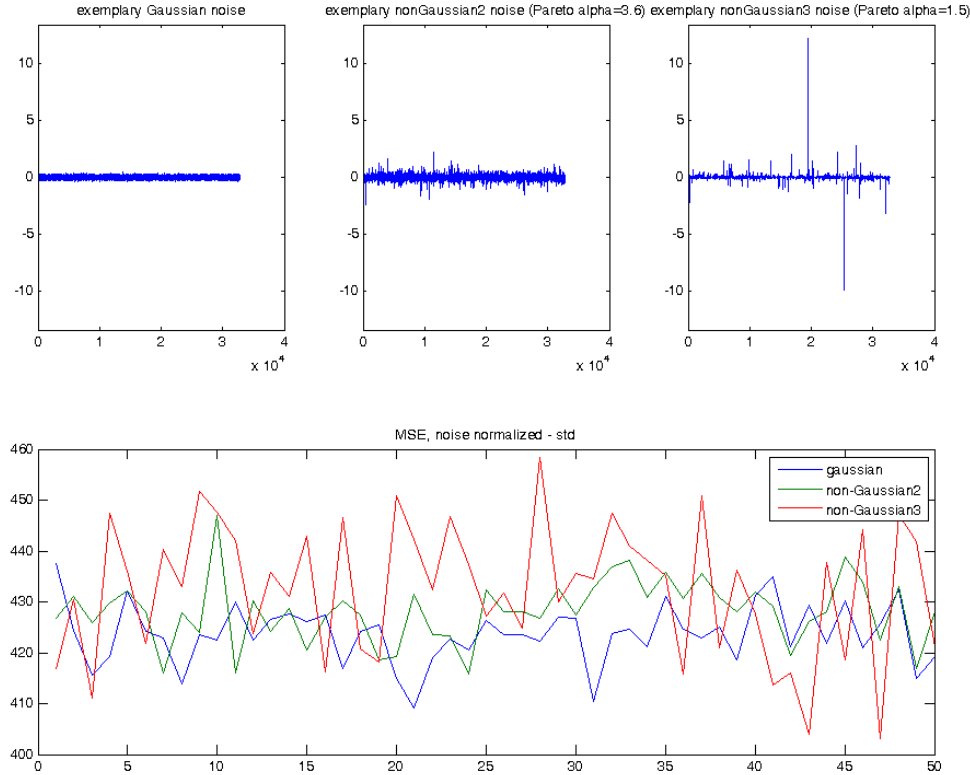


Figure 6.65: Exemplary noise (3 cases), MSE of frequency responses (3 cases). Not so large differences, probably because of normalization by standard deviation (energy)

consisted of 3 whole periods are significantly worse than other. Boxplots for period repetitions from 4 to 16 are similar, thus it is circumstantiated to see median of these values separately. Signals consisted of 17 and 18 period repetitions lead to the best results, i.e. the smallest MSE. Amplitude modulation of the noise does not introduce significant gain in MSE.

Medians of MSE between PAR parameters for the noiseless signal and PAR parameters for noisy signals of different lengths are presented in Fig. ???. One can clearly see general decreasing trend of the medians while the number of period repetitions gains. This result is consistent with dispersion illustrated by boxplots in Fig. ??.

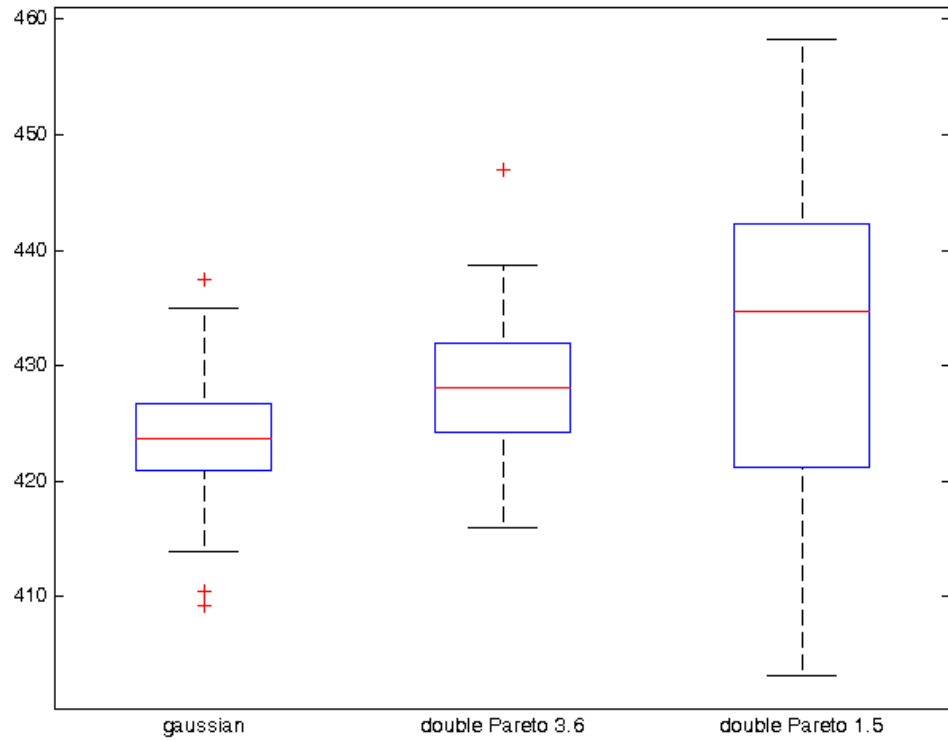


Figure 6.66: Boxplots of MSE from bottom panel of Fig. ???. Even for noises normalized by energy there is a visible difference.

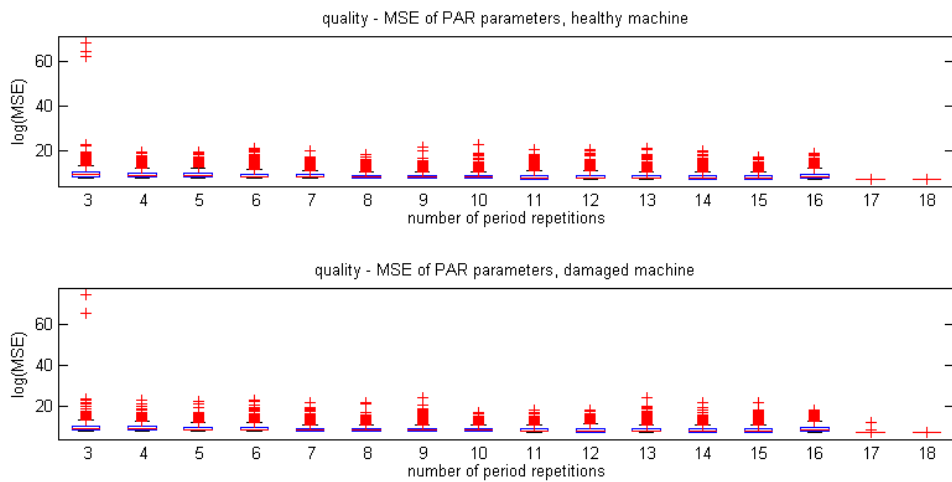


Figure 6.67: Boxplots of MSE for PAR parameters in case of healthy machine (top panel) and damaged one (bottom panel)

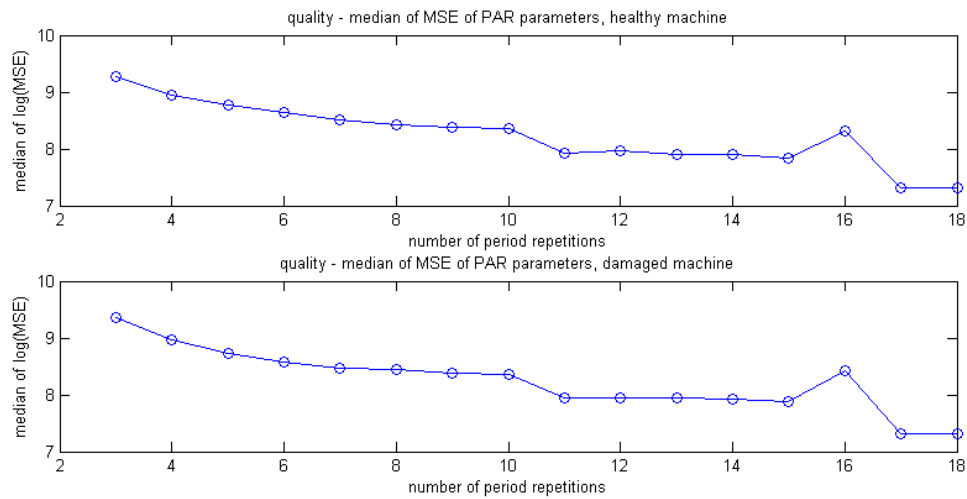


Figure 6.68: Medians of MSE for PAR parameters in case of healthy machine (top panel) and damaged one (bottom panel)

6.7 Conclusions

Podsumowanie rezultatow?

Chapter 7

Conclusion

7.1 Summary of Thesis Achievements

Jasne potwierdzenie udowodnienia tezy pracy. Lepiej nie rozbijac wnioskow na czesci, ewentualnie na akapity. Brak wyraznego rozbicia poprawi jednolitosc pracy.

7.2 Applications

Mozliwe zastosowania/komercjalizacja w systemach pomiarowych - czego brakuje do wyzszeego poziomu gotowosci technicznej

7.3 Future Work

Jak mozna ewentualnie rozwiazac problemy w przyszlosci, aby wszystkie te metody mogly byc stosowane w systemach pomiarowych w warunkach kopalni